Fabrication of thin film CZTS solar cells with Pulsed Laser Deposition

Cazzaniga, Andrea Carlo; Schou, Jørgen; Pryds, Nini; Petersen, Paul Michael

Publication date:
2016

Document Version
Publisher's PDF, also known as Version of record

Fabrication of thin film CZTS solar cells with Pulsed Laser Deposition

PhD candidate: Andrea Cazzaniga

Senior scientist Jørgen Schou

DTU-Fotonik, Risø campus
Roskilde, July 28^{th} 2016

To my three readers: James, Jørgen and Susanne.

Contents

Preface 5
Resume 8
0.1 på Dansk 11

Introduction **12**
0.2 The CHALSOL project 12
0.3 CZTS material 16
0.3.1 Motivations to CZTS 16
0.3.2 A complicated material 18
0.3.3 Alloying S with Se 21
0.3.4 Toxic and non-abundant device 23
0.3.5 Open problems with CZTS 23
0.4 Pulsed Laser Deposition 26
0.4.1 Unique features of PLD 27
0.4.2 Open problems with PLD 28
0.5 Is PLD suitable for CZTS? 30

I Background work **33**

1 Pulsed laser deposition of Cu, Zn and Sn **34**
1.1 Why PLD of metals? 35
1.2 Tuning the stoichiometry using multiple elemental sources . . 35
1.3 Multilayers of Cu, Zn and Sn 37
1.3.1 Cu-Zn-Sn alloyed target 38
1.4 Conclusions 39
Nanosecond laser ablation and deposition of silver, copper, zinc and tin 39

2 PLD of CZTS, first attempts **44**
2.1 Chalcogenide vs metallic target 44
2.2 First films and first problems 46

2.3 EDX measurements . . . 48
2.4 Substrate temperature . . . 49
2.5 Results and discussion . . . 50
2.6 First experiments with the annealing . . . 53

3 ZnS top layer for enhancement of the crystallinity of CZTS absorber during the annealing 55
3.1 Mistake it until you make it . . . 55
3.2 Let's write a paper . . . 57
3.3 Conclusions . . . 58

II Research activity 61

4 Breakthrough! 62
4.1 July 2015 . . . 62
4.2 Our first solar cell . . . 64
4.3 Our second solar cell . . . 67
4.4 The forgotten one . . . 71

5 Guidelines for PLD of chalcogenide targets 73
5.1 Choice of the laser . . . 73
5.1.1 Nd:YAG laser . . . 74
5.1.2 The KrF excimer laser . . . 75
5.2 Laser alignment . . . 76
5.3 Target morphology . . . 77
5.4 Rastering design . . . 78
5.4.1 Beam Stability . . . 78
5.4.2 Rastering speed . . . 81
5.4.3 My choice . . . 82
5.5 Measuring the laser spot size . . . 83
5.5.1 Against the Cu plate standard . . . 84
5.5.2 Analytical tools . . . 85

6 Pulsed Laser Deposition of thin films of CZTS and CTS 87
6.1 Introduction - what is laser ablation? . . . 87
6.2 The effects of laser fluence and wavelength . . . 91
6.3 Structure of the precursors . . . 93
6.4 Other groups doing PLD of CZTS . . . 94
Ultra-thin Cu_2ZnSnS_4 solar cell prepared by pulsed laser deposition 96

7 Double absorption onset of monoclinic Cu2SnS3: experimental features explained by DFT 112
7.1 Pico-introduction to CTS material 113
7.2 Experimental work 113
7.3 Conclusion 114
Conclusions 116

Preface

Pauca, sed matura
Carl Friederich Gauss

Here I go, the time has finally come to writing about my research activity. My work lies at the intercept of two very far fields in Physics: Pulsed Laser Deposition and Solar Cells. Altogether it sounds like the title of a sci-fi movie from the 70's, if you like the genre (I do not). The mistake that I will try to avoid, for as long as I can keep my scientific judgement detached from personal involvement, is to write for myself rather than for those who read. As a writer, one firstly wants to show that he has done a good work, a hell of a lot of work, and that he deserves the title of PhD. As a reader, one would possibly aim at (1) learning something new and (2, as a professor) having enough elements to judge if that person over there can be awarded by the *scientific community* with an "official licence to talk about science". In an era of super-experts of nothing, this is quite a task. The scientific method has never been so misused that, beside one's contribution to scientific progress, the scientific community needs valuable people with a clear say on what is scientific and what is not. Or at least, that is what I, as a physicist and citizen, feel more urgent.
For what concerns #1, I think there are results enough to bring some novelty to both the fields of Pulsed Laser Deposition and CZTS solar cells (Chapters 6 and 7). We talk very clearly of humble contributions, which can be considered "remarkable[1]" only in the fact that I achieved them with my own two hands, as result of a hard learning process.
Regarding #2, even more, if I wasn't myself able to only pick the good stuff out of all what I have, how could I demonstrate any scientific insight into what I have done? And I really would not need a hundred pages for this. Unfortunately, the thesis must be written according to some criteria, of which brevity is not the privileged.

[1]Everything has to be remarkable nowadays.

Thus, the thesis is divided into two parts, sketched in Figure 1 with different colors. Part 1, "Background work", contains Chapters 1, 2, and 3. This part is an account of the activity done to start up the project, roughly the first two years of my PhD. While writing it, I tried to enlighten the most significant progress and mistakes done, trying to show the logic behind, when possible. **There is not much scientific novelty in Part 1 and the reader who is not interested can safely skip it entirely.**
Part 2, "Research activity", contains the most important outcomes of this project. It contains Chapters 4, 5, and 6 and the paper(s) which were published (or submitted for publication).
I do not assume that every reader is interested in the whole work, so I tried to keep the chapters rather independent, hopefully one can easily see if the topic suits his own interest or not. The section on PLD is written for somebody who is familiar with solar cells, and vice-versa for the section on solar cells. I did not attempt to give an exhaustive review of the fields, there are good books for both of them and no one would benefit from a beginner's summary. Briefly, I tried to select which contribution each field can offer to the other and what are the warnings that one should be aware of before throwing himself into a new field.
Finally, Chapter 5 is fully dedicated to the experimental technique which I developed for our particular setup. It is rather extended and may be mostly for internal use, for the lucky few who will want to carry on this project. There is no scientific novelty in it[2], and I could have made it much shorter just writing a protocol (and I have almost never read or followed a protocol in my life). However, if there is one thing that should never be overlook, this is the scientific method, whose strength lies in the experimental reproducibility. Reproducibility was the main hurdle in this work, and only came after a breakdown analysis of every single step in the PLD process. The chapter is thus an attempt to make people aware not just of what have I done, but also to warn them against the effects of seemingly equivalent choices, which sometimes are not.
The learning process of the basic physics behind PLD, and PLD of CZTS, came along with experimental reproducibility, and I couldn't say which one led the drive. More likely, it was a self-regulating process. Thus, Chapter 5 rightfully belongs to Part 2 of this thesis.

[2]or maybe yes, I honestly don't know. Certainly, very few people nowadays spend time writing about experimental practice

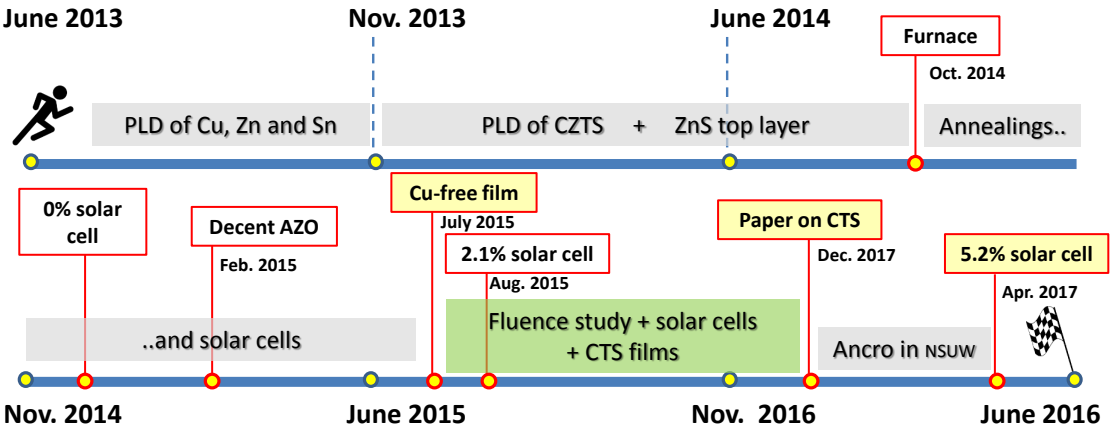

Figure 1: Timeline of my PhD project. The grey bars contain the activities belonging to the "background work" (First part of this thesis). The green bar indicates the period and the activities from which the main results came out (Second part of this thesis).

Resume:

This project was about making CZTS solar cells using PLD for the fabrication of the absorber layer, and using standard techniques for the rest of the device. The solar cell is a very complicated device and all the steps in the fabrication are very important. It doesn't matter if PLD brings the best absorber layer, if one has a poor device processing the outcome will be disastrous. The converse holds true exactly in the same way. Developing the device-fabrication takes time, trials and errors. Unless one has a special PLD equipment for large area deposition, PLD's sample-throughput is too low to provide enough "dummy samples" to develop device processing. If one wants to try out PLD for making solar cells with a standard PLD setup, my suggestion is to first develop device processing with an alternative technique, *e.g.* sputtering, and with an established material, *i.e.* CIGS., easier than CZTS to handle. Once device processing is under control, the small area of the samples made with PLD may be a not-too-dramatic problem.
CZTS as absorber layer is a polycrystalline material with a complicated structure that tolerates deviation from exact stoichiometry. It is very difficult to characterize such kind of material since many parameters can modify the optical and electronic properties: grain boundaries, point defects, disorder and secondary phases are just a few. When the CZTS layer is integrated in the solar cell, interface physics can also become very significant to the final device efficiency. As consequence, one cannot always distinguish a "good" or "bad" CZTS only using conventional techniques (Raman, SEM, x-ray diffraction, photoluminescence..) on the absorber layer alone. The only meaningful information comes from the full solar cell operation, but at this stage everything is coupled together behind the Quantum Efficiency (QE) curve.

What do I learn by reading this thesis? You will learn how to deposit a thin film CZTS absorber layer with Pulsed Laser Deposition with the desired composition. In addition, you will see how material transfer in PLD, which is generally believed to be stoichiometric, can be very much non-stoichiometric.

How to do it? I suggest to do PLD on a single sintered target (2CuS:ZnS:SnS).

The films are deposited at room temperature and then annealed in a furnace with some sulfur powder aside. The annealing step is as important as the PLD step to the final device efficiency.

What is your best solar cells? With our own in-house device fabrication we reached a 2.6% conversion efficiency. With the absorber layer produced with our PLD setup followed by a well established annealing + device processing we reached a PLD record efficiency of 5,2%. The world record efficiency for this material is around 9%, with sputtering.

Did you manage to get good quality CZTS? We cannot evaluate the performance of our annealing step. We can only demonstrate that the precursors made with PLD can be used for producing state-of-the-art solar cells.

Is there anything left to do? Oh yes! Exploring the non-equilibrium properties of PLD for the production of CZTS films. This may enable one to deposit crystalline CZTS at lower substrate temperature, with no requirement for an annealing step afterwards. Preliminary results do not seem too encouraging. The main obstacle to this approach may be that droplets do not have enough thermal energy to dissociate and merge in the absorber layer.

Any further suggestions? Learn by doing. Results from other group are more-often-than-not system dependent. Select your references very carefully. If the paper doesn't come from a group that has ever reported making solar cells, there is almost no point in reading it (and they are the vast majority).

Vox auctoritatis :

"[..] the thickness of annealed films was $1.7\mu m$ for CZTSSe, and $0.9\mu m$ for CZTS (significant cracks will develop for a thicker CZTS film).", from a footnote in IBM's [34], Dec. 2015. And I really wish they had written this before.

"[..] even rather detailed materials characterization was not able to resolve the particular chemical products that led to the large differences in device performance. The devices in this study varied from 0.3% to 7.9% efficient, but no strong differences were observed by Raman, SEM, or EDS mapping at the surfaces and back contacts. This means that the causes of the electrical differences are on a smaller scale than the resolution of these techniques and could be, for example, very finely distributed secondary phases, changes in grain boundaries, or of course, point defects.", from a paper by J. Scragg dated 2013 [29]. Which basically says that if you do not make a solar cell,

you do not understand much about this material.

"of course you can talk about XRD, at some point you've got to write something to finish your phD, but people mostly care about optical and electronic properties of this material, and of course, the efficiency of the solar cell above all". Private discussion with S. Siebentritt.

"[..] you just need to have the right composition in your precursors and the annealing pretty much does the job". Private discussion with T. Teodorov, from IBM's lab.

"[..] reproducibility of the results is an issue. Reproducibility of our best solar cells is below 30%". Private discussion with S. Tajima, from Toyota's lab.

0.1 på Dansk

Her er et lille resumé, fordi lille er min dansk sprog-skill. Har du nogle spørgsmål, så kontakt mig når vi komme til mit forsvar. Vi ønsker jer en dejlig læsning.

I denne afhandling er det beskrevet, hvordan man deponerer en tynd-film med den ønskede sammensætning af et CZTS absorber lag med pulset laser deponering (PLD). Man vil her se, at materialet , der overføres fra target til et substrat med PLD, som normalt vil have en lignende sammensætning som target, d.v.s. være støkiometrisk overført, faktisk kan være meget ustøkiometrisk. Man bør derfor benytte PLD til et enkelt sintret target (2CuS:ZnS:SnS). Filmene deponeres ved stuetemperatur og bliver derefter udglødet, "annealet ", i en ovn med ekstra svovl pulver. Selve annealingen er lige så afgørende som PLD processen for den endelige effektivitet af solcellen. Med den bedste celle og hele fabrikationsprocessen af solcellen internt på DTU har vi opnået 2,6% effektivitet. Ved kun at producere CZTS absorber laget med vores eget PLD system og derefter færdiggøre filmen i et veletableret, anerkendt annealing og celle processesserings laboratorium, har vi opnået en rekord-høj effektivitet for CZTS-lag produceret med PLD på 5,2%. Verdensrekorden er omkring 9% for CZTS absorber lag fremstillet ved sputtering deponering. Selvom det nu er lykkedes at fremstille høj-kvalitets CZTS, er det svært ved at vurdere, hvor god vores annealing på DTU er. Men det er klart, at vores PLD precursors kan bruges til at producere "state-of-the-art" solceller. Man mangler stadig at udforske ikke-ligevægts fænomener ved PLD-processen under fremstilling af CZTS tyndfilm. Dette ville kunne gøre det muligt at deponere krystallinsk CZTS ved lave temperaturer, uden at en efterfølgende annealing kunnen være nødvendig.. De foreløbige undersøgelser har dog ikke været særlig lovende, og den største udfordring kan være at droplets, mikrometer store partikler fra target, ikke har tilstrækkelig termisk energi til at dissociere og smelte sammen med absorberlaget. Dette felt bærer præg af "læring ved handling". Resultater fra andre grupper er ofte meget afhængige af den opstilling, der er brugt! Vælg referencerne med omhu. Kommer der en artikel om en fungerende solcelle fra en gruppe der aldrig før har produceret en celle, er der oftest ingen grund til at læse den (og til denne gruppe hører de fleste artikler).

Introduction

0.2 The CHALSOL project

In 2013 our group received a Danish grant of 16 MDKK (2 M €) to start working on earth abundant and non-toxic materials for solar cells. The choice was specifically on CZTS (Cu_2SnZnS_4), a direct band-gap semiconductor with high absorption coefficient in the visible range. Many groups were already working on this technology, and many more have joined the community in these last 3 years. Back in 2013 the record was IBM 8.4%[8], a record which has lasted until 2015, when researchers form Toyota brought it up to 8.8%[9]. My part in the research project was to exploit Pulsed Laser Deposition for the production of the CZTS absorber layer for solar cells. Indeed, among the many groups that were already working on this material, none of them was using PLD. After 3 years I now hope to have set some reasonable bounds on what PLD can and cannot do with regards to CZTS (in particular) and solar cells (in general). About a dozen people have been involved into the project, some directly part of our *Optical Microsensors and Micromaterials* group at DTU Fotonik and others from DTU Nanotech and DTU Energy, with whom we are collaborating. At the time of starting the project none of us had experience in making solar cells, nor a facility was dedicated to this project. The first thing we had to tackle was assembling our own labs, designing a furnace for the annealing, setting up a chemistry lab for the chemical bath deposition of the buffer layers and all the things that one needs to set up before making the first solar cell. This preparatory phase took a long while and is the result of combined efforts, discussions, trials and errors and perhaps some good ideas as well. Our first working solar cell came after more than 2 years from the start of the project.

Structure of the project

All the work discussed here was carried out between DTU Fotonik (Risø Campus) and DTU Nanotech (Lyngby Campus). At Risø Campus we had the

equipment for the production of CZTS thin films with two different methods: Pulsed Laser Deposition (PLD) and Wet Chemistry (WC). After the samples were fabricated, either with PLD or WC, we would send them to our colleague Andrea Crovetto at DTU Nanotech to carry out the characterizations needed (SEM, PL, Raman). Unfortunately the two campuses are more than 40 km away from each other, and there is no internal mailing service: often times the exchange of samples and analysis suffered delays from this separation.

Fabrication at Risø

The following equipment for the fabrication of the solar cell is at Risø Campus: PLD chamber for CZTS precursors, sulfurization furnace, fumehood for Chemical Bath Deposition (CBD) of the CdS buffer layer and sputtering chamber for the deposition of the ZnO:Al Transparent Conductive Oxide (TCO). In Figure 2, Risø Campus (left) and a sketch of the PLD setup (right) are shown. The PLD chamber is equipped with a Lambda Physics LPX 248 nm excimer laser (KrF) and can reach a vacuum level of $1 * 10^{-7}$mbar. The chamber is very simple, it can only host one target and substrate at a time. The substrate holder can be heated up to 800°C via resistive heating. There is no fast entry for handling substrates and targets, so the maximum production rate is one or two samples/day. Typical sample size for such PLD equipment is 5×5 mm^2. Unfortunately, this chamber was not fully dedicated to this project, but shared with another group that used it for depositing thin films of doped zinc oxide materials. For one year (all 2015) we have shared the use of the chamber, switching between the two groups every second week. Special care to avoid contamination was taken every time we exchanged the chamber by doing a bake-out at more than 100°C for several hours. In Figure 3 is shown the home made furnace we built for the annealing step.

Another PLD setup is also available at Risø, a solid state Nd::YAG laser working at 355 nm coupled to a vacuum chamber that reaches a vacuum level of $1 * 10^{-6} mbar$. A comparison between the performance of these two PLD system is given in Section 5.1. After depositing the films with PLD, their atomic composition is quickly characterized with Electron Dispersive x-ray (EDX) analysis. This was done with a Hitachi Tabletop Microscope TM 3000. The max magnification of this microscope is × 30k, which makes it not suitable for imaging features of less than 1 micron. After measuring the EDX spectrum, the samples are placed in the furnace for the sulfurization treatment3, which we have appositely designed for this project. The furnace consists of a 70 cm long quartz tube with 10 cm diameter, which can be evacuated down to $1 * 10^{-4} mbar$ through a pumping system and then sealed

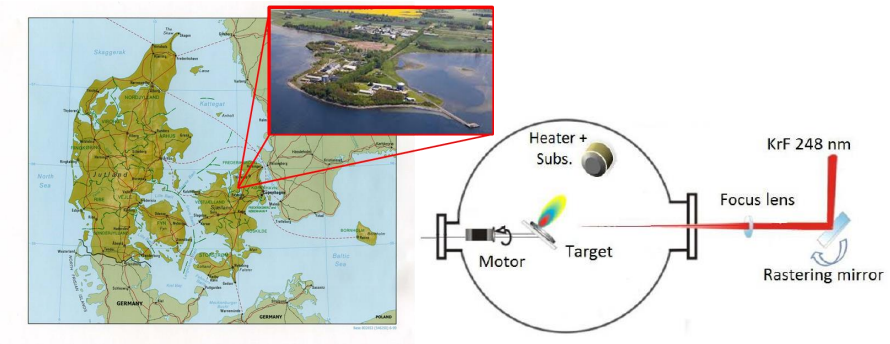

Figure 2: Left: Risø Campus, Frederiksborgvej 399, 4000 Roskilde, (DK). Right: Sketch of PLD chamber at Risø Campus.

and filled with nitrogen gas. The samples are placed in the hot zone inside a home-made graphite box together with sulfur powder. The maximum heating rate attainable with this furnace is around 800C/hr and no active cooling is present. More details on the furnace and on the annealing step are given in Figure 3.
After the annealing step, the solar cell can be completed right away by Andrea Crovetto, who set up in an adjacent room the equipment for chemical bath deposition of the CdS buffer layer and sputtering deposition of the i-ZnO and Al:ZnO layers. For details about these two last layers the reader is referred to his thesis.
Last, at Risø we could also use a Bruker D8 powder diffractometer to measure the x-ray diffraction pattern of our films.

Characterization in Lyngby

Although I did not do myself the characterizations, as the equipment is part of DTU Nanotech - Lyngby, they are included here for completeness. They were used by Andrea Crovetto to characterize the samples coming from me, Rebecca and Sara. All the electron microscopy, Raman, and photo-luminescence measurements in this work were done by Andrea Crovetto, or any the students working with him. List of the equipments, or techniques:

- FE-SEM, Supra 60 VP, Zeiss
- Raman spectra with multiple excitation wavelengths (455, 532, and 780 nm) are measured on a DXR Raman microscope (Thermo Scientific) in backscattering configuration, with a laser power of 1.5-2 mW and a spot size of approximately $2\mu m^2$.

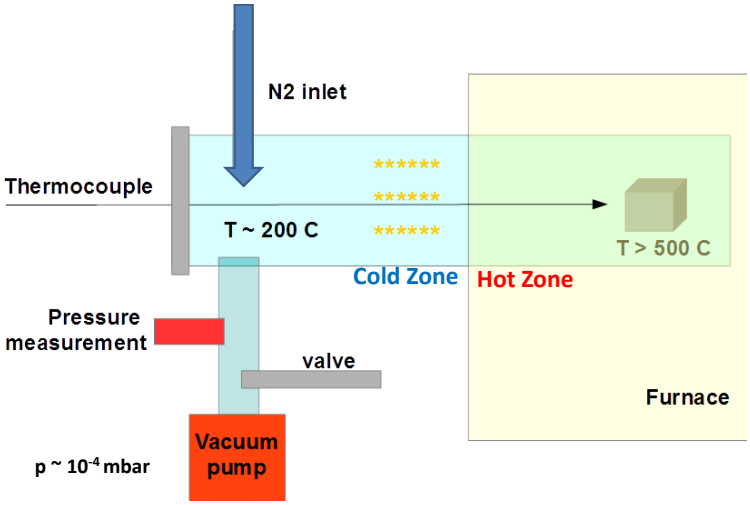

Figure 3: Schematics of our home made furnace for the annealing. The furnace is a resistive oven with maximum heating rate of 800°C/hr. Inserted in it, a quartz tube sealed at one end with a vacuum flange, which can be opened to insert the graphite box. The quartz tube is 50 cm long, has a diameter of 10 cm and is 3 mm thick. One third is inserted in the hot zone of the furnace. In the cold zone sulfur vapour condenses on the walls. A pressure gauge and a N_2 inlet are connected to the vacuum flange at the other end. The temperature is measured by means of a thermocouple placed inside the hot zone of furnace but outside of the quartz tube, to avoid corrosion and contaminations during the sulfurization process. From our calibrations with a thermocouple inside the quartz tube, we have seen a difference of less then ±5°C between the two values *Working procedure*: After the samples and the graphite box are put in place, the quartz thube is sealed and the system is evacuated down to 10^{-4}mbar. The valve is then closed and N_2 gas is purged into the chamber to obtain a static atmosphere of 100 mbar p_{N2}. The heat treatment is then started (ramp rate: 600°C/hr, setpoint temperature: 560°, annealing time: 5 min, natural cool off). During the heating stage the pressure inside the furnace raises up to 350 mbar. The natural cooling from 560° to 400° takes only few minutes, from then on more than 8hrs to a complete cool down at room temperature. The pressure at the end of the cycle was exactly the same as at the beginning.

- Steady-state photoluminescence (PL) spectra were measured with an Accent RPM2000 system at an excitation wavelength of 532 nm and power density 50-100 mW/cm^2. PL mapping measured with a CCD detector camera.

- JV curves were measured with 1 sun illumination (1000 W/m^2, AM1.5G) using a Newport Oriel 92190 large-area Xe light source and a Keithley 2400 source meter. Setup calibrated with reference Si solar cell (Newport)

0.3 CZTS material

0.3.1 Motivations to CZTS

The two leading Thin-Film Photovoltaic (TFPV) technologies, CIGS and CdTe, have been consistently improved during the last decades and have now demonstrated lab. cell efficiency above 22% and commercial module efficiency above 16%. TF-PV technologies have a key advantage on silicon PV in terms of energy pay-back time (EPBT), material utilization (g/kWatt) and higher efficiency at high temperatures and illumination conditions[10, 11]. Indeed, to date the largest utility-scale PV plants all rely on CdTe modules[3]. New applications on light-weight and flexible substrates are also envisaged. So, how is it possible that the total market share of TF-PV is still below 10% of the total PV market[10], and why are there serious doubts whether they will ever play a significant role in the global energy market? The reasons lie in the scarcity and toxicity of their constituents In, Cd, and Te, as can be seen in Figure 4. In Japan, for instance, the sale of CdTe solar panels is already forbidden by law due to toxicity of Cd. Indium is expected to limit CIGSe production to between 20 and 100 GWp/year [12]. The low annual production of tellurium (250–300 t/year) will limit CdTe module production to 4–5 GWp/year [13]. Thus, despite many advantages of thin-film technologies in terms of material utilization and EPBT, we are still lacking a champion material for large scale deployment.
To this end, CZTS has received a lot of attention, due to its earth-abundant and non-toxic constituents. It is a direct bandgap semiconductor with optimal gap of 1.5 eV, which gives it a theoretical conversion efficiency limit above 30%. Due to its direct bandgap, the absorption coefficient is very high, ($> 10^5 \mathrm{cm}^{-1}$), so that a thin layer of less than 2μm is enough to absorb all the incident sunlight.

Another aspect which makes CZTS appealing is the fact that it is a very similar material to the well-established $CuIn_xGa_{1-x}Se_2$ (CIGS). It is believed that a good deal of "CIGS know-how" can be directly transferred to CZTS technology, making the steps towards commercialization faster and cheaper. Indeed, most of the research on CZTS so far has made use of the CIGS solar cell architecture and fabrication methods with discrete success. Furthermore, similarly to CIGS, the bandagp of the absorber layer can be tuned across the optimal range 1.0-1.5 eV for PV devices by alloying sulfur with selenium.
In Section 0.3.3 the technical advantages of using Se or a S-Se mix are discussed. From the standpoint of device fabrication there is no doubt that

[3]https://en.wikipedia.org/wiki/List_of_photovoltaic_power_stations
https://en.wikipedia.org/wiki/Topaz_Solar_Farm

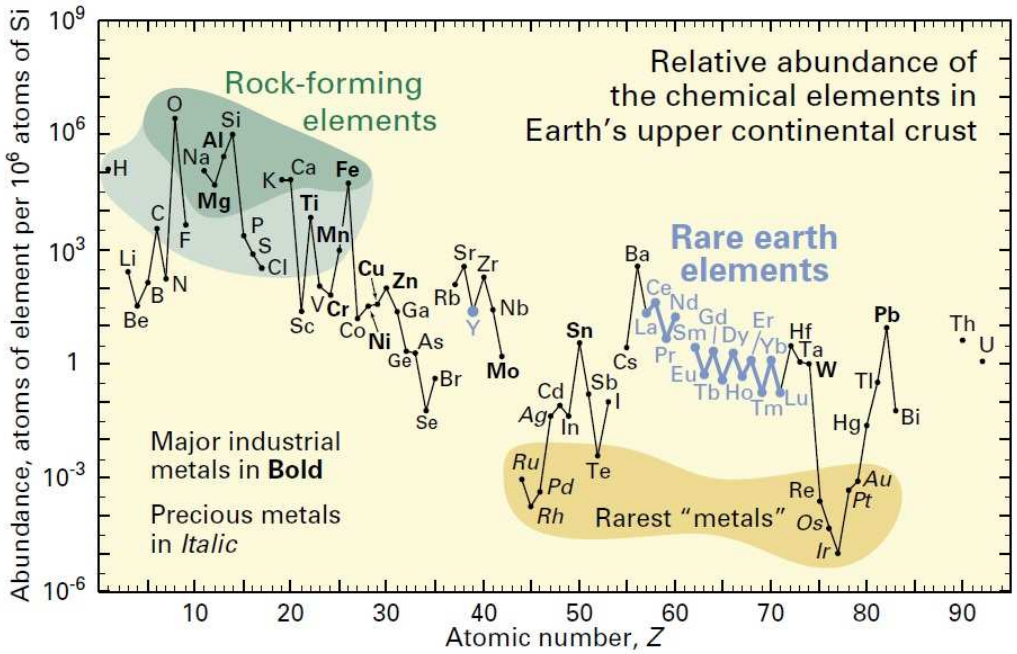

Figure 4: Abundance (atomic fraction) of the chemical elements in Earth's upper continental crust as a function of atomic number. (1) rock-forming elements (major elements in green field and minor elements in light green field); (2) rare earth elements (lanthanides, La–Lu, and Y; labeled in blue); (3) major industrial metals (global production ¿∼3×107 kg/year; labeled in bold); (4) precious metals (italic); and (5) the nine rarest "metals"—the six platinum group elements plus Au, Re, and Te (a metalloid). This plot is from a report of the U.S. geological associaition[14].

using a S-Se alloy gives better efficiencies and more reproducible results. However, despite the -*even greater*- technical hurdles, I very much favour the pure sulfide "high bandgap" CZTS, and in general high bandgap materials for TF-PV.
The two following economical reasons stems for this instance:

- High bandgap absorbers can potentially be integrated in a tandem structure with silicon, driving down the costs[4] much more than what any advance in a single junction PV technology can do.

- The US Dept. of Energy (through the Sun Shot Initiative) is clearly moving towards large scale PV systems, where PV is already competitive with other traditional technologies (gas and oil) and cost reduction as result of technical advance or simply by industrial up-scaling is predicted to be more effective. These utility scale PV systems are realized

[4]Levelized Cost of Energy (LCOE), in $\$/\mathrm{kW}_p$.

in areas of high illumination, where "high bandgap" (1.5 eV) devices are significantly more efficient than "low badgap" devices (1 eV or below).

0.3.2 A complicated material

However, for how ideal the bandgap of a semiconductor can be, it is definitively not the only parameter that turns "a possible candidate" into a "good candidate".

It's actually a pn junction

First of all, the elementary building block that defines a solar cell is more properly the pn junction, rather than just the absorber layer itself. This is especially true in TF-PV, where doping is generally intrinsic. This means that, *e.g.*, for a good p-type absorber layer, one must find a suitable n-type layer (or combination of layers) to complete the junction and make the solar cell. This n layer(s) must generally satisfy at least these requirements:

- Good lattice matching, to reduce interface recombination.
- Favourable band alignment, to allow for selective charge carriers collection.
- Be producible at conditions that do not alter the layer underneath.

An extremely good quality absorber layer can give a 0% efficiency solar cell if the pn junction is not well behaved. As can be imagined, finding such n-layer(s) for a completely new materials is not trivial and the search can take a very long time. Luckily for CZTS, it has a very similar lattice and band structures to CIGS, which makes it partly possible (further details in Section 0.3.5), to borrow the architecture of CIGS devices:
Mo/(p-type absorber)/CdS/ZnO/Al:ZnO. Thus, here I would make the first point which makes it challenging to understand this material:

- A good deal of information on CZTS actually comes from the full solar cell device (*e.g.* the bandgap is commonly extracted from the EQE), which is ultimately a pn junction and where also the other layers play an important role. Particularly critical is the junction with the CdS buffer layer, which is not completely understood. Furthermore, the CdS intrinsic doping is not easily measurable and it is probably system dependent. Some information can be retrieved from the CZTS layer alone (*i.e.* before device integration), but one must always keep

in mind that interface physics may well modify the properties that were measured prior to device fabrication. A bright PL spectrum on a bare CZTS layer can be reduced by non-radiative recombinations after CdS deposition.

Narrow phase diagram, disordered, off-stoichiometric poli-crystalline material

Even to study the bare CZTS absorber layer is, however, difficult. Very briefly, the properties of the poly-crystalline CZTS thin films (as used for making solar cells) are very far from those of a perfect crystal and depend also on the fabrication method. Results from different groups can only be compared with wariness.
As a matter of fact, precursors made with the exact stoichiometry of CZTS do not give good absorbers after the annealing, not even when loss of volatile S and SnS are compensated during the annealing. What is found experimentally is that Cu-poor and Zn-rich precursors give the best absorber layers [15]. This seems to contrast with the fact that the equilibrium thermodynamics predicts a narrow region of existence for CZTS in the compositional phase diagram [16], suggesting that deviations from stoichiometry would rather form secondary phases than a non-stoichiometric pure phase. Which secondary phases will occur depends on the structure and composition of the precursors and on the annealing procedure. Unfortunately, the most common secondary phases, ZnS and Cu_2SnS_3, cannot be detected with standard XRD and Raman investigations. As a consequence, it is always difficult to understand if the material/device properties described in one study are related to a pure phase CZTS material or to a mixture of CZTS and other secondary phases. Since the ultimate challenge is to assess the real potential of CZTS as absorber material for p-type absorbers, it would be very important to fabricate a phase pure CZTS thin-film. Deviations from exact stoichiometry can also result in defects in the lattice structure, instead of secondary phases. In this respect, a number of theoretical calculations based on Density Functional Theory (DFT) give some hints into which defects are more energetically favourable and which ones should be mostly avoided. In [17], a very concise plot, shown here in Figure 5, summarizes the main defects found for CZTS material.

The most detrimental are those located deep in the bandgap: V_S and Sn-related defects. Not all of them have the same formation energy, so they are not equally probable. V_{Cu} and Cu_{Zn}, which have a relatively low formation energy (below 0.3 eV) and which constitute shallow acceptor defects are responsible for the p-type conductivity of CZTS. Cu_{Zn} acceptor defect

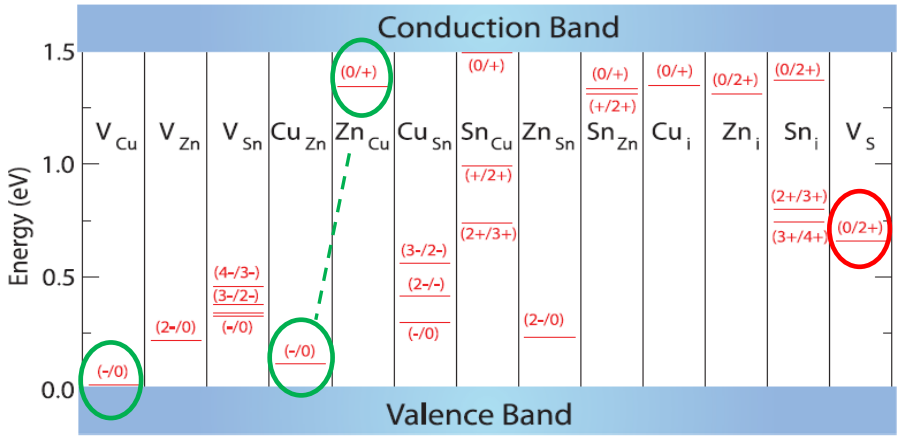

Figure 5: The ionization levels of intrinsic defects in the bandgap of Cu_2ZnSnS_4. The copper vacancy (green circle) results in a shallow acceptor level just above the valence band, while the Cu-on-Zn antisite (green circles) results in a level 0.12 eV higher in energy. The detrimental V_S is marked with a red circle. Figure from [17].

can be compensated by the shallow donor Zn_{Cu}, to give the compensated pair (Cu_{Zn} + Zn_{Cu}). The effect of this Cu-Zn disorder on the electrical and optical properties of CZTS is not fully understood and "ordered" CZTS absorbers do not give better efficiencies than "disordered" CZTS absorbers, even though a change in the band-gap in the ordered-disordered transition has been documented[18, 19].
Intermezzo: Could the V_{Cu} explain the Cu-poor stoichiometry of good absorbers? Likely not: the *p*-type conductivity in CZTS is usually associated to a charge carrier density of 10^{16}carriers/cm^3, while Cu-poor compositions (solid state density $\sim 10^{22}$atoms/cm^3) are of the order of 1.6<Cu/(Zn+Sn)<1.9, a difference of about four order of magnitudes.
Sulfur vacancies and Sn-interstitials are associated with higher formation energies (particularly relevant here: V_S has a formation energy between 0.9 and 2.5 eV [20]), thus their formation should be less likely to happen. However, the formation energy is calculated for bulk materials, while our material is a poly-crystalline film which experience sulfur evaporation from the top surface during annealing. Even without equations, recalling that sulfur atoms are the backbone of the CZTS lattice, it is easy to see why a - non compensated - sulfur loss results in a deep defect level V_S or in decomposition of CZTS into secondary phases, according to Equation 1.

To make this paragraph somewhat different from just a "homework-for-the-introduction-of-my-PhD-thesis", I would like to take few lines to tell how I

tried, perhaps naively, to render DFT into experimental practice. The prescription is clear: must avoid V_S.
The first graphite box we designed for the annealing had a thin lid for closing. In order to increase the partial pressure of sulfur during the annealing, I made a second one with a thicker lid. I have no clue if that had any effect or not. People at a conference told me they use screws to enhance the lid "sealing" effect. Due to the high reactivity of sulfur with metals, I am not very keen on this solution that may cause unknown contaminations.
Further, for my first annealing experiments I used 200 mg of sulfur powder in a graphite box that was less than 10 cm^3. Exfoliation of the films after the annealing was dramatic and we could not make films thicker than 500 nm. Eventually, I am now using 100 mg of sulfur pellets, and films up to 700nm thickness can be fabricated. Reducing the amount of sulfur was found beneficial to exfoliation. The use of sulfur pellets instead of powder should increase the time it takes to evaporate the material, since evaporation scales with exposed surface. I cannot quantify the time gained in this way, but I always used the shortest annealing time I could obtain in our setup: 5 mins (which is the time the oven takes to ramp up the last 10°C without overshooting). After the annealing no sulfur is left in the box, the annealing time is already much longer than what it takes for evaporating sulfur.

0.3.3 Alloying S with Se

The majority of the CZTS devices are actually done with absorbers whose chalcogenide elements are a mixture of sulfur and selenium. In this case the record efficiency reaches 12.6%[24] and experimental reproducibility is easier to achieve due to the lower volatility of the selenides Se and SnSe during the annealing [21, 22]. I will shortly discuss here the benefits and the disadvantages of alloying sulfur with selenium, and why we did not make any attempt in this direction.
Alloying sulfur with selenium is easy, since they both belong to the same group in the periodic tables, group 6 the "chalcogenides". Their electronic configuration in the outer shells is $(...)2s^24p^4$, which makes them suitable for tetrahedral coordination. The chalcogenide elements are oxygen, sulfur, selenium and tellurium. Oxigen is sometimes not included in the group for its very unique importance on its own. In the case of CZTS, it is found that alloying S with Se allows one to tune the bandgap across the whole optimal range for PV devices, where the pure selenide CZTSe has a bandgap of 1.0 eV and the pure sulfide CZTS of 1.5 eV [23]. It is generally observed that Se rich compositions give the best solar cell efficiencies. Indeed, the record efficiency is currently achieved with a CZTSSe device of 1.12 eV bandgap [24].

The addition of selenium has many beneficial advantages to device stability and reproducibility [23].

First, sulfur vacancies (V_S) are more likely to happen than selenium vacanciesV_{Se}, due to higher volatility of sulfur. V_S introduces a very deep defect inside the electronic bandstructure [20], affecting negatively the V_{oc} of the device. Further, donor and acceptor defects (Cu_{Zn} and Zn_{Cu} antisites, Cu vacancies) are predicted to introduce shallower energy levels in the selenide phase compared to the sulfide[20, 26]. As a result, bandgap fluctuations resulting from the local electric field generated by the ionic cation sites are also reduced, with again a lesser impact on the final V_{oc} of the device. The sulfide compound also exhibits larger electron effective masses and a smaller dielectric constant compared to the selenide [27], which means reduced screening effect of charged point defects and smaller mobility.

Lowering the bandgap by adding selenium gives the possibility to find the best band alignment between the absorber and the buffer layer, which is optimal when the bandgap of the p-type absorber layer is around 1.2 eV[5]. This is analogous the case for CIGS technology [28], where the bandgap can be varied in the interval from 1 to 1.5 eV by alloying In and Ga. A non-optimal band alignment at the junction implies that at the CZTS/CdS there can be a spike in the conduction band which constitutes a barrier to the flow of minority carriers from the CZTS to the CdS layer. Or that the junction is not fully effective in preventing majority carriers (holes) from moving across the junction, which results in a recombination current that again lowers the V_{oc}. There is no agreement in literature on the nature of the conduction band alignment at the CdS interface.
The last factor which greatly benefits from using a S-Se alloy is the back contact decomposition $Mo + S(e) \rightarrow MoS(e)$[29], which gets much worse for sulfides: pure sulfide CZTS cannot be fabricated with a thickness of more than 800 nm due to severe exfoliation problems, while CZTSSe and CZTSe can be fabricated with any thickness up to 2000 nm and no exfoliation is reported. Moreover, the MoS(e) thin layer at the back contact is affects the junction, making the back contact non-ohmic [41].

So, why are we even discussing if adding selenium or not? There are

[5]The band alignment does not depend only on the badgap, but also (among many others) on the nature of the orbitals originating the valence/conduction band and the position of Fermi energy level, and in this sense CZTS and CIGS are very similar materials. Very notable counter-example: CdTe solar cells (1.45 eV bandgap) also make use of a CdS buffer layer and no such problems with the band alignment are reported

two major drawbacks of using selenium, none of which is related to -*strictly speaking*- technical reasons. First, toxicity and non-abundance of selenium can pose a problem to up-scaling. In Japan the use of Se based technologies is already forbidden by law. Second, "high bandgap" (1.5 eV) solar cells like CdTe outperform silicon technology under high sunlight illumination and high temperatures, as was discussed previously in Section 0.3.1.

0.3.4 Toxic and non-abundant device

Two aspects should not be overlooked when talking too much about non-toxic earth-abundant material for solar cells. The CZTS absorber layer is not the only constituent of the solar cell. Secondly, its fabrication processing may very well make use of toxic substances.

If we consider the CZTS device as a whole, problems may arise from the use of toxic and not-abundant Cd in the buffer layer. To date the best devices are making use of a 60 nm thick CdS or $Zn_{0.35}Cd_{0.65}S$ buffer layer[30]. In_3S_2 was also found to give good efficiency devices[35, 36], but again it is made of both toxic (Cd) and rare (In) materials. Research is moving towards finding alternative buffer layers, especially in the case of pure sulfide CZTS, where it is likely that CdS does not even provide the best band-alignment [31]. In this direction, Zn(O,S) buffer layers would be natural candidates, since they are already successfully implemented in CIGS devices.
For the fabrication process on the other hand, many groups use the highly toxic H_2S gas during the high temperature sulfurization treatment. There are two key reasons for preferring the use of H_2S gas instead of dropping "some" sulfur powder into a "closed" graphite box. The first one is that hydrogen is well know for passivating vacancies, and the second one is that H_2S gas provides a highly controllable, uniform and reactive source of S atoms, which is otherwise more difficult to obtain when one is just evaporating sulfur powder, as discussed in Section0.3.5. In the Conclusions I state the reasons why I do not think we should worry too much about the issue of using toxic H_2S gas, especially when doing research.

0.3.5 Open problems with CZTS

There are several problems that need to be solved before the CZTS technology can be of any practical use. They can be presented under three, interrelated, categories:

- Low open circuit voltage.

- Reproducibility of the results.
- Mechanical stability.

Low V_{oc}

One cannot write a PhD thesis without a paragraph dedicated to the "low open circuit Voltage", which is unanimously recognized as the number one problem in this technology. A detailed break-down analysis of the loss factors in CZTSSe and CZTS devices is given in[33, 34]. In the Shockley Queisser (SQ) limit [32] (ideal solar cell) the limiting values of the diode parameters V_{oc}, J_{sc}, FF, and J_0 are only a function of the energy bandgap of the absorber. A more realistic model takes into account optical losses due to the top contacts and absorption in the TCO. Optical losses only affect the absolute value of the short circuit current J_{sc}, which is reduced by about 15% with respect to its SQ limit. If we compare state of the art CZTS and CZTSSe devices with state of the art CIGS devices we see that the photo-current collection is already at a level comparable with the best CIGS devices with similar bandgap and is comparable with the SQ limiting value corrected for optical losses.

Device	bandgap eV	eff. %	V_{oc} meV	J_{sc} mA/cm^2	FF %	J_0 mA/cm^2	R_{Sh} Ωcm^2
$SQ_{1.5}$	1.5	32 (27)	1210	30 (25)	90	10^{-20}	
Toyota	na	8.8	710	17.5*	71	na	1300
IBM	1.45	8.4	662	19.5	65.8	na	na
DTU	1.53	5.2	616	17.6	47.9	5*10^{-5}	1500
$SQ_{1.2}$	1.15	33 (28)	900	43 (36.5)	88		
IBM_{CZTSSe}	1.17	12.6	513.4	35.2	69.8	7*10^{-5}	
ZSW_{CIGS}	1.14	20.3	730	35.7	69.8	4*10^{-8}	

Table 1: Device parameters of the best pure-sulfide CZTS solar cells and of the device presented in this work. Data from[9, 8, 24], SQ limiting values from [25]. Between parenthesis the values after 15% optical losses as in [33], (*) indicates no anti-reflection coating.

On the other hand, the V_{oc}, FF and J_0 are well below their limiting value and there exist a clear relation with the bandgap (again similar to what found for CIGS), where devices with low bandgap (1.1-1.2 eV) are generally characterized by better diode parameters. The situation worsen by increasing the bandgap (*i.e.* the amount of sulfur) and gets at its worst for the pure sulfide CZTS. The low V_{oc}, FF and J_0 are all, to a first approximation, due to recombination of the charge carriers. Without going further into details, (at least)

one experimental finding marks the difference between CZTS (and CZTSSe) and well behaved absorbers [33]: at very low temperatures the V_{oc} does not approach the bandgap value, as it does for CIGS and CdTe. There are two major suspects to blame for this shortfall: (1) the CdS hetero-junction and (2) defects in the absorber layer. Regarding the pure sulfide CZTS, there are indications [33] that the heterojunction with CdS is characterized by a "cliff like" bending of the CZTS conduction band, which would result in lowering the effective bandgap of the device. This problem can be tackled directly by investigating alternative buffer layers (and/or overall junctions) and some encouraging results have recently appeared [9, 30, 31]. Regarding (2), it is not even yet understood which defects play a major role. It could be bandgap fluctuations due to the disordered structure of the kesterite phase, point-like defects like V_S, or micro domains of secondary phases(ZnS, SnS?) responsible for enhanced recombination.

Reproducibility of the results

There are two kinds of reproducibility issues that one is confronted with. The first one is reproducibility of results by independent laboratories. It is related to the fact that the fabrication process (deposition technique, structure of the precursors and annealing strategy) is closely connected to the quality of the CZTS and the final efficiency of the device. Unfortunately there are no standard procedures, and what can be best for one group might not work for another one. The etching of the CZTS before depositing the CdS buffer layer is one good example of this, where each group has developed their own best strategy. Few facts have been universally acknowledged: Cu-poor Zn-rich composition is beneficial for making good solar cells, CdS is (up to now) the best choice for buffer layer and the best annealing temperatures are in the range 540-580 C.
The second issue is reproducibility of the results within the same group itself[6]. Even the best laboratories are struggling with this issue, having a rate of reproducibility of their best results below 20%[7]. The variation in the efficiency can be dramatic even in the same batch of samples, from 8% to less than 1%. To my understanding there are two main reasons why this is so: inability to reproduce the same stoichiometry in the precursors, especially for vacuum techniques, and reproducibility of the annealing conditions, especially if using S powders or pellets, as discussed in 0.3.4.

[6]This fact is hardly mentioned in scientific literature, however it was acknowledged by all the people to whom we have talked to at conferences, meetings and symposia.

[7]Toyota labs, private communications.

Exfoliation and vacuum instability

CZTS at standard annealing temperatures 540-580 °C is not stable and can decompose via S and SnS evaporation [40, 21, 22] and secondary phases can segregate at the back contact due to reactions with the Mo layer[29]. The reaction of S and SnS evaporation is described in [40, 21, 22] and reads as follow:

$$Cu_2ZnSnS_4(s) \leftrightarrows Cu_2S(s) + ZnS(s) + SnS(s) + \frac{1}{2}S_2(g) \quad (1)$$

$$SnS(s) \leftrightarrow SnS(g) \quad (2)$$

where (s) and (g) denote the solid or gas state of the various compounds. Arrows in eq.1 and 2 indicate that the reactions would be reversible in presence of saturated SnS and S_2 atmosphere. The rate at which reactions 1 and 2 occur depends on ambient gas composition, pressure and temperature.
The condition of saturated atmosphere, which prevents decomposition reactions, is difficult to realize experimentally at standard annealing conditions, due to the very high partial pressure of S_2 required at T>500 C. Indeed, the high temperature annealing usually lasts for a max of 10-20 minutes. The reason is that sulfur is not a gas at the standard RTP conditions and needs to be evaporated from the solid phase. While it is true that sulfur is very volatile, it is also true that its most stable molecular form at typical annealing conditions is an octagonal ring molecule, which lowers its reactivity with the CZTS film. We recall from previous paragraph that sulfur vacancies are very bad for the electronic properties of the CZTS solar cell.

0.4 Pulsed Laser Deposition

In this section I will introduce the technique of Pulsed Laser Deposition, stressing out its unique features as thin film fabrication technique. It is beyond the scope of the present thesis to include a comprehensive review about PLD, and there are very good references available, for example[42, 43, 44]. My aim is just to touch those features of PLD that can be exploited to address the "Open problems with CZTS" listed in 0.3.5. The topic "PLD of metals" is deferred to next chapter.

Pulsed Laser Deposition is a non-equilibrium deposition technique where high power laser pulses are focused onto a solid state target placed in a vacuum chamber. When the laser beam hits the target the phenomenon of laser ablation occurs: the photons (generally nanosecond UV pulses) are absorbed

by the target material via instantaneous photon-electron interactions. The exited electrons then quickly (few ps) release energy to the lattice via phonon scattering and the material eventually vaporizes in the form of a partly ionized plasma. The material-laser interaction is very complex and a rigorous theory of plasma formation is not given [45, 49], but definitively it is not a simple evaporation process. Indeed, the effective temperature of the plasma can be much higher than the boiling point of the target and is usually in the range of 1 to 100 eV, depending on the laser energy density and interaction parameters. Once formed, the plasma expands from the target in the forward direction and reaches the substrate where it is deposited in form of a thin film. The high kinetic energy of the atoms arriving to the substrate can have many positive effects on the structure of the growing film and this makes PLD a "non-equilibrium" technique.

0.4.1 Unique features of PLD

The story of PLD begun in the late 80's. The first ground-breaking result was demonstrated in 1987 by Venkatesan and co-workers [50] at IBM labs, where they managed to deposit thin films of the high temperature superconductor $YBa_2Cu_3O_{7-x}$ (YBCO). Due to its complex stoichiometry, the only other techniques capable of producing such material as thin film were MBE and sputtering, but the fabrication process was slower and less controllable [42]. On the other hand, PLD provided an easy tool to transfer in just one step the complex stoichiometry of YBCO from a solid target to the thin film. This paper is very important in the history of PLD, and a thorough discussion in relation to this work will be given in Section 2.1.
Two years later, in 1989, another key feature of PLD was pointed out by Sankur et al.[51], who demonstrated that Ge homo-epitaxial growth at a substrate temperature of 300°C, while temperatures in excess of 700°C are required for thermal growth techniques (MBE in this case). The difference resides in the kinetic energy of the atoms and ions arriving at the substrate. In the case of MBE, atoms have a Maxwellian kinetic energy distribution peaked at the temperature at which evaporation occurs, range 0.1-03 eV $(1 - 3 * 10^3 K$). In the case of PLD, atoms arriving on the substrate have a (non-Maxwellian) kinetic energy distribution in the range 1 to 10 eV, which makes them reactive when they land on the substrate. Thus, even with modest substrate heating, incoming atoms posses enough kinetic energy to overcome activation barriers stemming against crystal growth.
In year 2000 Willmott et al. [52], demonstrated heteroepitaxial growth of the lasing garnet $Gd_6Sc_2Ga_6O_{12}$ doped with Nd and Cr (Nd,Cr:GSGG) on Si(001). This material contains 160 atoms per unit cell and has a very com-

plex stoichiometry with six different elements. In the words of the authors:*"It seems most improbable that this thin film system could have been synthesized using any thermal methods"* [42].
Along with the ability to realize epitaxial growth onto a crystalline substrate, PLD has proven the ability to create sharp, atomically flat interfaces between two adjacent layers. One famous application of this is the realization of a high mobility 2D electron gas at the interface of two perovskite oxides $LaAlO_3/SrTiO_3$[53]. In order to realize atomic flat heterojunction, the pulsed nature of the deposition flux and the stoichiometric transfer are essential. In[53], the chamber is equipped with a multiple target holder and a RHEED detector. The RHEED detector allows real time monitoring of the film growth with atomic layer sensitivity. When one film has grown to the desired structure, *e.g.* 15 complete unit cells, the laser is stopped and the deposition flux ceases immediately. This can be so due to the fact that the material deposited per pulse is less than 0.1 mono-layer/pulse. If mechanical shutters were used to stop a molecular beam or a sputtered continuous flux no such level of control could be achieved. The second layer can thus be deposited onto an atomic flat surface right away in the same deposition run.
Lastly, and of minor scientific impact (although perhaps most relevant for this work), PLD has proven to be an easy-to-operate and a successful tool for growing amorphous materials and super-saturated metallic alloys [54] with composition far from what is allowed by equilibrium thermodynamics. The strength of PLD in this latter case is the mechanism of adsorption and deposition of the incoming atoms. Due to the high kinetic energy, the species are highly insensitive to surface chemistry and the sticking coefficient is close to unity.
In summary, the key features of PLD which will be later discussed in this work are:

- Stoichiometric transfer from target to thin film.
- Enhanced crystal growth even at modest substrate temperatures.
- Amorphous films with homogeneous composition and structure.

It must be very clear that none of these points necessarily holds true *per se'*, they must be verified for each system case by case.

0.4.2 Open problems with PLD

Of course, any deposition technique has its advantages as well as its drawbacks. In the case of PLD one can face three major problems: molten droplets

ejected from the target along with ablated material, lack of uniformity of deposited films and coating of the laser viewport, which hinders the stability of the ablation process. Here follows a quick overview from state-of-the-art PLD literature. In Section 5.4 I will recall these points one by one in relation to this work.

Droplets

Droplets are molten particulates in the micrometer size range which are ejected from the target during the ablation process. Not all the target materials produce droplets, for example high melting point oxide materials generally withstand well the fast heating driven by the laser pulse [58, 59]. On the other hand, materials with high thermal conductivity, like metals, and(or) low melting point are likely to produce droplets. Tin, with a very low melting point at 230 °C is one such material [56, 1]. Targets made from sintered powders usually produce more droplets than single crystal targets. Target roughening, a consequence of the melting and re-solidifying process, is also responsible for droplet ejection, as loose ends or lumps of material can get easily detached before the full vaporization. For this reason, it is generally a good practice to make use of ablation parameters that reduce target modification: large beam spot and uniform rastering [60]. The CZTS target modifications are discussed in Chapter 5. One more possible cause of droplet formation is subsurface boiling, which can happen when the incident light penetrates well below the surface of the target material. For this reason shorter wavelength UV lasers and denser targets are preferred in PLD, since the absorption length is usually very small. Furthermore, the more the optical energy is confined near to the target surface, the more efficient is the ablation process, with less energy dissipated as heat.

Small area coverage

As recalled, material transfer in PLD is a consequence of plasma plume expansion, which originates from the small area of the laser spot and is narrowly peaked in the forward direction. Some hydrodynamical models describe this mechanism [46, 47, 48], the general conclusion is that the material is ejected with a super-cosine distribution $\propto \cos^n\theta$, $4 < n < 20$. This makes the thickness profile of the deposited film uniform over a length-scale comparable with the size of plume and the laser rastering area, typically no more than 1 cm^2 for a common 2" inch. diameter target. The only two options to increase the area of the deposited films is (1) to move and rotate the substrate or (2) to use high pressure background gas, which has the effect of increasing the

angular distribution of the plume[47]. In the first case the deposition time increases linearly with the size of the substrate and a specific equipment is needed, in the second case the non-thermal properties of the deposition flux are highly reduced by scattering events. Rastering the laser over a bigger target of, say, 10 cm^2, is not commonly possible, since the beam focusing cannot be kept constant over such large area[8].

Window coating

Controlling the laser fluence is of paramount importance to control film properties. Atomic composition, crystalline structure and atomic point defects have all been shown to be primarily sensitive to the laser fluence [61, 62], to give few examples. In particular, in [61] a change in the laser fluence from 0.3 to 0.4 J/cm^2 is shown to lead to significant changes in the structural and electrical properties of the films. While it is very easy to control the energy released by the laser, coating of the viewport can make the effective fluence on the target difficult to control. Absorption of radiation due to window coating can get as high as 70%[63]. This issue, which is very detrimental for PLD of CZTS, will be treated in Section 5.4.

0.5 Is PLD suitable for CZTS?

It feels natural to conclude this introduction by discussing which challenges in CZTS technology are worth exploring pursuing the strengths of PLD.
On a general sideline, it should be mentioned that the use of non-thermal deposition techniques has been suggested [38, 39] as it may avoid precipitation of thermally stable secondary phases, like ZnS, and/or it may promote Cu vacancies over Cu_{Zn} antisites, which are shallower acceptors in the energy diagram.
Let's now focus specifically on PLD. Indeed, since PLD is a non-scalable technique for PV applications, one should have clear scientific goal driving its research. Nobody can be interested in PLD of *any-kind-of-material* for solar cells if PLD does not provide any extra feature to what well established and up-scalable vacuum techniques offer.

In this sense, I see three research-lines worth pursuing:

1. Precursors made with PLD can be maximally amorphous. This feature cannot be easily achieved with sputtering or evaporation.

[8] unless the focal lens is also moved along with the rastering mirror

2. Growing CZTS crystalline films directly in vacuum at lower substrate temperature than that required by thermal growth techniques. Films produced in this way can have a different defect distribution in the electronic band-structure and do not suffer from adhesion problems.

3. PLD makes it relatively easy to incorporate doping elements in the deposited films (*if the target can be fabricated; Na-doping is a notable exception)

4. The use of any background gas is allowed in PLD in a wide pressure range from high vacuum to standard atmospheric pressures.

In this work I could explore in a -somewhat- satisfactory manner the first of these three points, mostly because the three other ones require the back up of a robust device fabrication process which we did not manage to achieve.
Regarding point N_o 2, as pointed out in Section 0.3.5, CZTS is not stable in vacuum at the high temperatures required by the annealing. Decomposition reactions are well documented both at the bottom interface and at the top surface [21, 29]. In particular, sulfurization of the Mo back contact and exfoliation of films thicker than 800 nm cannot be solved by any post annealing treatment. These problems are avoided if temperatures well below 500°C can be used for fabricating CZTS polycrystalline films. A thicker CZTS layer may enable a better collection efficiency and a pure Mo/CZTS back contact would be worthy to study, since the MoS layer in the Mo/MoS/CZTS structure makes the back contact non-ohmic[41][9]. This low temperature growth can only be achieved with a non-equilibrium growth process, such as that driven by PLD. The idea would be to deposit polycrystalline CZTS right away in the PLD chamber at substrate temperatures well below 500°C, avoiding the annealing step. Furthermore, the defect density in films grown off-equilibrium can be different from that resulting after the annealing. It is known that the thermal defect distribution in CZTS is non-optimal and that this may be the main cause for the low V_{oc} of CZTS devices, as was discussed here in Section 0.3.5.
Regarding point N_o 3, if doping atoms can be homogeneously incorporated in the target, they will be easily transferred to the growing film by the plasma plume. Indeed, the sticking coefficient of energetic particles, such as those in the plume, is close to unity, disregarding any possible surface chemistry. Clustering is also avoided, since the growing film is either amorphous or crystalline. To be very fair in the discussion, if one only wants to grow amorphous

[9]Disclaimer: it is by no means certain that a pure Mo/CZTS back contact is eventually better than the Mo/MoS/CZTS back contact, but it would be good to have an experimental insight.

or semi-amorphous X-doped CZTS precursors, sputtering deposition could provide exactly the same precursors quality. It is only in the case where crystalline films are directly grown (usually hetero-epitaxial structures) that the superior quality of PLD can be of any advantage, due to the narrow kinetic energy distribution of incoming species that distinguishes PLD from sputtering deposition. Thus, in my view, one should attempt (3) after being successful at (2).

Part I

Background work

Chapter 1

Pulsed laser deposition of Cu, Zn and Sn

All the beginnings are obscure.
Hermann Weyl

Time period: 1^{st} semester as PhD Student. Status of the project: Ground zero. My future colleagues have not been hired yet, I am getting started with the PLD technique, CZTS material and solar cell technology.

The very first idea in the project was to deposit a metallic film with the desired stoichiometry (Cu_2ZnSn) to be sulfurized in a furnace (to be set up) or using a sulfur cracker (to be bought and incorporated in the PLD chamber).
I would use three different metallic targets (Cu, Zn and Sn targets) and tune the overall composition by changing the number of pulses onto each target. By doing so, one is in principle able to make a multi-layered structure or a uniform Cu-Zn-Sn alloy, depending on how often the laser switches from one target to another. This pathway was soon abandoned after a preliminary study primarily because:

- High number of micron-sized droplets in the films
- Equipment limitations (no in-situ monitoring in the PLD chamber)
- No advantages compared to what can currently be done by sputtering or evaporation techniques.

However, the results on PLD of metallic targets were judged interesting by themselves and published in the paper "Nanosecond laser ablation and deposition of silver, copper, zinc and tin", on *Applied Physics A* [1]. The paper is enclosed in the appendix.

1.1 Why PLD of metals?

Regarding metallic films, PLD was successfully employed for the fabrication of metallic multi-layered structures and supersaturated alloys, as discussed in [64, 65, 66, 54]. Many deposition techniques are known for depositing metallic thin films, so why using PLD? A striking advantage of PLD, in this case, is the extremely sharp control over layer thickness and interface roughness, which can be both limited to well below 1 nm precision due to the pulsed nature of the deposition rate (0.001 to 0.01 nm/pulse typically). This is achieved by in-situ monitoring of the layer growth with Reflection high-energy electron diffraction (RHEED) technique[1], as also mentioned in Section0.4.1. This combination has proven to be crucial for the fabrication of, for instance, high quality X-ray optics [66], which are superlattices of alternating layers of high-Z (Ni, W, Ag, Au,...) and low-Z (B, Be, C,...) materials. Typical values of layer thickness are 1-10 nm, depending on the application. Good examples of state-of-the-art PLD of metal multi-layers can be found in [65, 66, 67], and are illustrated in Figure 1.1.

1.2 Tuning the stoichiometry using multiple elemental sources

For CZTS precursors, metallic or chalcogenide films, the level of control on stoichiometry is quantified by Katagiri and co-workers in [15]. The compositional ratios among which they have managed to fabricate $> 5\%$ efficiency solar cells are: $0.75 < \mathrm{Cu}/(\mathrm{Zn}+\mathrm{Sn}) < 0.9$ and $1.1 < \mathrm{Zn}/\mathrm{Sn} < 1.2$. Thus, the ability to control the "$\mathrm{M}_1/\mathrm{M}_2$" ratio must be of the order ~ 0.05.
Limiting our discussion to vacuum techniques using multiple targets, there

[1]RHEED technique is sort of a shallow incidence XRD measurements, but with electrons. Between one laser pulse and the next one, the chamber is under high vacuum, so a coherent beam of electrons can be shot on the growing films and a diffraction pattern is detected. When one atomic mono-layer is completed, the intensity of the diffracted peaks has a maximum and the film growth can be sharply interrupted by stopping the laser pulses.

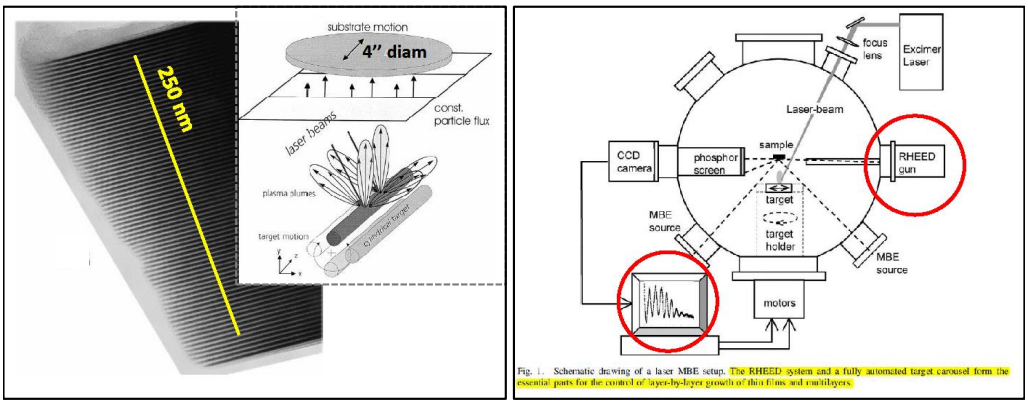

Figure 1.1: Left: Morphology of 75-period Ni/C graded multilayer stack with mean period thickness t=3.65 nm. The substrate is a 4 inches diameter wafer. Such large area uniformity was obtained by using the special PLD equipment in the inset. Image from [65].
Right: typical PLD equipment for the fabrication of multi-layered structures. Figure from [66].

are two ways by which one can monitor and control the stoichiometry of the precursors:

- Staking different layers of metals or chalcogenides, or a mixture of them. This is the most effective method to precisely know the absolute value of the compositional ratios by looking at the thickness of the different layers. However, the stacking sequence can have big influence on the crystallization process during the high temperature sulfurization, leading to preferential segregation of secondary phases or non-uniform mixing of the constituents. Thickness uniformity must be carefully evaluated.

- Doing co-sputtering or co-evaporation with real time monitoring of the individual elemental sources. By tilting the substrate along one axis one can also obtain a smooth compositional gradient in one element, as reported by NREL[39] and IREC[37]. The precision to which the gradient can be known corresponds to the detection limit of the compositional measurements. A systematic error can originate from the calibration of the mass deposition monitors.

In our specific case, we can take the example of the stacking sequence "glass/Mo/Zn/Sn/Cu". The overall stoichiometry depends on the thickness ratios of the layers. Given the fact that one wants the absorber layer to be 800-1000 nm thick, a first estimate on the thickness of the layers could be:

150 nm for copper, 120 nm for zinc and 150 nm for tin. If we assume a thickness uniformity of ±5 nm, it is easy to show that tuning the stoichiometry within the desired range can be achieved.
In this respect, the deposition of the Sn layer may be the most critical part since Sn has the tendency to wet the surface instead of growing as a uniform layer. For this reason often times it is seen that deposition is made from a Cu-Sn alloyed target instead. Another solution is to make use of mass-rate deposition monitors, which measure the mass deposited and is, to a first approximation, insensitive to the structure of the films.

1.3 Multilayers of Cu, Zn and Sn

PLD of Sn

In figure 1.2 we see the morphology of thin films of zinc and tin fabricated with PLD at the laser fluence of 2 J/cm^2 at room temperature.

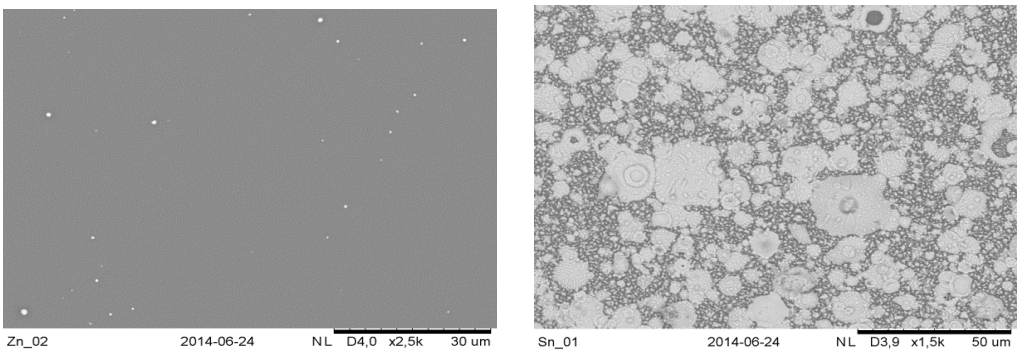

Figure 1.2: SEM top view of thin films of zinc (left) and tin (right) made with PLD at the laser fluence of 2 J/cm^2. Thin films of copper are deposited without visible droplets (picture not shown).

Already from these pictures it is clear that PLD of tin is very problematic due to the huge amount of micron-sized droplets, which make any attempt at quantifying the deposition rate insignificant. The high production of droplets in PLD of Sn was already documented in [56], and is related to the low melting point at 230°. A way to reduce the number of droplets for low melting point materials was found by making use of liquid targets [57], but this was not a feasible option with our setup. Working with a Cu-Sn alloyed target might have alleviated the problem of droplets, as the melting point

of the Cu-Sn alloy at 2Cu:Sn composition is around 750^{o}C. However, we did not try this option for the reasons explained in the following Section.

Multi-layered structures

Even if one solves the problem of droplets, stacking two (or more) layers of more than 150 nm thickness in a chamber that is not equipped with a multiple target holder and that has no tools for real-time deposition control is not an easy task. In fact, the only option to mount different targets at once was to cast them together in a single target (of 1 inch. diameter) subdivided in two (or three) different "slices". The laser would then be directed to one or another of the slices. With this strategy and with our setup that does not provide substrate motion[2], due to the narrow spatial confinement of the ablation plume, the thickness profile of the deposited films can only be uniform over an area smaller than the size of the ablation region on the target, much less than 1 cm^2, which is commonly not a problem for films deposited with PLD (typical sample size is 5×5 mm^2), but which is absolutely insufficient when it comes to making solar cells.
The maximum degree of sample uniformity achievable with our setup is illustrated in Section 6.3, Figure 6.5. Clearly, stacking two or more films with such degree of uniformity does not enable any control over the stoichiometry of the precursors.

1.3.1 Cu-Zn-Sn alloyed target

After deciding that casting multiple targets in one was not an option, the only metallic target left to consider was a Cu-Zn-Sn alloyed target, but eventually we decided to move instead to a chalcogenide CZTS target. In the next Chapter, in Section 2.1, a detailed comparison between these two targets is done. Here, briefly, we note that metallic targets are generally associated to low deposition rates. In our case, as reported in the paper [1], at standard working conditions it takes more than one hour to deposit a film thicker than 100 nm. In the view of installing the sulfur cracker in the PLD chamber to combine PLD and sulfurization, such a long deposition time is not desirable, due to the instability of CZTS in vacuum at high temperatures. Plus, the Cu-Zn-Sn system is very easy to alloy, so there is no interest in using PLD to fabricate such kind of thin films. If it is just for depositing a simple metallic film to be sulfurized afterwards, this can currently be done much faster and on larger area with sputtering deposition.

[2]which is the only effective way to increase the size of the deposited films

1.4 Conclusions

Laser ablation and deposition of Sn have proven not to be an option because of unavoidable ejection of micron sized droplets from the target. This fact is due to the very low melting point of tin and was previously documented in PLD literature [56]. The use of multiple targets for tuning the stoichiometry via a multi-layered approach was assessed not feasible without a special equipment for large area PLD and a multi-target holder. With our simple setup, the best uniformity conceivable would be achieved on a sample area <1 cm^2, with a huge lateral thickness gradient (>100 nm/cm, see the figure in Section 6.3), which is not suitable for making solar cells.
The use of a single Cu-Zn-Sn alloyed target was discarded mostly for the low deposition rate and because of the lack of motivations in using PLD for this particular metallic alloy. Thus, it was decided to change direction in the project and to start working with a sintered (2CuS:ZnS:SnS) CZTS target, since PLD seemed the right technique to "easily allow a stoichiometric transfer even for complex materials".

Appl. Phys. A (2014) 117:89–92
DOI 10.1007/s00339-013-8207-0

Applied Physics A
Materials Science & Processing

Nanosecond laser ablation and deposition of silver, copper, zinc and tin

Andrea Cazzaniga · Rebecca Bolt Ettlinger · Stela Canulescu · Jørgen Schou · Nini Pryds

Received: 8 November 2013 / Accepted: 10 December 2013 / Published online: 7 January 2014

Abstract Nanosecond pulsed laser deposition of different metals (Ag, Cu, Sn, Zn) has been studied in high vacuum at a laser wavelength of 355 nm and pulse length of 6 ns. The deposition rate is roughly similar for Sn, Cu and Ag, which have comparable cohesive energies, and much higher for the deposition of Zn which has a low cohesive energy. The deposition rate for all metals is strongly correlated with the total ablation yield, i.e., the total mass ablated per pulse, reported in the literature except for Sn, for which the deposition rate is low, but the total ablation yield is high. This may be explained by the continuous erosion by nanoparticles during deposition of the Sn films which appear to have a much rougher surface than those of the other metals studied in the present work.

1 Introduction

Pulsed laser deposition (PLD) is a well-known and established technique to produce thin films of metals and metal oxides. It is possible to a high degree to control the stoichiometry of the films and to produce accurate interfaces for multilayer devices. The applications span from superconductive metal oxides to Fresnel lenses for X-ray focusing [1–4], to mention the most important. In this work, we report on UV laser ablation of four different metals Zn, Ag, Cu and Sn in the nanosecond regime under typical working conditions for a deposition experiment, i.e., when the target is subjected to a very high number of pulses (up to 10^5) over an area (~ 1 cm^2) scanned by a rastering system. Cu, Zn, Sn, with S and Se, are the elementary constituents of the chalcogenide materials CZTS/Se, which are semiconductors potentially very attractive for applications as solar cell absorbers [5]. However, control of the crystal growth is still an issue due to both defects and mixing of secondary phases, such that there is a demand to improve the crystal quality and tune the stoichiometry of the deposited layer. Ag has been included as well since its ablation properties are well known [6–10]. As a matter of fact, there are already a number of experimental [11–15] and theoretical [16–18] studies on laser ablation and deposition of metals, but a comprehensive investigation of the deposition of all these metals is not yet available. We have investigated the fluence range close to the ablation threshold of metals, from 0.5 to 4 J/cm^2, which is particularly suitable for thin-film deposition due to low re-sputtering and low implantation yield. In this fluence interval, there is a transition [19] from the evaporation regime, where the evaporated species are not ionized, to the plasma regime, where more and more emitted species are ionized and the kinetic energy of the ions rises up to more than 500 eV [9]. However, below 4 J/cm^2, the plasma may not be fully ionized and plasma shielding may not be significant. Re-sputtering effects on the growing films above 4 J/cm^2 have been reported in several cases [12–14], as well as re-sputtering at an interface [15], but this effect is clearly more important at lower fluence for materials with smaller cohesive energies [20]. A second effect is recoil implantation [21, 22] which tends to smear out the interface. This effect is

A. Cazzaniga (✉) · R. B. Ettlinger · S. Canulescu · J. Schou
DTU Fotonik, Technical University of Denmark, Bygning 343, Ørsteds Plads, 2800 Kgs. Lyngby, Denmark
e-mail: andcan@fotonik.dtu.dk

N. Pryds
DTU Energy Conversion, Technical University of Denmark, 4000 Roskilde, Denmark

relatively insignificant at low fluence, but has been observed at higher fluence [14, 15].

2 Experimental setup

The laser used was a Nd:YAG with a fundamental frequency at 1,064 nm working in the UV regime at 355 nm and with a pulse duration of 6 ns. The experiments have been carried out as follows: the laser pulses were focused on the target in a HV chamber ($p < 10^{-6}$mbar). The spot size was estimated to 0.3 mm^2 after irradiation of 1–3 pulses on a silver target. Such a small spot size minimizes the non-Gaussian shape of the up-converted laser pulses. The energy of the laser pulses has been measured with a power meter before, during and after each deposition. The fluence variation during a long deposition experiment (2–3 h at a pulse repetition rate of 5–10 Hz) was found to be around 10 %. During all the experiments, the laser beam was scanned over a rastering area of 0.35 cm^2, and the metal targets were rotating at the speed of 1 rotation/min. The target was placed at 45° with respect to the incident laser beam (Fig. 1), with a variation of <1° introduced by the rastering system. The deposition yield and the film thickness were measured at a fixed distance of 5 cm normal to the target surface and centered with respect to the rastering area. The deposition rate was monitored with a quartz crystal microbalance (QCM), as shown in Fig. 1. The crystal is a standard AT-cut crystal with a diameter of 14 and 0.3 mm thick. The deposition area on the center of the crystal surfaces is covered with a silver electrode with a thickness of 400 nm and with a diameter of 6 mm. The resonance frequency (~5 MHz) is measured with accuracy of 1 Hz, corresponding to a mass variation of $\sim 1 \times 10^{13}$ atoms/cm^2. For the direct thickness measurements, the films have been deposited under the same conditions as with the deposition on the QCMs on Si substrates. The thickness was measured with a DEKTAK profilometer with overall accuracy of 5 nm.

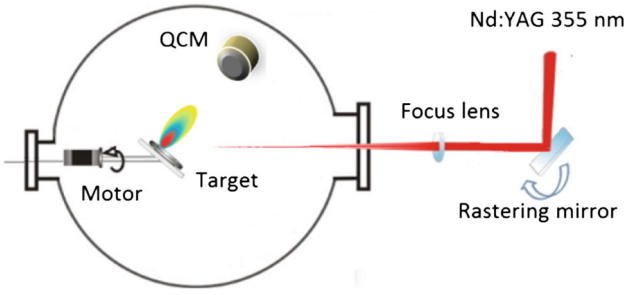

Fig. 1 Experimental setup for thickness measurements using a quartz crystal microbalance (QCM). The focussed laser beam is hitting the target at an angle of incidence of 45°. Distance from target to substrate/QCM device is 5 cm

3 Results

The deposition rate of Ag, Cu, Zn and Sn has been studied as a function of the laser fluence in the range 0.5–4 J/cm^2. For each value of the laser fluence, the deposition has been carried out over a period of 20 min at a repetition rate of 2 pulses/s. The frequency shift observed was between 50 and 200 Hz. The various deposition rates as a function of the laser fluence are shown in Fig. 2 and summarized in Table 1.

In addition to mass area density measurements with the QCM, we have performed thickness measurements on thin

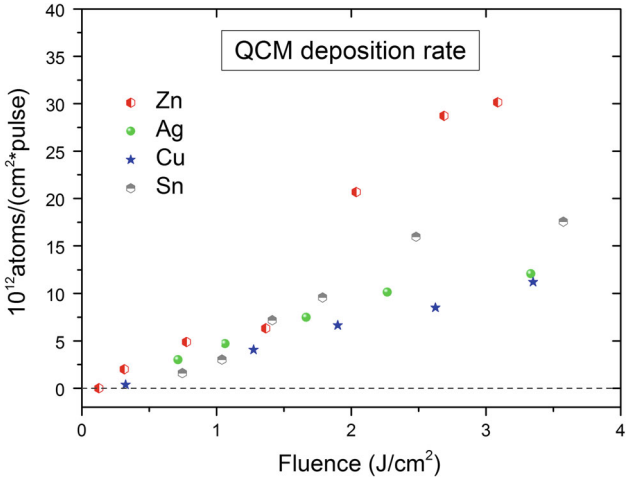

Fig. 2 Deposition rates at 355 nm for zinc, silver, copper and tin as measured by a quartz crystal microbalance placed at a distance of 5 cm from the target. Laser working at pulse repetition rate of 2 Hz

Table 1 Summary of the value given in Fig. 2 for a laser fluence of 2 J/cm^2 (after linear interpolation of the data) together with the time needed to deposit a single layer of 100 nm

	Zn	Ag	Sn	Cu
Cohesive energy (eV/atom)	1.35	2.95	3.14	3.49
Melting temperature (C)	420	962	232	1,085
Ablated atoms/pulse* ($\times 10^{15}$)	4	1.9	7	1
Deposited atoms/pulse* ($\times 10^{12}$)	17	8	9.5	7
Time to deposit 100 nm* (at 10 Hz)	01 h 20 min	04 h 30 min	–	03 h 40 min

For the accuracy, see Fig. 3. A comparison with the cohesive energy and the total ablation yield from [11]

* At 2 J/cm^2

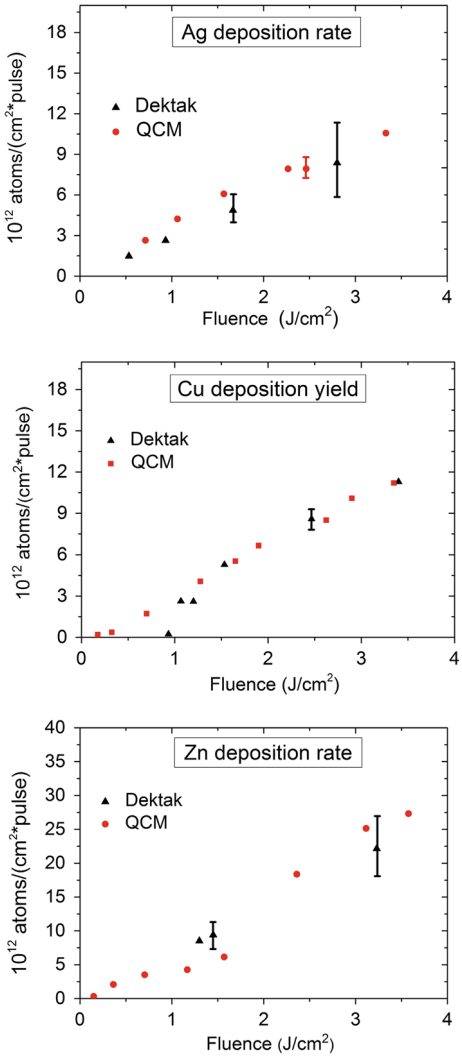

Fig. 3 **a–c** Comparison between the number of atoms deposited per pulse as given from the QCM measurements and as deduced from the Dektak profilometer assuming bulk density. Disagreement of the data at the ablation threshold may merely originate from scattering of the data points [11]

films of Zn, Ag, Cu and Sn deposited on Si substrate with the profilometer to gain information about uniformity, density and texture. For Zn, Ag and Cu, there is a fair agreement between mass area density and thickness measurements when the number of atoms is calculated assuming bulk density, as shown in Fig. 3. For the thin films of Sn, it was not possible to provide a thickness value due to the roughness of the surface. In Fig. 4, a typical thin film of Sn is shown with an irregular surface with many craters and droplets.

3.1 Reflectance measurements

In order to try to understand the role of target roughening on light absorption and plume collimation, we measured

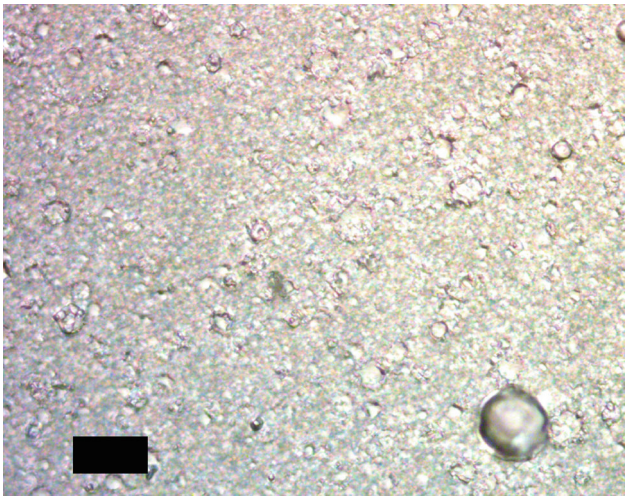

Fig. 4 Image with optical microscopy of an Sn layer after 4 h of deposition at 3 J/cm^2 and with 10 Hz of pulse repetition rate at room temperature. The average film thickness was estimated to 500 nm. The black rectangle has dimensions of 10 μm × 20 μm. Many craters are seen on the Sn film surface. A big droplet of dimensions >2 μm is seen in the *lower right corner*

the total reflectance spectrum of the target in the range 300–1,000 nm before and after the ablation from a polished surface at two different fluences of 2 and 4 J/cm^2. For the noble metals Cu and Ag, we can observe only a small increase of the reflectance in the UV spectrum while the value in the visible regime is the same with $R_{vis} > 0.9$. For Zn and Sn, the increase is significant and still it is more pronounced in the UV spectrum. At a wavelength of 355 nm, the total reflectance for Sn rises from 0.35 to 0.65 after the ablation, and for Zn, it changes from 0.6 to 0.8. The roughness of the target surface induced by laser irradiation is determined by the type of material, the total number of pulses and the laser fluence, but a clear result is that it reaches a stable value independent of the fluence, at least up to 4 J/cm^2.

However, the change in reflectivity does not seem to be related to the deposition rate, a possible reduction of the amount of energy absorbed by the target or by any change of the ablation plume direction. The reason is that the reflectivity changes dynamically during the nanosecond pulse and reaches a stationary reflectivity after the laser pulse terminates [23]. The role of reflection needs to be further investigated.

4 Discussion

The deposition rate for Ag is in agreement with the values reported in [11], which is not trivial due to the longer duration of the deposition and the rastering conditions. Typically, discrepancies would occur due to roughening of

the target and uncontrolled window contamination by the ablated particles. For Sn, there is no deposition rate reported in the literature, and we can notice a very big difference between the number of ablated and collected atoms compared with the other elements (see Fig. 2 and Tabel 1). In fact, Sn has the largest ablation yield among metals, but a modest deposition rate. One difference may arise if the ablation of Sn is violent from a very early stage of the laser heating with emission of big chunks or nanoparticles from the target. The emission of big chunks with relative low kinetic energy from the target may induce desorption of loosely bound Sn atoms at the impact on the film surface and result in surface smoothening, while the most of the chunk material may stick to the surface [24]. Generally, a large flux of smaller nanoparticles with high kinetic energy that may produce the many highly regular craters seen in Fig. 4 will usually not occur during nanosecond laser beam impact, but only for ultrafast laser beam impact [25]. However, the thermodynamic pathways during nanosecond heating and subsequent cooling in Sn are not known, and a part of the ablated volume may reach a metastable, thermodynamic zone, since Sn has a very low melting point as seen in Table 1. Nanoparticles from such a process would be emitted from an Sn with a typical velocity below 1 km/s. In any case, it does not seem possible that the craters in Fig. 4 with diameters up to 1 μm are produced by impact of single atoms from the target. The crater form is typical for bombardment by low-energy nanoparticles [26]. An additional effect is that the crater size induced by cluster ions increases with decreasing melting temperature [27] and that may happen for an Sn film that is heated by the arriving flux of ablating particles. These points may explain why only Sn shows a film surface covered by craters of micrometer size. More studies are required to understand the behavior of Sn during the deposition process.

5 Conclusion

The deposition rate for different metals has been determined in the fluence range from 0.5 to 4 J/cm^2. Cu, Zn and Ag metals have a very similar deposition rate as a function of the laser fluence with a value of 7–9 $\times$ 10^{12} atoms/cm^2 deposited at a fluence of 2 J/cm^2. Zinc deposition is more efficient with a deposition rate of 17 $\times$ 10^{12} atoms/cm^2 at the same fluence, which is in good agreement with reported values on laser ablation of Cu, Ag and Zn [11, 12]. The situation is completely different for Sn, which shows the highest ablation yield while the deposition rate is only 9 $\times$ 10^{12} atoms/cm^2 at 2 J/cm^2. This behavior may be related to the low melting point of Sn such that the ablation process could be very explosive at a late stage of cooling after the laser impact. This may lead to the ejection of fast nanoparticles, which not only produces craters by bombardment of the film but also leads to a significant mass loss from the films. This explains why the deposition rate for Zn is comparatively low in contrast to the high ablation yield. Moreover, due to the roughness of the Sn thin films, it has been impossible to perform reliable thickness measurements by the profilometer. For Zn, Ag and Cu, the thickness measurements are in good agreement with the QCM data, assuming bulk density for the thin film produced.

Acknowledgments This work has been supported by a grant from the Danish Council for Strategic Research.

References

1. H.U. Krebs, in *Pulsed Laser Deposition of Thin Films,* ed. by R. Eason (Wiley, New York, 2007), p. 363
2. D. Bäuerle, *Laser processing and chemistry*, 4th edn. (Springer, London, 2011), p. 759
3. P.R. Willmott, J.R. Huber, Rev. Mod. Phys. **72**, 315 (2000)
4. F.A. Döring, A.L. Robisch, C. Eberl et al., Opt Express **21**, 19311 (2013)
5. B. Shin, O. Gunawan, Y. Zhu, N.A. Bojarczuk, S.J. Chey, S. Guha, Prog. Photovolt. Res. Appl. **21**, 72 (2013)
6. W. Svendsen, O. Ellegaard, J. Schou, Appl. Phys. A **63**, 247 (1996)
7. T. Hansen, J. Schou, J.G. Lunney, Europhys. Lett. **40**, 441 (1997)
8. H.U. Krebs, Bremert, Appl. Phys. Lett. **62**, 2341 (1993)
9. B. Toftmann, J. Schou, S. Canulescu, Appl. Surf. Sci. **278**, 273 (2013)
10. B. Toftmann, J. Schou, J.G. Lunney, Phys. Rev. B **67**, 04101 (2003)
11. J. Schou, Appl. Surf. Sci. **255**, 5191 (2009)
12. S. Fähler, S. Kahl, M. Weisheit, K. Sturm, H.U. Krebs, Appl. Surf. Sci. **154**, 419 (2000)
13. J. Gonzalo, J. Siegel, A. Perea, D. Puerto, V. Resta, M. Galvan-Sosa, C.N. Afonso, Phys. Rev. B **76**, 035435 (2007)
14. K. Sturm, H.U. Krebs, J. Appl. Phys. A **90**, 1061 (2001)
15. C. Eberl, T. Liese, F. Schlenkrich, F. Döring, H. Hofsäss, H.U. Krebs, Appl. Phys. A **111**, 431 (2013)
16. S. Amoruso, F. Bruzzese, R. Velotta, N. Spinelli, J. Phys. B **32**, R131 (1999)
17. J. Lunney, R. Jordan, App. Surf. Sci. **127–129**, 941 (1998)
18. S. Amoruso, J. Appl. Phys. A **69**, 323 (1999)
19. R.W. Dreyfus, J. Appl. Phys A **69**, 1721 (1991)
20. P. Sigmund in, *Sputtering by Particle Bombardment I*, ed. by R. Behrisch (Springer, Berlin-Heidelberg, 1981), p. 9
21. P. Sigmund, Appl. Phys. Lett. **14**, 114 (1969)
22. P. Vajda, Rev. Mod. Phys. **49**, 481 (1977)
23. K. Ujihara, J. Appl. Phys. **453**, 2376 (1972)
24. I. Yamada, J. Matsuo, Z. Insepov, T. Aoki, T. Seki, N. Toyoda, Nucl. Instrum. Method B **164–165**, 944–959 (2000)
25. P. Balling, J. Schou, Rep. Prog. Phys. **76**(036502), 1–39 (2013)
26. R. Aderjan, H.M. Urbassek, Nucl. Instr. Meth. B **164–165**, 697 (2000)
27. K. Nordlund, K.O.E. Henriksson, J. Keinonen, Appl. Phys. Lett. **79**, 3624 (2001)

Chapter 2

PLD of CZTS, first attempts

If you can't say something nice, do not say anything at all Thumper (Bambi)

Time period: 2^{nd} and 3^{rd} semesters as PhD Student. Status of the project: I will start using one single CZTS target, first experiments to see what comes out. The other PhD students are hired and will start working on the project. We complete the furnace for the annealing and eventually set up the apparatus described in Section 0.2, Figure 3. Andrea Crovetto starts working on the fabrication of the top layers CdS and Al:ZnO (AZO). I write a paper on the first CZTS films, and the paper is rejected right away.

2.1 Chalcogenide vs metallic target

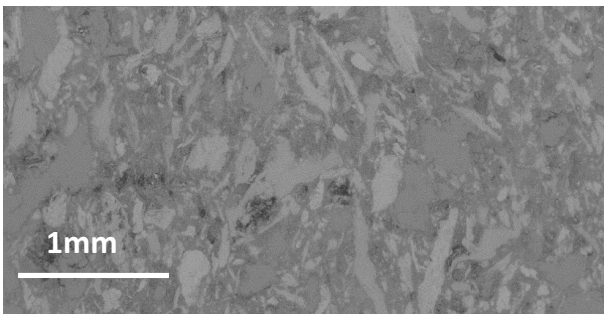

Figure 2.1: Top view of the 2CuS:ZnS:SnS sintered target. The different phases are clearly visible and extend over a typical length scale of a few hundred μm. The melting point and the vapor pressure of the main phases are summarized in the paper enclosed at the end of Chapter 6.

In general, metallic targets require tight focussing of the laser beam in order to produce significant deposition rates, which is an important parameter if the aim is for films thicker than 100 nm. Indeed, metals tend to have high boiling point, low volatility, high reflectivity and, above all, are good heat conductors. This means that the local heat generated by the laser pulse readily diffuses away, making the local heating process more energy demanding. For example, in [42] is observed that heat dissipation accounts for more than 70% energy loss of the incident laser pulse in an experiment of UV nanosecond laser ablation of Zr. On the other hand, high band-gap semiconductors do not suffer so severely from heat dissipation, as they are not good heat conductors. For example, a value as low as 0.2 J/cm^2 is reported to be optimal for achieving stoichiometric transfer from a single crystal $SrTiO_3$ target[61]. This value is very close to, or even below, the ablation threshold for many metals. The very confined heating induced in high bandgap semiconductors usually results in films with less droplets compared to those fabricated from metallic targets. In addition, target modifications are also less severe.
In our case, the sintered CZTS target (Figure 3 of the paper enclosed at the end of Chapter 6), contains binary phases with very different properties. ZnS and SnS are semiconducting and volatile, while $Cu_{2-x}S$ phases behave as semi-metals. Thus, an intermediate situation between the two is expected. A detailed analysis of the phases in the target and their interaction with the laser pulses is given in Chapter 6. The task of doing PLD with such a multiphase target is not standard in PLD, if available single crystals or poli-crystalline single phase target are used. However, for the case of CZTS this option is not commercially available, although single crystals of CZTS have been successfully fabricated for research purposes [68, 69].
After the first ablation experiments it was clear that the target was heavily modified by the ablation process and that a lot of material was lost to evaporation, as could be already seen by the strong coating found on the laser viewport and on the walls of the chamber. In Figure 2.2 are shown (left) a top view of the target after one deposition run and (right) a detail of the effect of 5 laser pulses on a fresh target surface. The morphology of the deposited films was very irregular due to the high amount of droplets, as illustrated in Figure 2.4 (right).
Summing up, we had the the first experimental observations on PLD of CZTS:

1. The deposition rate was much higher than with metallic targets, about 500 nm/20 mins.

2. The deposited films had plenty of droplets, whose composition was mostly Cu-S (Figure 2.4, right).

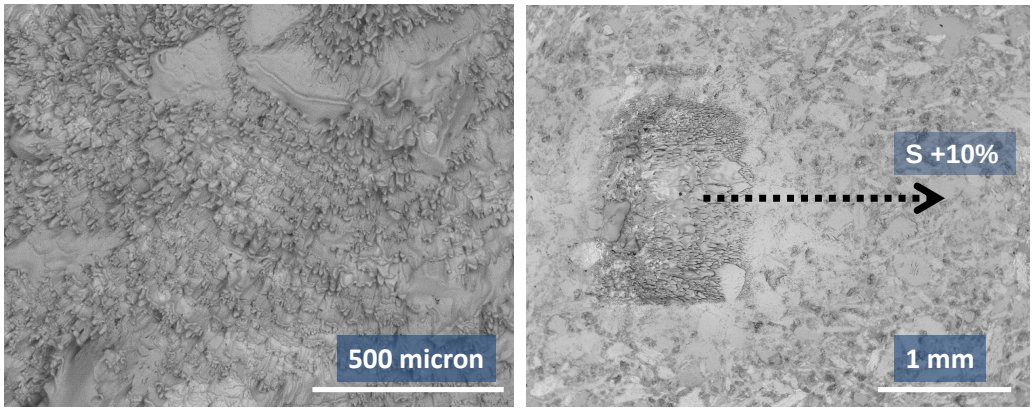

Figure 2.2: Left: SEM image of the CZTS target surface after ablation. Right: ablated area (5 shots at 1.5J/cm^2) VS non ablated area. The arrow indicate the gradient of sulfur signal in EDX mapping, which increases by 10% moving out of the ablated spot. These images show that target modification after ablation involves both morphological and compositional changes.

3. The target was severely altered by the ablation process (Figure 2.2).

2.2 First films and first problems

First, I was happy with the deposition rate: 15-20 minutes for fabricating a film was a reasonable time. However, the films had a very poor morphology and any attempt at quantifying thickness and composition was arguable. Stability of the target surface was clearly an issue and was likely related to the high number of droplets observed in the films. Coating of the the viewport was also a problem, as the fluence on the target was being severely altered during the deposition. Eventually, as described in Chapter 5, I found a solution to many of these problems, but for that time being I was clueless. Now, I estimate that the fluence fluctuated by about 50% during the depositions due to non-optimal procedure. Thus, to mitigate all these problems and aiming at reproducibility, I adopted the practice to always refresh the surface of the target after every deposition and to clean the viewport with some dishwasher powder and diluted HCl. Which means dismounting a vacuum flange and clean the viewport every single time: it is a huge load of work. Did I have another option? Maybe. Lowering the fluence is also a documented strategy for reducing droplets, if one can afford working at low fluence. Looking backwards, that would have been a very wise decision. Unfortunately many things lead me to think it would have been the wrong direction to try: the vast majority of papers on PLD con-

tains the claim that "PLD preserves the stoichiometry" of the target to the thin film as long as the fluence exceeds a certain "ablation threshold". The most popular view is based on a very famous paper from Venkatesan and co-workers (1988) entitled "Observation of two distinct components during pulsed laser deposition of high T_c superconducting films" [50]. The authors observe a broad evaporative component, predominant at low fluences and a narrow, forward-directed, stoichiometric plasma plume at high fluences. *The evaporated component is non-stoichiometric, as one would expect, whereas the forward-directed component has a composition close to that of the pellet. Further, the forward-directed stoichiometric component increases with the laser energy density in comparison with the evaporated component.* Conclusions: for stoichiometric transfer, move towards increasing the fluence. The success of Venkatesan's group in fabricating thin films of high T_c super conducting materials contributed to a wide (and uncritical) acceptance of the aforementioned statement, which was only verified with regards to that particular target and to the fact that, for that material, a tight control over stoichiometry is not required [1].
Thus, since our CZTS target was made of different phases, each with a different ablation threshold, and that evaporation was already a clear problem, my first worry about lowering the fluence was to even increase the evaporated component and to fall in the "non-congruent evaporation regime". All in all, I though, the morphology of the precursors may not be a problem if during the annealing these droplets will merge entirely into the poli-crystalline films. Several groups, [37] for instance, reported making CZTS by sulfurization of a stack of metallic precursors. Some Cu-S droplets must not be too bad, if the stoichiometry was the right one. Was it?

The first films produced at room temperature (Figure 2.4, right) were characterized with SEM images and EDX analysis. I started to work in the fluence range from 1 to 3 J/cm^2, where the plasma plume is bright and well visible. As discussed earlier, I wanted to avoid the evaporation regime. The first results were rather inconclusive.

Assessing the deposition rate was the first problem: due to micron sized droplets, the roughness of the films was of the same order as magnitude of the thickness itself. The amount of droplets from one film to another seemed to change, but it wasn't clear that the fluence was responsible for

[1]The class of high T_c oxide semiconducting materials tolerates deviations from the exact stoichiometry up to few percent'*s*. In the case of thin-film electronic devices, way more stringent conditions are required on the stoichiometry of the deposited films. Yet, this fact seems to be mostly overlooked, as already pointed out in [61].

this fact. It could have been related to other causes, such as the status of the target, as well as a different thickness of the film.
Assessing the fluence was the second problem: due to volatile ZnS and SnS in the target, the evaporated component was responsible for harsh coating of the laser view-port. The laser fluence on the target diminished between 30% and 70%, depending on deposition time and initial fluence. I took the average value for the fluence, measuring the fluence at the beginning and at the end of the depositions, assuming (arbitrarily) a linear decrease in the viewport transmission. Those numbers were not trustful.

2.3 EDX measurements

From the harsh coating all over the deposition chamber and the observed modifications on the target after the ablation, it was clear that the assumption of stoichiometric transfer was difficult to justify. Thus, we investigated both the target and the deposited films with EDX analysis, Figures 2.2 (target) and 2.4 (films). According to the EDX software the films were rich in copper and tin and poor in sulfur and zinc. The target was found sulfur-poor in the ablated area as compared to the "fresh" surface. The results were qualitatively consistent with expectations of evaporation of ZnS and S, but.. could the results be trusted? No, for several reasons. First of all, the EDX data processing was not calibrated using binary standards. Without standards, the quantification can be easily wrong by 10%, or even more. This can be easily checked by processing the experimental data with different algorithms available within the same software[2].

Beside choosing one algorithm or another, the signals from S and Sn are in the low-energy side of the EDX spectrum, below 3.5k eV, where the background noise also affects the overall quantification[3].

The aforementioned problems would only induce systematic errors in the EDX quantification, which would have been not a huge problem: one could use the numbers just as phenomenological parameters.

The major hurdle, however, was that the morphology of the films (and of the target) was very irregular. The software that does the EDX data processing must always assume a uniform elemental distribution for the sample

[2]There are two mainstream algorithms, namely "ZAF" and "ϕ-ρ-z". The latter is reported to be more suitable for light elements, which would actually be our case if we consider the large amount of sulfur in our films. Nevertheless, I selected the ZAF one since I was not interested in a quantification of the sulfur content, rather the Cu/Zn was more important.

[3]Furthermore, sulfur signal overlaps with that coming from the molybdenum substrate

investigated. When this assumption is not true, the peak-intensity of each element can be altered dramatically. For instance, Cu has a K_α^{Cu} transition at 8.04 keV, while Zn at 8.63 keV. Thus, the signal emitted from Zn atoms can be re-absorbed by Cu atoms, which then re-emits a signal at K_α^{Cu}=8.04 keV. On the other hand, the signal coming from Cu atoms does not have enough energy to excite the K_α^{Zn} at 8.63 keV. The software is programmed to take into account for this absorption/re-emission mechanisms, but the emitter is assumed spatially homogeneous. Our films had plenty droplets, whose composition was mostly Cu-S, as we documented in [4]. How much was that altering the estimation? one cannot know the answer. Why using EDX at all then? First, there is no better option: if the sample is not uniform, no technique is able to give a reliable quantification. Second, I still hoped I could deduce the *ratio* behind the EDX numbers after seeing the results from raman and XRD.

2.4 Substrate temperature

Due to difficulties in assessing the laser fluence during the depositions, we decided that it would be meaningful to start by investigating the effect of the substrate temperature. The hope was that, at higher temperatures, droplets would merge in the growing film and a more regular, crystalline morphology could be obtained. For anybody familiar with PLD, this is the most natural way to fabricate films. We did not have a furnace for the annealing yet, but the hope was that we would not even need it.
I would do all the films in exactly in the same way (cleaning the laser viewport and refreshing the target surface every time, same laser energy, p.r.r and deposition time for each film) in order to single out the effects related to substrate temperature. I decided to lean on the "high fluence" side of my experimental range, in order to minimize the evaporation component and have as much possible "stoichiometric plasma". The nominative value for the fluence used was 3 J/cm^2. I deposited five CZTS films on quartz substrate in the temperature range 25 to 500°C. The SEM top views of four of these films are illustrated in Figure 2.3. To be more precise, the substrates were clamped to a the resistive heater, whose temperature was controlled by a thermocouple. That is the value reported for the substrate temperature[4]. Since heat transfer in vacuum is very poor, it is very reasonable to think that a difference of more than 100°C existed between the heater and the quartz substrate, at least for the film done at 500°C.

[4]This was the first and last time we used a clamping system for high temperature depositions.

As expected, substrate temperature proved to be a relevant parameter. In Figure 2.3 the SEM top-views of the films from 275°C to 500°C are shown. The morphology of the film deposited at 275°C was very similar to that of the sample deposited at room temperature (not shown).

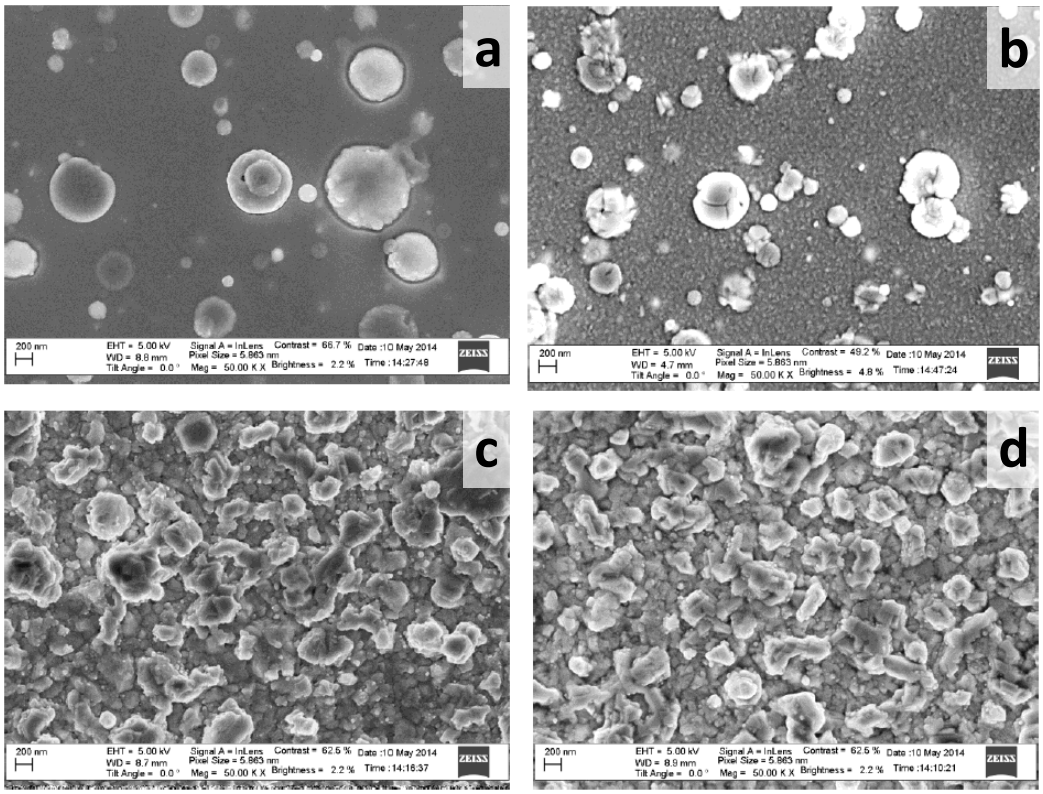

Figure 2.3: SEM top views of the CZTS films produced at: 275°C (a), 350°C (b), 425°C (c) and 500°C (d). Films were produced in high vacuum, p<10^{-6}mbar at 5 Hz p.r.r and deposition time of 90 min. The long deposition time was chosen so to have thick samples (>2 micron) and avoid collecting EDX signal from the substrate. The film deposited at room temperature (not shown) had a very similar morphology to the one deposited at 275°C.

Further investigations were conducted by means of EDX, XRD and Raman analysis, Figures 2.4 and 2.5.

2.5 Results and discussion

By comparing the results of Raman and XRD analysis, none of the films was promising as absorber for solar cells. The films deposited at a temperature of

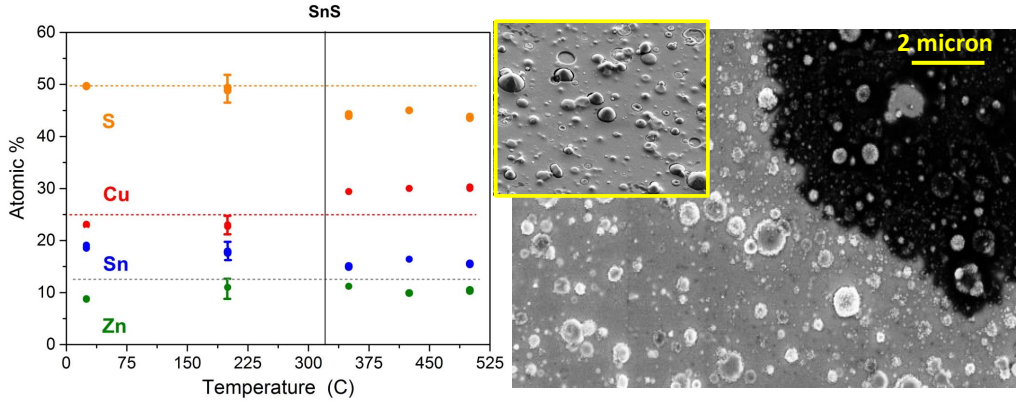

Figure 2.4: Left: EDX estimate of the atomic composition of films deposited at different substrate temperature. High energy electrons of 15 keV were used to stimulate the x-ray signal. The temperature of 310^{o}C at which SnS becomes sensibly volatile in vacuum is marked by a black bar. Right: Top view of the sample deposited at room temperature, with Cu-S droplets removal after KCN etching shown in the inset.

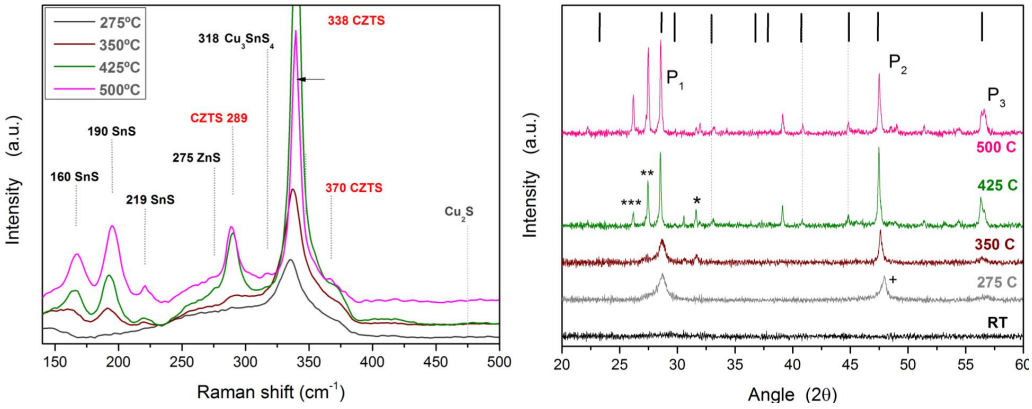

Figure 2.5: Left: Raman fluorescence spectra of the films in Figure 2.3. Spectra recorded at room temperature using a Thermo Scientific DXR Raman microscope with a diode laser (λ= 455 nm at 0.4 mW). Right: XRD patterns of the same films, plus the sample deposited at room temperature, which is completely amorphous. Black lines indicate the peaks related to the CZTS Kesterite phase, "*", "**" and "***" indicate SnS, $Cu_{2-x}S$ and Cu_2SnS_3 identified peaks, respectively.

350°C or below did not show enough features under XRD or Raman analysis to identify unambiguously a CZTS kesterite phase and Cu-S droplets have not merged into the layer. The films deposited at higher temperatures showed strong signs of secondary phases, especially SnS under Raman investigations, which is a very surface sensitive technique. $Cu_{2-x}S$ and Cu_2SnS_3 were identified with XRD analysis, and probably more other Cu-Sn-S phases were

affecting the samples, but we simply could not identify them all. According to EDX, the films deposited at lower temperatures were Sn-rich and Zn-poor and a reduction in the Sn content was observed for samples deposited at temperatures higher than 400^oC, which could be attributed to SnS evaporation, in agreement also with SnS phases individuated with Raman spectroscopy and with what expected from literature [40]. From EDX it wasn't clear if we had a loss of volatile phases or not, or if the transfer was stoichiometric, as stated in the vast majority of papers about PLD.
However, the vast amount of secondary phases in the samples deposited at high temperatures was a sign that the composition of the films was likely Cu-rich, since it is widely reported that more and more Cu-related secondary phases appear when the stoichiometry of the precursors is Cu-rich. Another option was that the transfer was indeed stoichiometric, but there was a non-compensated evaporation loss of S and SnS, which again brings to Cu-Sn-S phases, as discussed in [21]. Either way, the result was not satisfactory.
Furthermore, there were concerns regarding sulfur loss. The experience with PLD suggests that oxygen is always used as background gas during the depositions, whenever oxide materials are involved. Likewise for nitrides [55], where N_2 background gas is used. Indeed, the "stoichiometric transfer" discussed for PLD does not usually concern the very light and volatile elements or molecules that can be supplied in gas phase during the deposition.

The limits of this fabrication approach seemed very hard to overcome, even changing some of the deposition parameters, like the laser fluence or the pulse repetition rate. I did try to use at least 10 Hz p.r.r (thus shortening the deposition time) but I did not notice any significant difference.

Thus, the priority in the project became the completion of the furnace, to be able to implement a more standard fabrication procedure: deposition of precursors followed by sulfurization in a furnace. Among the benefits, this was the most common fabrication strategy and we could benefit from having reliable benchmarks from literature.

2.6 First experiments with the annealing

Summing up from the previous experience: samples were Cu and Sn -rich and S-poor. A vast amount of Cu-S and SnS secondary phases was visible for the films deposited at higher temperatures. We had two issues to tackle with the new furnace for the annealing:

- compensate for the sulfur loss during PLD
- achieve a good polycrystalline structure while avoiding SnS evaporation.

A soon as the furnace was finally up an running (November 2014, half of my PhD), I deposited a new series of thin films of CZTS at different substrate temperatures alike the ones already described before [5] and measured the composition before and after the annealing. The results of the EDX study are illustrated in Figure 2.6. We started with mild annealing conditions, as described in the figure, by keeping the annealing temperature below 510^oC. It is seen that (1) according to EDX, the sulfurization is effective and the sulfur content increases as result of the annealing. Surprisingly, the numbers returned by the EDX software round exactly to 50%, a coincidence that still struck me. (2) The Sn content is now finally correlated with the substrate temperature, and [Sn]% drops significantly whereas the substrate temperature is above 310^oC, where SnS is reported to become volatile in vacuum [40]. XRD analysis were also conducted, finding a closer resemblance to what expected for CZTS material, but still with some visible problems of Cu-S secondary phases. These results are discussed in the next chapter, along with our following attempt to put a ZnS cap layer on top of the CZTS.

[5] Except for using silver paste for glueing the substrate to the heater, no clamping any more.

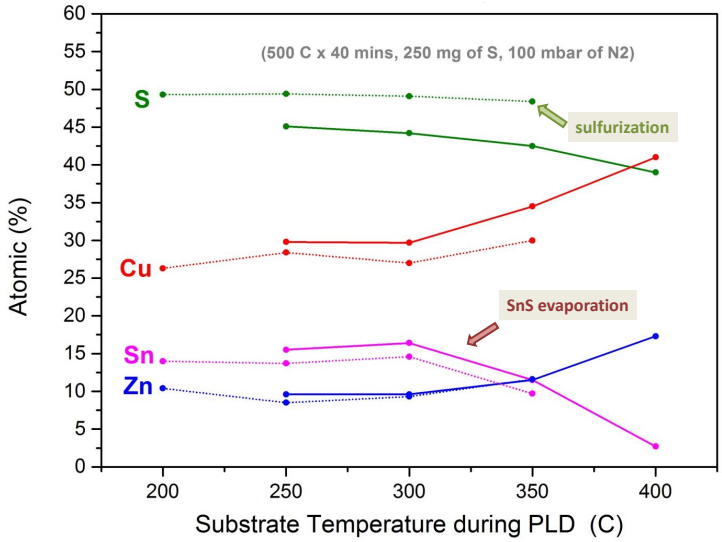

Figure 2.6: EDX estimate of the atomic composition of CZTS films deposited at different substrate temperature before (solid lines) and after (dotted lines) the annealing experiment. The annealing was carried out as indicated in figure, note the relatively low temperature of only 500°. This time, samples were glued with Ag paste onto the heater, so the temperature indicated in the graph closely represent the experimental conditions.

Chapter 3

ZnS top layer for enhancement of the crystallinity of CZTS absorber during the annealing

An expert is a man who has made all the mistakes which can be made, in a narrow field. Niels Bohr

Time period: 3^{rd} and 4^{th} semesters as PhD Student. Status of the project: The first solar cells did not work at all: both the CZTS and the top layers were not functioning. I needed to get a better quality CZTS and we needed to improve the fabrication process of the solar cells. None of this is going to be achieved here.

3.1 Mistake it until you make it

This chapter is a pedagogical example of how wrong one can go while trying to make solar cells. As illustrated previously, all the CZTS films made up to that point were Cu-rich and S-poor. After the annealing there were plenty of $Cu_{2-x}S$ secondary phases, and the few attempts to make solar cells had failed miserably. We also tried KCN etching, which selectively removes Cu-S phases, without any success: the problem was not just at the surface. There were a lot of problems: the top layers were still "under way", the oven had just started to work. Thus, the fact that the solar cells did not work was not really pointing at any specific problem. Nonetheless, from XRD and Raman it was clear that there was a problem with $Cu_{2-x}S$ secondary phases, at least one problem was clear.

The solution we came up with was adding a ZnS top layer to the Cu-rich CZTS. This should have had to positive effects:

- Adjust the Cu/Zn ratio by changing the thickness of the ZnS top layer.
- Prevent S and SnS evaporation during the annealing.

Tuning the Sn content was not an option with this fabrication strategy, but, if the results with the ZnS layer had been promising, I would have thought of adding a third layer of SnS.
The first step was PLD of ZnS: morphology of deposited films and deposition rate. ZnS is a very friendly material to deposit with PLD: films are amazingly flat and droplet free. A promising start! Coating of the view-port was still a problem: the brightness of the ablation plume diminished over time during the deposition. Since that was the case for CZTS as well, I did not see a big problem.
I begun to deposit bilayered CZTS/ZnS films with different thickness and at different substrate temperature. The results were all invariably encouraging: the XRD patterns did not show any $Cu_{2-x}S$ secondary phases after the annealing, as shown in Figure 3.1. What a success!

Unfortunately (1), I only had XRD to investigate my samples, which is not much but at least detects $Cu_{2-x}S$, our mayor problem. Andrea Crovetto at DTU Nanotech, in Lyngby, had access to Raman and SEM equipments, but he was busy with the deposition of the top layers CdS and AZO. It took a couple of months before I could understand what was going on in my samples, *i.e.* that the ZnS layer was forming a stable phase which did not merge with the CZTS layer, as shown in Figure 3.2. For the time being I was just delighted by my beautiful and very reproducible XRD patterns.
Unfortunately (2), I even got convinced that the best substrate temperature for the depositions was 300°C, right below when SnS starts to evaporate[40]. I did not have any evidence that 300°C was better than room temperature, but it seemed to me reasonable that enhancing the crystallinity in the first step would have resulted in a better crystallinity after the annealing. As I said, this is a chapter about mistakes.
In the meantime, since we also needed to take a study of the annealing step, I started to change the annealing conditions (background pressure, amount of sulfur, temperature, time) to see what would happen with my samples. Nothing: the XRD patterns all looked more or less the same to what was already shown in Figure 3.1 (Right). The problem of $Cu_{2-x}S$ secondary phases seemed to be solved forever.

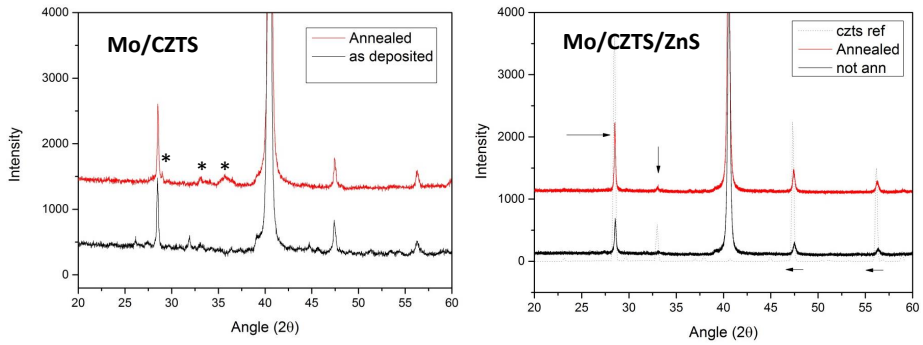

Figure 3.1: (Left) XRD patterns of the CZTS sample without the ZnS top layer. (Right), with ZnS top layer. In this case the estimated thickness for the CZTS layer was 500 nm, and the ZnS was estimated to 60 nm. I could show countless figure alike these ones

3.2 Let's write a paper

The deadline for abstract submission to PVSC2015 was getting closer and I was suggested to send an abstract and to write a paper about my results. This gave us the kick for taking a closer look to what I really had done so far. For the paper we decided to compare three films annealed together. One sample should be only Cu-rich CZTS, one should have a ZnS top layer and the third one a ZnS bottom layer. The attempt was to discriminate the effect of changing the stoichiometry from that of preventing S and SnS evaporation during annealing. Making these samples was very challenging[1] how could I manage to deposit three CZTS similar layers and two similar ZnS layers? Reproducibility was still an unsolved issue and controlling the thickness was difficult.
I wanted to add 80 nm'*s* of ZnS to a 500 nm CZTS layer, which seemed to me to be a good guess on how much ZnS we should add in order to target an active composition with 1.7<Cu/Zn<1.9. I had to minimize experimental errors. Using substrates small enough (10×5 mm^2) it was possible to deposit two samples at the time (the heater is 1 cm^2).
After I got an estimate for the deposition rates of ZnS and CZTS, I took the following strategy for the depositions:

- #1 deposition run: only one substrate inside the camber, deposition at 300°C of the CZTS layer (500 nm expected) for the Mo/CZTS/ZnS sample.

- #2 deposition run: adding a second substrate right aside the first one,

[1] And indeed, I failed

deposition at 300°C of the (80 nm expected) ZnS layer on both the samples, to fabricate in one step both the top and the bottom ZnS layer.

- #3 deposition run: removing of the Mo/CZTS/ZnS sample and deposition in one step of the CZTS layer for both the Mo/ZnS/CZTS and the SLG/Mo/CZTS samples (laser energy, p.r.r. and deposition time as used in #1)

The obtained films were analysed with XRD, Raman and SEM imaging, both top view and cross section. The first thing that came out was that the thickness was quite off with respect to what expected. The CZTS layer made in run #1 was 500 nm thick, but the CZTS layer deposited in #3 was only 250nm. How could that happen? Well...I did not clean the view-port after every deposition run, so coating set up during the first two deposition runs, and the third layer was done at a much lower fluence and hence lower deposition rate.

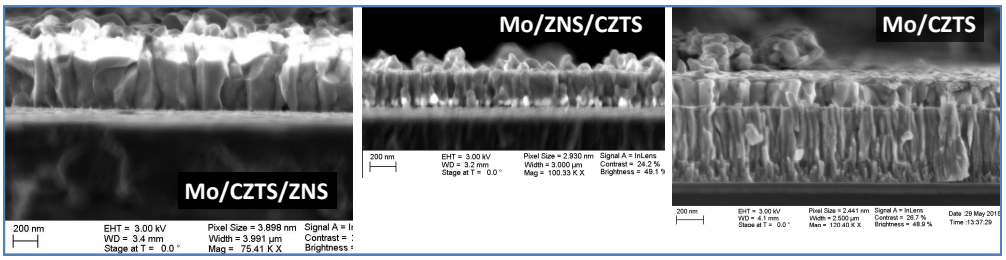

Figure 3.2: SEM cross sections of the samples prepared for this study after the annealing at 560°C in sulfurized atmosphere. The bright layer in (I) and (II) is ZnS that did not react with the CZTS. These images were taken by bachelor students at Nanotech, as part of their Bachelor project.

3.3 Conclusions

We have learnt that, if you add enough ZnS to your *randomly-made* CZTS films, the XRD pattern will show you the signature of CZTS. Which is also that of ZnS, and of CTS, and of many more other secondary phases. You may enjoy not seeing CuS_x anymore, but your films are not going to be of any use for making solar cells. This chapter was about mistakes, and so are the conclusions.

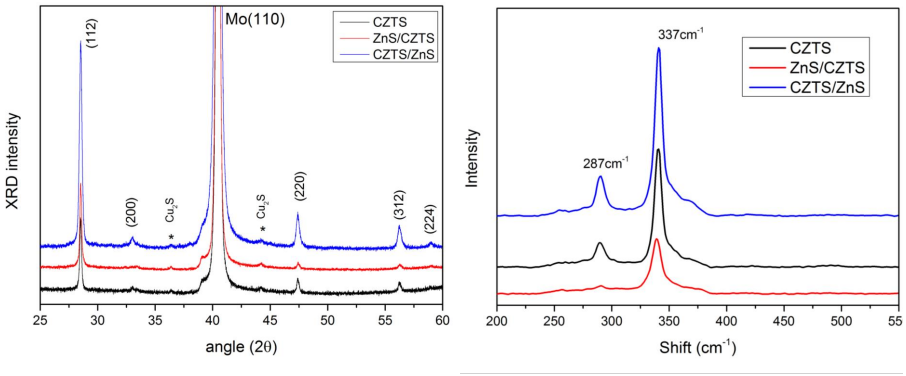

Figure 3.3: XRD pattern (left) and Raman spectra (right) of the samples shown in fig. 3.2. The XRD patterns have been normalized with respect to the Mo peak, as described in the paper to account for the different thickness of the samples. At the time of writing, I cannot explain what was my idea behind doing so, but it was certainly wrong.

First mistake: Adding complexity (ZnS top layer) to a process that was already not well understood/reproducible. The idea was very difficult to realize experimentally in a reproducible way, due to window coating. Moreover, it was also time consuming, since our chamber does not have a fast entry for the substrates nor a multiple target holder. I had to break vacuum twice for every sample. It would take two days to fabricate a (non-reproducible) sample of just 1 cm^2.

Second mistake: Not using the proper techniques (SEM and Raman from the start) for investigating the samples, followed by overlooking the easiest hypothesis: ZnS segregation. ZnS is known for being a very stable compound, therefore one must suspect that Zn will not incorporate into the CZTS layer, but rather segregate as ZnS secondary phase. Unfortunately, instead of checking this first, I spent a long time only looking at the XRD patterns of these bi-layered films, not aware of what their morphology was. I took a very inconclusive study on the annealing parameters (temperature, pressure, amount of sulfur, time), where the only tool for evaluating the results was XRD. A huge waste of time and work.

Third mistake: I will do it myself, no matter what. I should have asked Andrea Crovetto for Raman and SEM analysis well before the time I finally did it. I was reluctant because I knew he was working hard on the other layers [2] and, to both of us, that was the priority. I thought I could get away

[2]Plus, we work in two different departments 40 km away from each other. I told myself: "what is the use of only having just a few analysis here and there, if it cannot be made

with only doing XRD by myself, at the end for detecting $Cu_{2-x}S$ phases XRD is enough, isn't it?

systematic?"

Part II

Research activity

Chapter 4

Breakthrough!

Somehow,
I have to make this final breakthru.
Now!
Freddy Mercury

This chapter is dedicated to an experimental result which I did not have time to investigate in further detail, to my great regret. It was undoubtedly the most important result for my phD, after which the fluence dependence of the atomic composition of CZTS films became immediately clear, even before taking the rest of the experimental data. The rest of the chapter is dedicated to our in-house solar cells.

4.1 July 2015

It was July, 2015, right after the end my second year as PhD student. My results were going absolutely nowhere. Best case scenario I was going to finish my PhD with few useless papers on the deposition rate of CZTS with PLD. Or I would quit my phD, maybe a more dignified conclusion. But then, all of a sudden, within one month, we had our first working solar cell and the fluence plot was fully disclosed. So, what happened? I was perfectly clear that those Cu-rich films with huge droplets would have never led anywhere. Thus, I decided to lower the fluence below the "ablation threshold" and see what would come out of the "incongruent evaporation regime" [50]. Indeed, the main goal of lowering the fluence was to eliminate the droplets. Lowering the fluence often reduces the number of droplets, it was even mentioned in

one of the very few papers on PLD of CZTS [76][1].
The main hurdle brought by droplets is that any meaningful characterization of the films is impossible. One can not even hope that EDX only makes systematic errors if the films are covered with such a random number of droplets of size from 500 nm to 2-3 μm of diameter.
There are several warnings against doing PLD near or below the "ablation threshold":

- the transfer may be non-stoichiometric (but it wasn't already).
- the deposition rate drops considerably, probably a couple of hours for depositing a 100 nm thick film.

To cope with the low deposition rate, I completely removed the aperture used to shape the laser beam before focussing (Figure 5.6) in order to maximize the energy on the target, and brought the focal lens as close as possible to the quartz viewport, in order to de-focus the beam and get the biggest beam spot. Pulse repetition rate was set to 20 Hz, let it be a drastic change. I did not even try to guess what the spot size was, but the fluence was definitively lower than ever used before: the plasma plume was barely visible, but still narrowly forward directed. During the deposition, the visible part of the plume extended to maximum 1 cm over the target.
When I measured the thickness of the film with the Dektak profilometer, I could not see any droplet at the optical microscope. Excited for having apparently solved the issue with droplets, I gave the sample to Andrea Crovetto to take some good SEM pictures and EDX data. The result was a big surprise: a perfectly smooth, droplet-free and Cu-free film, as shown here in Figure 4.1. EDX could not detect any signal from the $Cu_{K\alpha}$ transition. This was a real breakthrough.

First, it was demonstrated that the laser pulse was inducing different ablation[2] mechanisms (and ablation rates) upon hitting onto different phases. This was something that I was convinced of, but could not demonstrate anyhow. The question if in this case we have laser ablation or laser induced evaporation is discussed later in Section 6.1, where it will be argued that it

[1] I did not pay the right attention to this paper before, since it was blended in my personal bibliography with all the other papers on PLD of CZTS, and a coherent synthesis was not possible. My approach was then to discard all of them, as a beginner my filter to select good and bad papers was very crude. Now, I would still discard the other ones, but pay the right tribute to [75] and [76].

[2] It wasn't immediately clear if we were doing laser ablation or just laser induced evaporation. As we will see in Section 6.1, it was laser ablation.

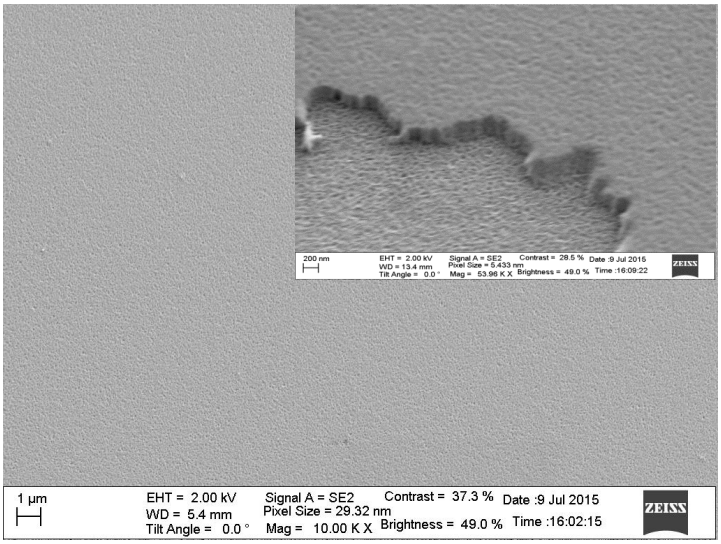

Figure 4.1: SEM images of the droplet-free and Cu-free Zn-Sn-S thin film done at very low laser fluence F<0.2J/cm^2. The composition according to EDX was sulfur 57%, Sn 19%, Zn 24% and Cu 0%. Whether or not one believes the numbers for S, Zn and Sn, one number could be finally trusted beyond any doubt: [Cu]=0%. SEM images courtesy from Andrea Crovetto.

is selective ablation of ZnS and SnS phases.

Second, we could finally achieve Cu-poor precursors by doing PLD at a laser fluence somewhere halfway in the range between "no-Cu-at-all" and "Cu-rich" transfer. The Zn/Sn ratio might still be off the desired range, but that is a minor problem: a Sn deficiency can be adjusted during the annealing by using SnS powder, and a Sn excess should just result in SnS evaporation, as discussed in [22].

Third, fluence control was finally correlated to the most important experimental parameter: precursor composition. If the way forward was to balance ablation of different phases at once, the first experimental challenge was to achieve an extremely tight control over the laser fluence. The good news was that there was no need to go for high fluence, even better: low fluence was needed. I could (I had to, see the next chapter) work with a dirty viewport: the cleaning days were over!

4.2 Our first solar cell

Few weeks later came our first 2.1% efficiency solar cell. The progress was striking. I made a couple of films in the fluence range where Cu-poor com-

positions could be expected and EDX confirmed that the Cu/Zn ratio was finally Cu/Zn<2. I still did not trust EDX in assessing the precise value of this ratio, but sure there was less copper here than in any previous film. There were still a few, small droplets, but nevermind a few droplets. Thus, we attempted an annealing with one sample, named optimistically SC01 (solar cell #1): 560°C for 10 minutes, same graphite box as usual, and 200 mg of sulfur powder. Then, the samples were given to Andrea Crovetto to have some SEM images [3]. The morphology seemed to be perfect, as well as the Raman spectrum, shown here in Figure 4.2. We decided right away to try to make some solar cells. Luckily, there were three more "SC01" samples which I have not annealed yet [4] .

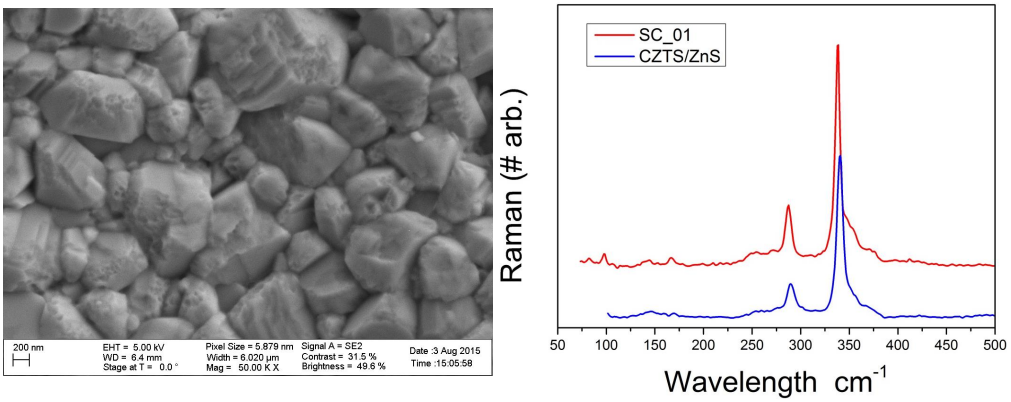

Figure 4.2: Left: Top view of the Cu-poor SC01 film after annealing. Right: Comparison of the two raman spectra. The blue line is from the previous work with CZTS/ZnS top layer, after KCN etching to remove CuS_2 phases, the red line is the raman spectrum of the annealed SC01. SEM images and Raman courtesy from Andrea Crovetto.

Bearing this in mind, I had put four 1×1 cm^2 substrates at once onto the substrate holder, in order to have samples ready if we wanted to make solar cells after seeing something promising. In Figure 4.3 the position of the samples with respect to the deposition area can be inferred. In Figure 6.5 one can estimate how much non-homogeneous could the samples have been. Thus, all the three SC01-samples left were annealed at once under the same conditions and Andrea Crovetto completed the solar cell by depositing the CdS buffer layer and the Transparent Conductive Oxide (TCO) layer, which

[3] I still remember when, a few days later, he called me asking if I had stolen some CZTS from IBM's laboratories, or what the hell I had done.

[4] Methodological note: the Chemical Bath Deposition (CBD) of CdS must be done right after taking the samples out of the annealing furnace, a few minutes later is the maximum delay time. Thus, the samples used for characterizations, like SEM, Raman, PL and so on, cannot be subsequently re-used for making solar cells.

was a double layer of i-ZnO/Al:ZnO. Before choosing the spots where to make the solar cells (it was a hand-made scribing process, with Ag paste for the top contact, Figure 4.9), he took a PL mapping study, shown here in Figure 4.3. Unfortunately, due to mild exfoliation of the CZTS during the annealing, Figures 4.5 and 4.6, it was not possible to make solar cells on most part of the samples. Only one tiny corner offered a suitable spot, where such problems were not visible (arrow in Figure 4.3).

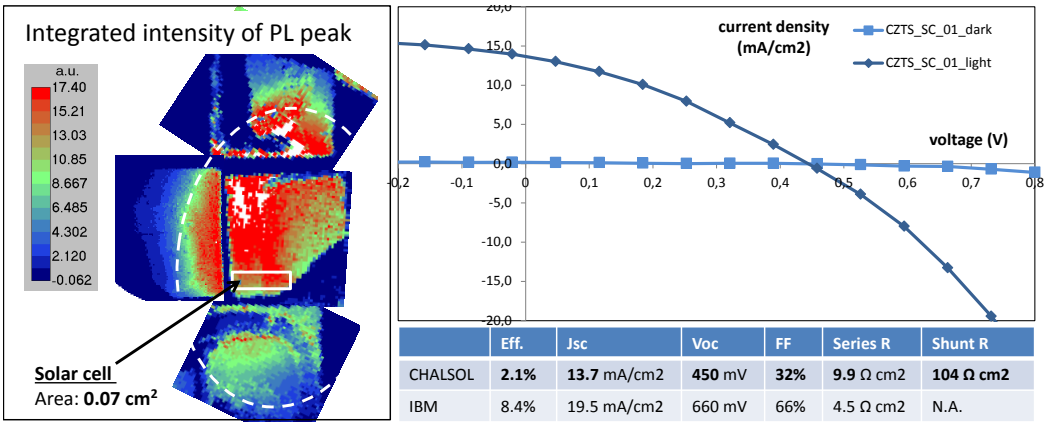

	Eff.	Jsc	Voc	FF	Series R	Shunt R
CHALSOL	**2.1%**	**13.7** mA/cm2	**450** mV	**32%**	**9.9** Ω cm2	**104 Ω cm2**
IBM	8.4%	19.5 mA/cm2	660 mV	66%	4.5 Ω cm2	N.A.

Figure 4.3: Left: Photoluminescence (PL) intensity map of the deposited samples. The position of the samples reflects their position in the deposition chamber, and the white dotted ellipse indicates the area of the deposition (see also Figure 6.5 for further details). Due to exfoliation (see Figure 4.5 and discussion therein) the device could not be fabricated in the area with highest PL signal. NB: the color scale in figure is related to the signal intensity at the wavelength of 900 nm, where the PL spectrum has a maximum. On the right side, the JV curve of the solar cell device under AM 1.5 illumination and in dark, pg. 13. The diode parameters are indicated in the table together with those reported by IBM for their record device. At that time we did not have any equipment for EQE measurement. The discussion on the JV curves is postponed to Section 4.3. PL map and JV curves courtesy from Andrea Crovetto.

In Figure 4.4, the cross section of the full solar cell fabricated and the top view of the sample after chemical bath deposition are shown. The cross section shows a very good, compact morphology and no obvious segregation of secondary phases are seen at the back contact. However, the CdS layer suffers from many pin-holes, which should not appear. The origin of these pin-holes can only be speculated, but two factors may have played a major role: the use of an "old batch" of ultra-pure water for the CBD solution and the long bath deposition time of 20 minutes. This was intended: we wanted to obtain a better coverage by increasing the deposition time, at the expense of optical absorption. It seems, however, that films deposited by CBD may start to peel off if the films grow too thick. These pin-holes were a problem

for few following months and eventually almost disappeared after improvements in the CBD process, *i.e.* better temperature control of the solution, use of a shorter deposition time (10 minutes) and of a new, certified, batch of ultra-pure water.
The CdS buffer layer was not the only thing that went "wrong" with our first solar cell. As mentioned, all the SC01 films suffered from exfoliation after the annealing and only a minor part at the periphery survived the CDB process. In Figures 4.5 and 4.6 some examples of exfoliated samples. The cross section in Figure 4.5 is taken in proximity of a "flake like" irregularity indicated by the yellow arrow in the image aside. From EDX and Raman measurements on some of the exfoliated material we can conclude that those flake-like structures were SnS secondary phases segregated at the bottom. These are known for having such morphology and have already been reported even in high efficiency CZTS devices [73]. Exfoliation has been a major problem for us for several months, and we did not easily realize that thickness of the CZTS was the most important parameter. Indeed, this problem is scarcely mentioned in literature, even if, as a matter of fact, very few groups report CZTS solar cell devices with absorber layer thicker than 700 nm[5]. At first, we thought it was related to SnS secondary phases or to some problems related with the deposition of the Mo substrate. Shortly after that we figured out that the problem was mainly related to the thickness of the CZTS precursors, a paper from IBM came out, where, in a very minute comment, it was mentioned that "a thickness below 800 nm .. to avoid exfoliation.."[34]. Just a bit too late.

4.3 Our second solar cell

After the achievement of the 2.1% solar cell at fist try (with the new Cu-poor precursors) we were expecting big improvements quickly. All the subsequent attempts, however, resulted mostly in failures. Exfoliation was the major problem: many samples did not survive the annealing. A few solar cells reached around $\sim 1\%$ efficiency, still not good enough. It took us four months before we managed to fabricate our second solar cell with a record 2.6% power conversion efficiency, in November 2015. It happened after realising that we needed to make thinner films in order to avoid exfoliation. In Figure 4.7 and **??** are shown the JV curve, the External Quantum Efficiency, and the cross section of our new record device. As can be seen from Figure 4.8, the thickness is significantly lower than our previous device. The morphology is compact, even though grains do not seem here to extend from bottom to top,

[5]Even more, we were really wondering what kind of top secret physics was the reason.

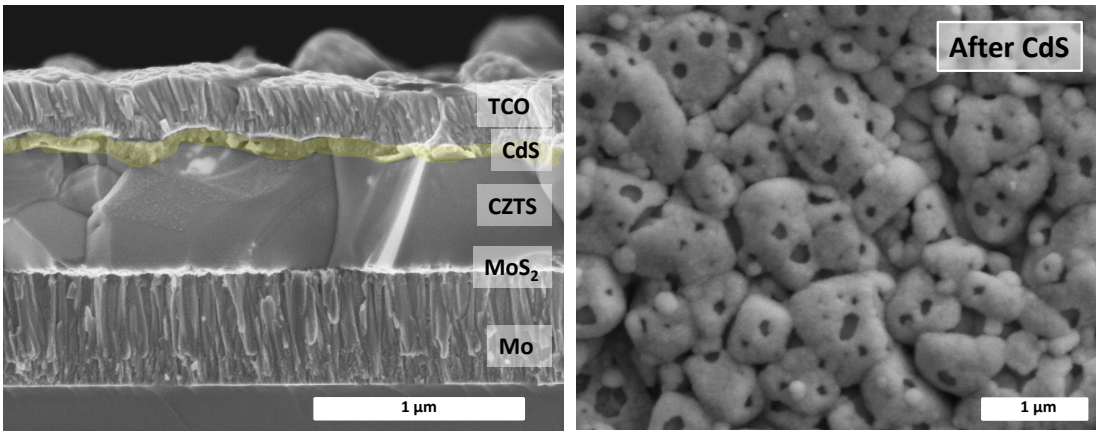

Figure 4.4: Left: Cross section of the 2.1% efficiency solar cell, with corresponding layers aside. Note the compactness of the CZTS film. Enlightened in light yellow the CdS buffer layer. Right: Top view of the CdS buffer layer. The large amount of pin-holes in the layer are probably responsible for several problems in our first device. SEM image courtesy from Andrea Crovetto.

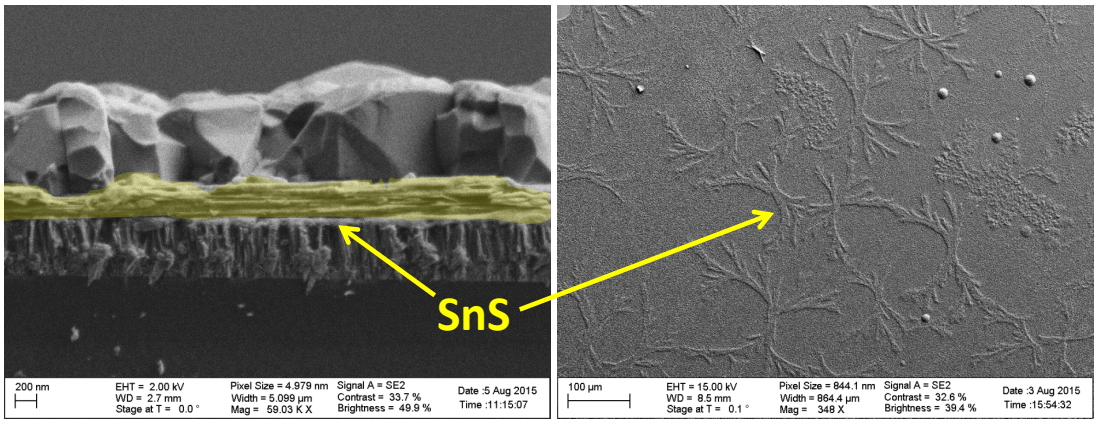

Figure 4.5: On the left, a cross section of the sample SC01 in proximity of a "flake-like" irregularity. A SnS secondary phase (highlighted in yellow) is clearly segregated at the back contact and is responsible for the strange morphology seen from the top view, image on the right. The identification of the phase as SnS is drawn after Raman and EDX measurements. SEM images courtesy from Andrea Crovetto.

but rather form a bi-layered CZTS. This is quite unusual with respect to the standard morphology that we see for our annealed CZTS, which resembles more the one shown for SC01.
From a comparison of the JV curves we can see that, owing to a lower thickness, the short circuit current collected by the SC016 solar cell is inferior to that of the previous device, while the FF and the V_{oc} are significantly

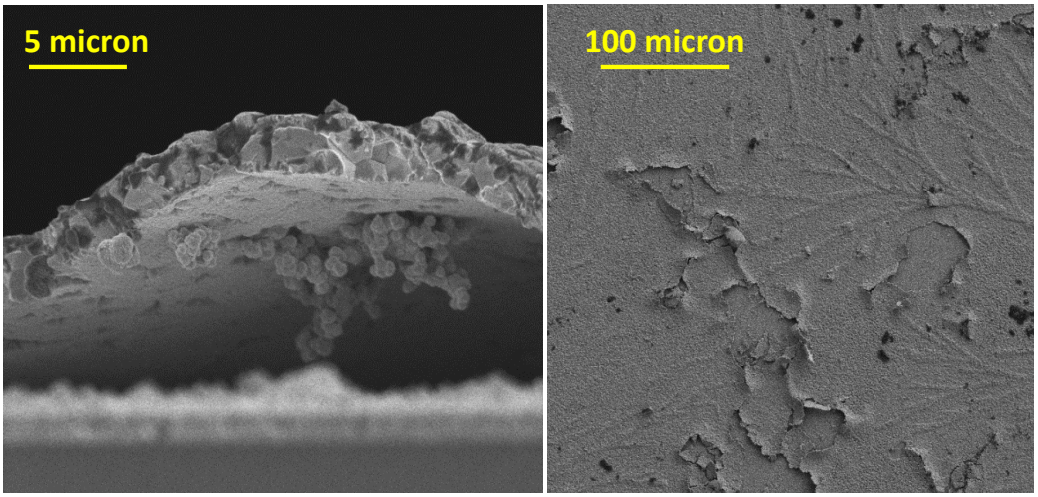

Figure 4.6: SEM images of exfoliation after annealing . In some cases both the CZTS and the Mo layers exfoliated, leaving nothing but a piece of glass with some dust on top. Exfoliation of CZTS is barely mentioned in literature, but, as a matter of fact, few groups report making CZTS solar cells with thickness significantly greater than the limit above. The extent of this phenomenon depends, to the best of our experience, other than CZTS thickness, on annealing temperature, and amount of sulfur in the graphite box. As said in the text, it took us several months before we realized that the thickness of the CZTS precursors was the major problem. SEM images courtesy from Andrea Crovetto.

improved. Note also that the dark-light crossover (the point where the dark and light curves intersect) is also improved, as consequence of a better behaved dark JV curve for the SC016 device. In fact, for an ideal device, the dark and light JV curves should be nothing but the same curve translated by the amount of the short circuit current collected under illumination. The crossover point would then be very far from the V_{oc}. If we look at our first device, SC01, the dark JV curve looked more like a straight line rather than the solution of a diode equation. We explain this huge difference between the dark and the light JV curves of SC01 to be due to an anomalous behaviour of the CdS junction under dark conditions. Indeed, CdS electrical conductivity is light-dependent, where light-activated defects increase the conductivity. For a well behaved CdS buffer layer this difference should not be so large, but clearly SC01 did not have an optimal CdS. Regarding SC016, the dark JV curve shows a reasonable diode behaviour, indicating that the CdS has improved its quality. This is confirmed by SEM images, shown in Figure 4.9, where it is possible to see that the density of voids has been significantly reduced (although some voids are still visible). From the EQE, Figure 4.7, it is also possible to see that the CdS buffer layer induces light-dependent junction properties, as the collection efficiency of the solar cell increases sig-

nificantly at 600 nm, showing that sub-bandgap[6] light-activated defects play a significant role in modifying the diode behaviour. This can be seen from the fact that this EQE curve is taken without any light bias during the monocromatic measurement, as usually done. Unfortunately our setup does not provide this extra feature. Regarding the strong cut-off for wavelengths below 550 nm, we note that the CdS layer in our device has a thickness of about 90 nm, which explains why the optical losses are so important, if compared to state-of-the-art devices.

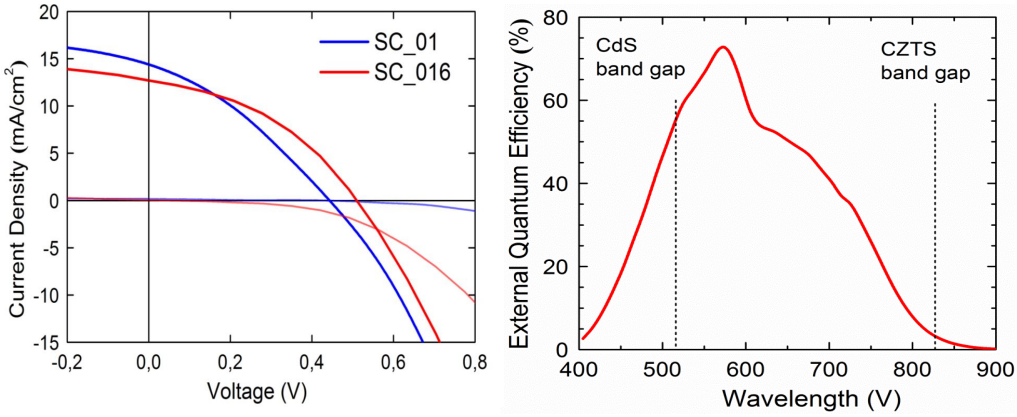

Figure 4.7: Left: light and dark JV curves of the η=2.6 device (SC016, red lines) compared to our previous η=2.1 device (SC01, blue lines). Right: EQE curve of the SC016 device, taken without light bias. JV curves and EQE courtesy from Andrea Crovetto.

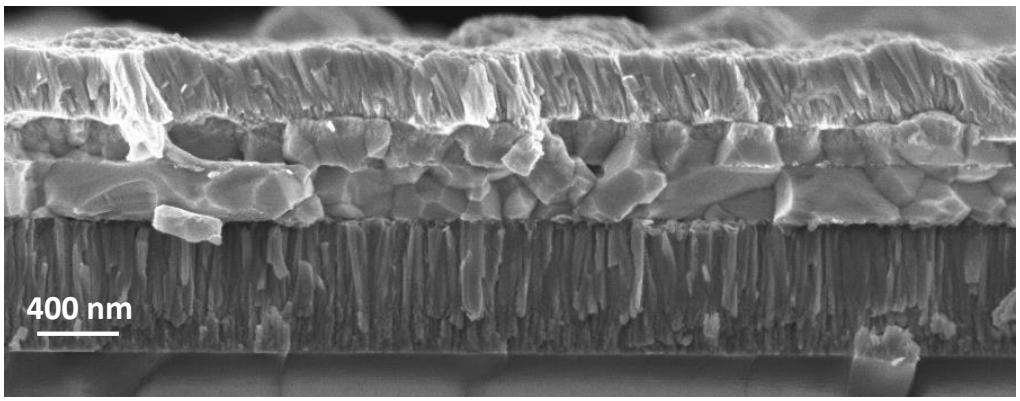

Figure 4.8: SEM extended cross section of our in-house champion device. SEM image courtesy from Andrea Crovetto

[6]CdS bandgap, which is at 2.42 eV (512 nm)

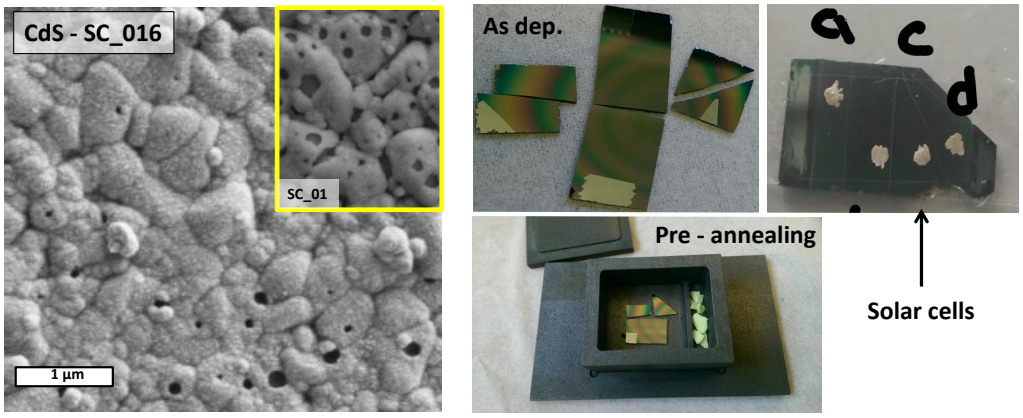

Figure 4.9: Left: SEM top view of the CdS buffer layer (90 nm thick) in the SC16 device. In the inset, a detail of the CdS layer of our first device, same magnification. Right: Collection of images that show our fabrication process, from as-deposited precursors to the final solar cell devices. Note that the precursors are characterized by significant thickenss gradients, as revealed by the optical interference fringes. A quantification of this thickness gradient is given in Section 6.3. SEM image courtesy from Andrea Crovetto.

4.4 The forgotten one

I started this chapter by saying how I very much regret not to have had time for investigating in more details the "most important" experimental result of my phD. So then, what can be interesting about an amorphous film of Zn-Sn-S composition, which, by itself, has no use for solar cell application? Well, it turns out amorphous thin films of chalcogenide materials are very interesting for many advanced applications. Here below some of the highlights, taken directly form the book "Amorphous Chalcogenide Semiconductors and Related Materials", ed. by K. Tanaka and K. Shimakawa, Springer, 2011.

- Infrared transmission is a unique characteristic of the chalcogenide glass.
- The most widely commercialized product using chalcogenide films at present is undoubtedly the optical phase-change disk, named DVD (digital versatile disk).
- Unique photo-conductive properties of amorphous Se have been utilized for a long time. The most known is the xerography, patented by Carlson in 1937, which was commercialized by Xerox Corp in 1950.
- Amorphous solar cells are also mentioned as possible applications, together with ionic memories, ion sensors, and ionic selective membranes for batteries applications.

Beside[7] applications, another fact makes this amorphous film interesting from the scientific point of view: Sn and Zn are two strongly non-miscible metals. The limit of solubility of Zn in solid Sn is below 5%, and vice-versa for Sn in Zn. The situation does not change if the chalcogenides are involved. This means that the amorphous state is the only possible, and that to produce such material with conventional techniques is, probably, very difficult as Sn and Zn would tend to cluster and segregate as the film is deposited. Indeed, the production of this material perfectly suits the features of PLD! Here, I can only show the one measurement I had done, which is the absorption coefficient as function of the photon energy for a 400 nm thick amorphous Zn-Sn-S film deposited on a double-side polished quartz substrate. At least, it confirms that the film is an amorphous semiconductor of the kind described in the book.

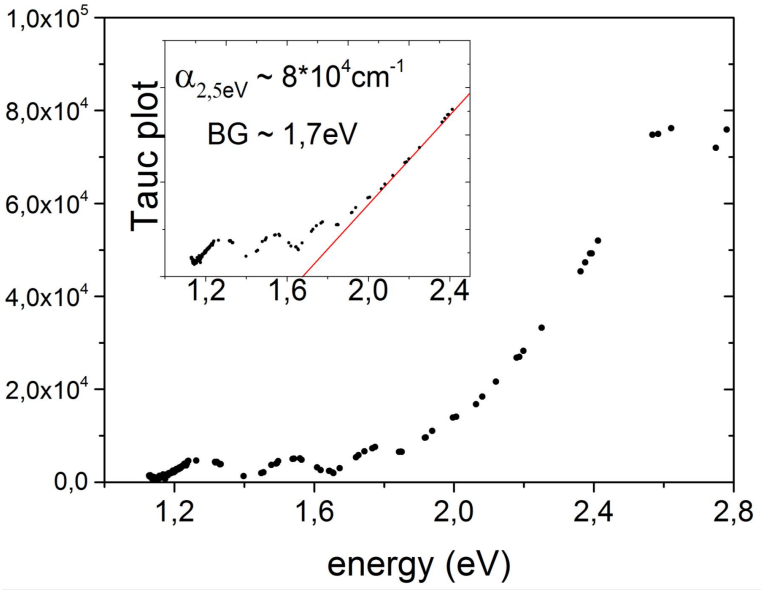

Figure 4.10: Absorption coefficient for the amorphous Zn-Sn-S films deposited on a quartz substrate. A bandgap of about 1.7 eV is extracted from a Tauc plot, shown in the inset.

[7] futuristic

Chapter 5

Guidelines for PLD of chalcogenide targets

This chapter is about experimental practice, which is always improvable. It is a tutorial that explains in detail the experimental method which I developed for this work, and which enabled reproducibility in the PLD of CZTS and CTS materials. The content is related to the particular equipment used and the problems faced. For the rest, there already exist PLD systems for large area deposition, and so do systems for preventing coating of the viewport, although not widely used.

Conclusions: (1) Use the biggest beam size and laser spot on the target. (2) Change the fluence by moving the focal lens closer-further away. (3) Estimate analytically the variation of the beam spot along the whole rastering path. (4) Measure the energy on the target and the transmission at the quartz viewport before and after every deposition (fig. 5.3). (5) Look at the target: the ablated area must look homogeneous (fig. 5.4). (6) Look at the plume: its shape, direction and color must always be uniform during the deposition. Check every film right after making it, do not make 10 films in a row and post-pone the analysis.

5.1 Choice of the laser

The laser and the target are the first things to look at when one starting a PLD experiment. Let us start discussing some aspects related to the laser. Needless to say, the choice of the laser, and how to operate it, is connected with the properties of the target to be used. Light-matter interaction determines the properties of the plasma and hence of the films deposited. We

could use two UV lasers: a solid state Nd:YAG laser, with fundamental mode at 1064 nm up-converted to 355 nm and a KrF excimer laser working at fundamental wavelength of 248 nm. The properties of the two lasers are summarized in Table 5.1. In general, the shorter the wavelength, the higher the absorption coefficient; for this reason UV lasers are generally preferred to IR-vis lasers.

5.1.1 Nd:YAG laser

This solid state laser produces a Gaussian mode at the fundamental wavelength of 1064 nm, which is up-converted to 355 nm. This up-conversion process in general goes along with the generation of higher order harmonics, influencing the beam profile. Although it was not possible to measure the beam with a beam profiler, some rings of higher order modes could be seen with the help of optical paper in the far field mode. Thus, before focusing on the target, the laser beam was let through a circular aperture of 7 mm diameter (about 0.4 cm^2), to cut-off as much as possible of these unwanted higher order modes. The pulse-to-pulse stability can be rated to about 20%, as measured by our power meter.
The use of this laser may not be optimal for the ablation of high bandgap semiconductors or insulators, since the wavelength of 355 nm is associated to a photon energy of 3.49 eV, and can below the absorption edge of the material under investigation. In relation to this work, we note that 3.49 eV is just below the bandgap of ZnS, which is 3.54 eV. For laser ablation of the CZTS target, which has plenty of grains with ZnS phases, this means that light absorption will be less efficient, leading to preferential absorption/ablation of other phases. For laser ablation of the CTS target this problem does not arise, as all the Cu-Sn-S binary and ternary phases have a bandgap well below 3.5 eV. For this reason, the use of this laser was mostly dedicated to the study of CTS and other Cu-Sn-S materials, as presented here in Chapter 6, and in our works [6, 2].
As the last point, the pulse width of the Nd::YAG laser is 7 ns, about 3 times shorter than the KrF laser, leading to 3 times higher intensity for a given value of the fluence. If uniform heating of different phases is desirable, then shorter pulses (considering the ns range) are not the first options, as the faster heating process will stress out markedly the differences between phases with different thermal properties.

5.1.2 The KrF excimer laser

The 248 nm excimer laser does not produce higher order harmonics, as it works directly with the fundamental frequency. The beam profile is a top-hat with a beam width of several cm and pulse-to-pulse stability about 10%. The pathway between the laser and our PLD chamber is of several meters with 3 high-reflective mirrors used to steer the beam direction to the chamber. This optical path leads the beam to experience a 40% overall energy loss and to become more Gaussian in distribution and with a wider beam waist. Thus, before focusing the beam into the chamber it was let through an aperture of 1.0×1.5 cm^2, positioned to capture the original "top-hat" part of the beam and to cut-off the low energy edges. Care must be taken when focusing a top-hat beam. Unfortunately there are no closed solutions for the propagation of top hat beams, numerical analysis is required for any specific case [74]. Briefly, lenses are Gaussian passive optical elements, meaning that a Gaussian beam passing through maintains its Gaussian profile. Gaussian beams are the ones with minimum divergence and are more robust to focus. A top hat beam is not a Gaussian beam and has a worse divergence, such that after focusing the beam profile may become shattered and develops many fringes of high/low intensity contrast[74]. In practice, all these problems become relevant for beam profiles very close to a step-like function or when the beam waist is focused down to a size comparable with the wavelength. In our case here, with a beam waist focused down to a maximum of 1 mm^2 and a wavelength of 248 nm, these problems should not matter. But, at least, the beam at the target cannot be considered a top-hat, rather a gaussian-like beam.

Laser	wavelength nm (eV)	Width ns	Beam profile	Fluence mJ/cm^2	Stability
KrF	248 (5.0)	20	Top hat	50	10%
Nd:YAG	355 (3.49)	7	quasi-Gaussian	200	20%

Table 5.1: Laser parameters, Nd::YAG vs KrF excimer laser. The fluence value reported is the beam fluence right before being focused onto the target

5.2 Laser alignment

Here I will describe the procedure to align the laser and the set of parameters needed to fully characterize the laser beam at the target surface.
Safety warning: If you are working with a material that induces strong coating on the viewport, there will always be a component of the incoming laser beam that will be reflected back. Never forget that this component has passed through a focal lens, so it is a converging beam. Avoid perfect normal incidence for the beam to the viewport and make sure that the reflected component is absorbed by a shield.

Laser output mJ (/kV)	Aperture cm^2	Energy after aperture - mJ	Lens f cm	Lens-target cm	On target mJ
300 (19-21)	1.0×1.5	68-72	75	60-70	24-36

Table 5.2: Set of parameters used to characterize and reproduce the KrF beam at the target surface.

Right before being directed onto the target by the rastering mirror, the laser beam passes through an aperture that gives it a definite beam profile. This aperture must be carefully centred to the beam intensity profile. In order to do so, one must make visual the beam intensity profile. I used a yellow post-it covered with semi-transparent tape: after several shots a slightly burned profile appears on the tape, indicating where the beam intensity profile has a maximum. Using common optical paper for imaging would not work, it is far too sensitive and the blackened area extends over a much larger area. Same problem occurs if one the use of a fluorescent screen is attempted, e.g. an aluminum foil. At first I tried to align the laser and the aperture by maximizing the energy flux through the aperture, but ultimately it is very difficult to use the power meter as feed-back monitor while adjusting micron-precision aligned mirrors. I recommend to "burn" the post-it.
After getting the beam aligned it is a good practice to measure the energy right after the aperture and to always check that the energy flux is still the same before starting every deposition. Otherwise the beam must be realigned. Never change the laser parameters, setting a different energy output (or HV) would alter the time width of the pulse and the beam divergence, as discussed in [62]. The same goes for cutting the energy with passive optics such as glasses, since these tricks can induce thermal focusing and are anyway not easy to reproduce.

5.3 Target morphology

Two sintered targets from Testbourne Ltd were used, one stoichiometric CZTS target (powder ratios 2CuS:ZnS:SnS) and one stoichiometric CTS target (powder ratios 2CuS:SnS). Due to the complexity of the Cu-Sn-S system, it is not possible to fabricate single phase targets. The targets from the sintering process are multi-phase and multi-crystalline in nature, as can be seen in fig. 5.1 and with the help of XRD.

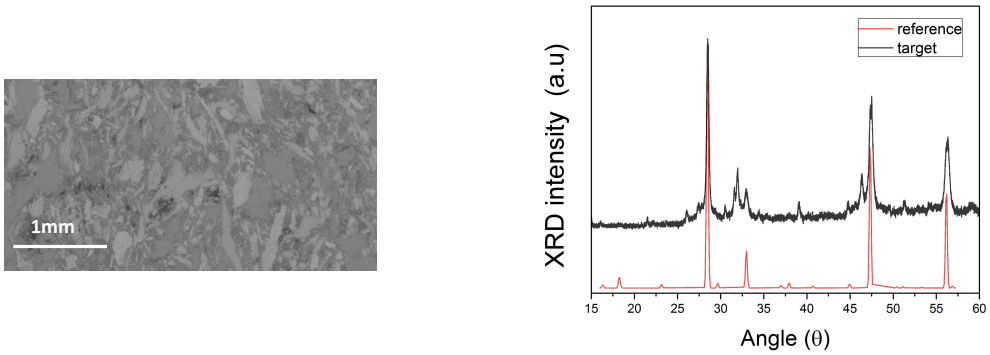

Figure 5.1: Left: SEM image of the CZTS target before ablation. Clearly visible its multi-phase morphology, with different grains extending for hundreds of μm. Right: XRD pattern of the CZTS target, with other peaks clearly not belonging to CZTS (reference is CZTS pattern). The same multi-crystalline morphology is seen for the CTS target.

The detailed discussion of the interaction of such multiphase targets with the laser pulses is given in the following chapter, in relation to the discussion of the non-stoichiometric transfer. From a general point of view, when one is confronted with targets like this, there are few considerations to keep in mind. The beam spot on the target must be big enough to sample a statistical relevant portion of the target. In this case a spot of about 1 mm^2 is the minimum dimension one can afford to use. If the different phases have very different melting and boiling point, one should expect in general a non-stoichiometric transfer. If material removal from the target is phase-selective, stable conditions cannot be reached. In case one wants to refresh the surface of the target, I suggest to use a sharp blade and to mechanically scrape-off the ablated surface. The use of sanded paper should be avoided, as there is a risk of contaminating the target surface with left-overs from the paper. If one still uses sand paper, rinse the target afterwards in ultra pure water using the ultra sound bath. These targets are soft and porous.

5.4 Rastering design

The rastering design is not trivial, as it has to address all the problems anticipated in section 0.4.2, i.e. fluence drop as consequence of window coating, target damaging and ejection of droplets. We stress that the key to achieve reproducibility is to minimize everything that alters the fluence.
Summing-up: a simple line-scan is the best rastering strategy, with a small compromise to stay on the depositing area. Coating of the viewport cannot be avoided, but transmittance reaches a stable value when, for each pulse, laser removal of the coating is equal to the added coating material.

5.4.1 Beam Stability

PLD problem #1: small area coverage

For making solar cells it is very desirable to deposit uniformly over the largest possible area, since much can be learnt by comparing the performance of different solar cells made in the same processing batch. In our setup the substrate is fixed in front of the target, therefore, in theory, the largest area coverage has the same extension of the target, $\sim$4 cm^2. In practice, it is much less.

In principle, the maximal coverage could be achieved by rastering the laser beam uniformly all over the target, with a 2D rastering system. However, we must consider that the beam is impinging on the target at 45^o deg. incidence, so rastering in one direction (Horizontal) is not equivalent to rastering in the other one (Vertical). When the beam is rastered in the direction where the target is tilted by 45^o, the laser spot on the target also changes, as illustrated in Figure 5.2 (Left). How much does the spot change from one end to the other of the target? It is indeed very much. In Figure 5.2 (Right) this variation is calculated for our system as a function of the Lens-to-Target (L-T) distance, see the caption for details. The variation is always significant and never below 10%. It becomes very relevant ($>$ 20%) when the L-T distance approaches the focal length. In particular, at the L-T distance of 62-64 cm, which we used for producing our best solar cells, the variation is above 20%. It is very clear from these numbers that, in order to obtain careful control over the laser fluence, the rastering can only be done in the vertical direction, where the target does not introduce any extra component L2 to the optical path L1[1]. One could still think of keeping a "small" horizontal component

[1]To be extremely precise there is still an extra component to the optical path, say L3, when doing vertical rastering, but this contribution is negligible, as $L3 = \sqrt{L1^2 + \frac{D}{2}^2}$ and $L1 >> \frac{D}{2}$.

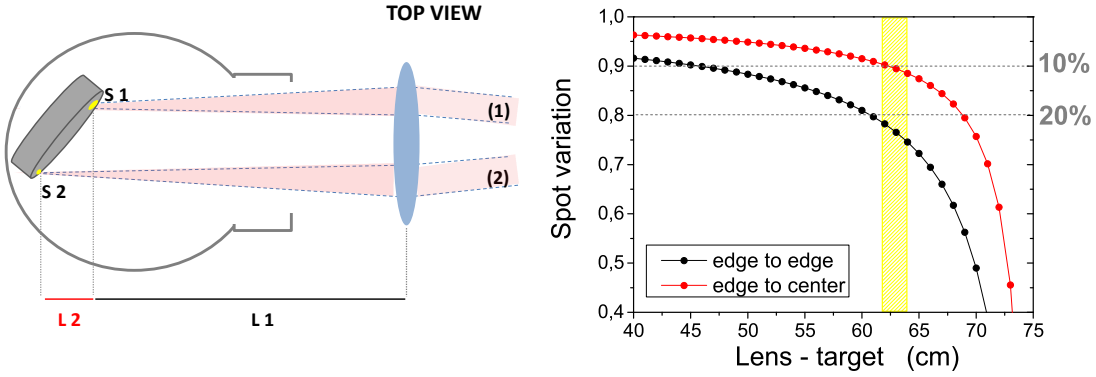

Figure 5.2: Left: Change of laser spot on the target as consequence of rastering along horizontal direction. The two beams (1) and (2) are directed from the lens to the target in the vacuum chamber. The optical path of beam (1) is L1, while beam (2) has to travel a further L2 distance introduced by the target-beam angle of incidence of 45^o. For our case of $2.5cm$ diam. target, this component is: L2 = 2.5 cm $\times\cos(\frac{\pi}{2}) \sim 1.7$cm.
(Right): Spot-size variation S2/S1 as function of the lens to target (L-T) distance if rastering in the Horizontal direction (from S1 to S2). The numbers are calculated using linear optics equations for a beam of 15×10 mm^2 and a focal lens with $f = 75$cm, as in our system. The yellow shaded region indicates the "sweet range" for optimal Cu-poor CZTS. The red dots indicate the variation if the H-rastering is limited to half of the target (edge to center). A variation $\geq 10\%$ in the "sweet range" is still expected.

along with the full vertical scan as compromise between controlling the fluence and covering a larger area of the substrate, but new factors come into play and rule out this option. First, the minimum significant horizontal displacement of the beam on the target is about 1 cm, which would introduce a $> 10\%$ variation on the fluence, as seen from Figure 5.2 (Right). This is so because 1 cm is roughly the plume size at the substrate, as can be seen by measuring the thickness profile of the samples fabricated, see fig. 6.5. The two other reasons are covered in the next paragraphs.

PLD problem #2: window coating

Due to volatile components in the target (S, SnS and ZnS), window coating is very harsh and gets responsible for as much as 70% absorption of the laser energy at the quartz viewport, as shown in 5.3. If we worried about a 20% fluence variation due to a change in the spot size, a loss of more than 70% of the laser energy during a deposition run is even worse. Since coating cannot be avoided[2], we must at least make sure that coating effect is very uniform

[2]Unless one makes use of mechanical wheel filters triggered by the laser pulses, but it was not a compatible option with our small deposition chamber

during the whole deposition time and throughout the whole laser rastering path. First, we notice from Figure 5.3 that the transmission drops regularly over time, but eventually reaches a stable value. As consequence: **do not clean the viewport!**
When the quartz window is very clean, the transmission loss rises very fast as the window gets gradually coated. However, the thicker the coating grows, the more it absorbs the laser light and at some point the energy absorbed is large enough that "laser cleaning" sets in and a balance is reached between how much coating there is deposited and how much material there is removed. Locally this "cleaning effect" is related to the number of laser pulses per unit time. On the other hand, the coating effect is just proportional to the total number of pulses on the target. Thus, if one uses a complicated rastering path, one cannot make sure that all the local points will experience the same balance condition and cannot ensure uniform transmission.

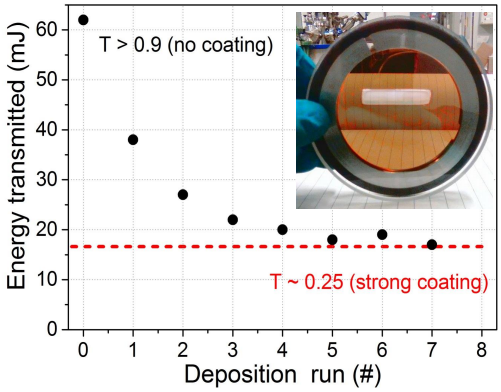

Figure 5.3: In the plot, the laser energy transmitted through the quartz window as function of deposition run is shown. Each deposition run corresponds to the laser working for 30 minutes at 10 Hz, vertical rastering only. The laser energy right before the quartz window is 68 mJ ±2mJ. The regime of stable transmission is reached after 4 or 5 deposition runs. In the inset, an image of a coated window with stable transmission (T∼ 25%), where the laser "self cleaning" effects are visible.

Given the extent of the absorption, even a small change can have a very significant consequence. This fact lead me to keep the rastering as simple as possible, just scanning the laser along the vertical direction. In this way it is quick to measure the transmission over the full scan-length and after each deposition and make sure that it is uniform. It is a good practice, however, to clean the viewport from time to time, say every 10-15 depositions, as the "laser cleaning" is a rather harsh process that can damage the viewport.

PLD problem #3: droplets

There is also a third reason that contributed to use a very simple rastering path. Due to mechanical inertia in the picomotor actuators that drive the rastering mirror, changing direction requires about 0.5 seconds. During this time the laser is standing still, hitting the same spot on the target. In section 5.3 we have already discussed how bad this can be for the chalcogenide

targets. To minimize this detrimental effect, this "pit stop" should always happen at the outer edge of the target, where the radial velocity is maximal. Actually, on one side I allowed the laser to run off the target, such that it would hit an external shutter, instead of letting the laser hitting on the target on the target, see Figure 5.5. In the table 5.3 below a comparison of the pulse density over different areas of the target. In fig. 5.4 one can see the effect of this phenomenon. For this reason, the simplest rastering path is also the one that allows the user to minimize target damaging.

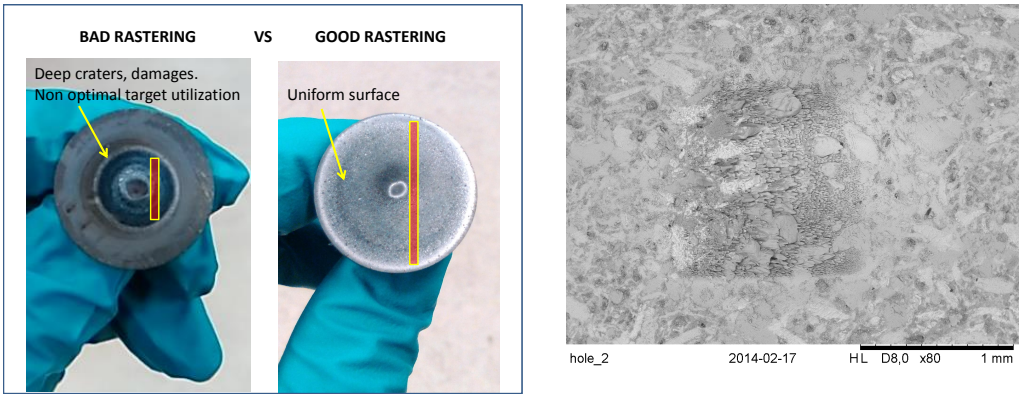

Figure 5.4: Left: Bad rastering VS good rastering. In red is depicted the corresponding rastering path. Note that the laser beam passes right close to the center, but not exactly by the center to avoid target damaging related to excessive $\frac{\#pulse}{u.area \times u.time}$ as discussed in the text. Right: SEM image of target damaging as consequence of laser ablation. The morphology keeps worsening as the number of pulses increases.

5.4.2 Rastering speed

At which speed should the rastering run? Let it be the choice of a simple line rastering path, as in fig.5.4. One can set a uniform rastering velocity $v = v_R$ or a more sophisticated function $v = v(x,t)$. This choice require some considerations, so let us make the example of a deposition which lasts T_{dep}=1 hr at 10Hz pulse repetition rate, with a 2.5 cm diam. target rotating at 10 rpm, as used in this work. If one sets a constant velocity v_R, the local density of pulses on the target will be different, since the radial speed of the target is fastest at the edge and close to zero at the center. In this case, no matter what value for v_R is chosen, the target usage will not be even, and deterioration will be faster towards the center, as shown in table 5.3. On the other hand, setting a velocity profile that sweeps the laser faster when it is at the center and that slows down towards the edges would allow one to obtain a constant pulse density per target unit area. This would be

very desirable, since uneven target deterioration may cause reproducibility problems and droplets ejection. But there are two drawbacks to this strategy: (1) Window coating will also be non-uniform, as the local density of pulses on the quartz window will follow the same variation as that of the rastering velocity. We have seen what a serious threat this can be in the previous paragraph. (2) Due to the narrow plume geometry, the thickness profile of the deposited films will also reflect this non-uniformity, the film growing thicker in correspondence to where the scan speed is lower and thinner vice-versa. As anticipated, one must make a compromise at some point, and here is the point. The target can be refreshed more often to overcome uneven-deterioration, or one can leave with a thickness gradient on the films and perhaps a bit uncertainty over the fluence value. At this point it really does depend on which applications and properties are sought.

zone	radius r_i	area	time	#pulses	pulse density
	mm	mm^2	(s/round)	(/round)	(#pulses/(mm^2*round)
1	10	140	0.1*4+1	14	0.1
2	6	100	0.1*4	4	0.04
3	3	50	0.1*4	4	0.08
4	0	π^2	0.1*2	2	0.22..

Table 5.3: Pulse density on different zones (see figure 5.5 for reference) of the target for rastering in one direction end-to-end of the target. The numbers are calculated assuming constant rastering speed (V_R=20 mm/sec) and a pulse repetition rate of 10Hz, as used in this work. Zones are 2 mm thick circles, "radius" refers to the the inner radius, thus area $= \pi * \left((r_i + 2)^2 - (r_i)^2\right)$. "time" indicates the seconds (/round) for which the laser is shooting onto each zone. Zone "1" has an extra contribution "+1" due the pit-stop time of 0.5 seconds when the laser changes direction (x2/round). Crossing the zone takes 0.1 s each time (x4/round). Zone "4" is a $D = 2mm$ circle centered in the origin, thus $r_i = 0$ and it is only crossed (x2/round)

5.4.3 My choice

My rastering strategy is synthesised in Figure 5.5. Since the laser fluence is strongly related to film composition, which in turn is the most important parameter in CZTS devices, I privileged the fluence control over anything else. Thus, the choice is that of a single line scan with constant rastering speed. Note: from what was said about the window coating, if one wants to change the fluence from one deposition to the next, it only makes sense to change the fluence by moving the lens and changing the beam spot size. In this way, one can be sure that the transmission at the viewport will not

change[3], as well as the energy on the target and, in first approximation, the deposition rate.
Using a constant rastering velocity leads to uneven target usage and deterioration, which becomes critical in the inner area close to the center (circle "3" and inside in Figure 5.5). The target starts to show signs of deterioration after about 10-15 depositions; it must be refreshed with a sharp blade, as discussed in Section 5.3. It is important to not use sanded paper or anything that can leave residues on the target.
As shown, the scan is actually not going from end-to-end of the target. This would have been the preferred choice, but the reduced size of the lens (plane-concave 2 inch. diameter, f=75 cm) was a limiting factor in the maximal scan length achievable[4]. Thus, the rastering scan goes from the top end of the target at r_1 down to a spot located between r_2 and r_3. This second "pit-stop" is chopped by an external shutter, to minimize target damaging.

5.5 Measuring the laser spot size

As critical as the rastering design, a correct measurement of the beam spot on the target is of paramount importance when one wants to "reproduce experiments under the same conditions". We spent a long time seeking a correlation between the fluence and films properties without reaching any conclusion: everything we would measure (EDX composition, droplets size and distribution) did not show any significant trend, only scattered inconclusive results. Indeed, we were using a not-suitable, (although common[5]) technique for measuring the laser spot on the target: the contour of the ablated area on a copper plate. Ideally one would measure the area of the ablated spot on a copper plate and, when in need of reproducing the same experiment after some time, adjust the experimental parameters (lens position, slit aperture) until it gets back with same spot. By doing so, one can be easily off by 30% or more. In fact, the two experimental parameters that can be effectively controlled and reproduced with negligible error are the slit aperture area and the lens-target distance, so only they should used.

[3]The change in beam size at the viewport is not significant (unless one does a very dramatic change in the focusing).

[4]Unfortunately bigger lenses are not readily available for f=75 cm focal length.

[5]as it happens to read in the literature, when even mentioned at all

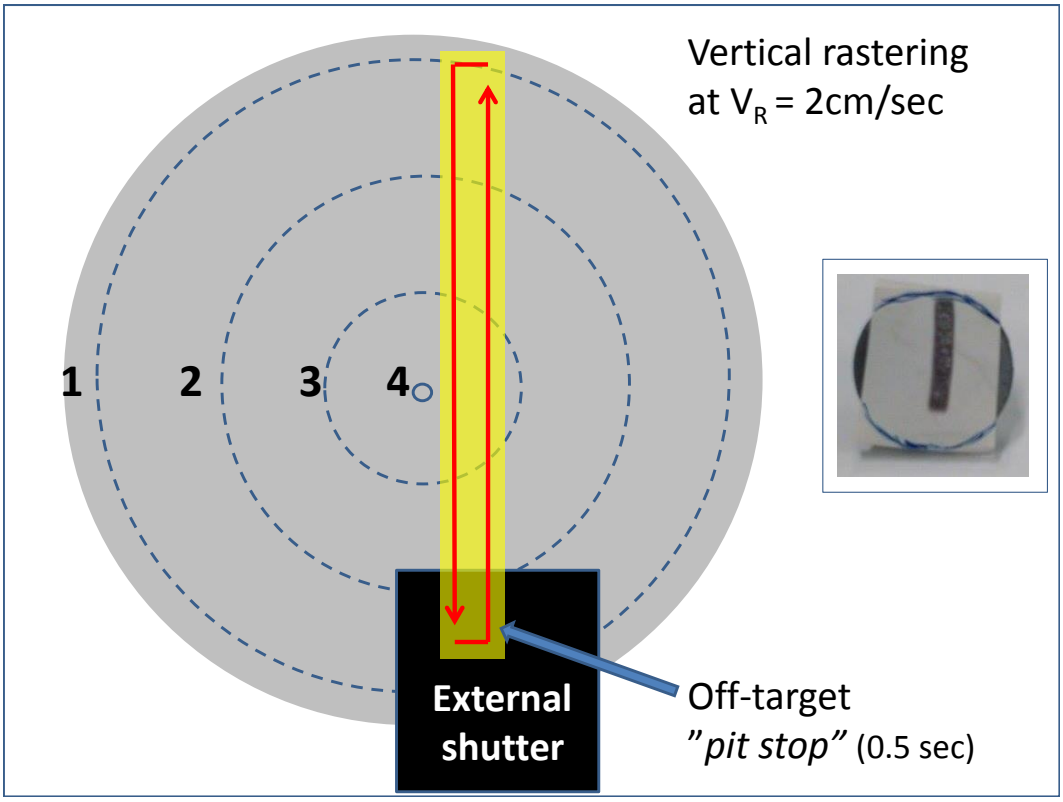

Figure 5.5: Sketch of the rastering design used for the production of CZTS and CTS films. The meaning of the numbers 1-4 is discussed in the text and in table 5.3. In the inset is shown the image on optical paper of the full-line rastering scan on the target. Note the max. scan length achievable due to the limited size of the lens.

5.5.1 Against the Cu plate standard

First: Let us first consider the beam profile and the way it changes with propagation, as sketched in Figure 5.6. After the focal lens the top hat beam is characterized by an intensity profile distribution rather than a step function, and this distribution gets sharper and sharper towards the focal point[6]. The visible ablated area on the Cu plate corresponds approximately to the area where the beam fluence is above the ablation threshold for the copper plate, say F^{o}_{Cu}. During propagation, the beam profile changes due to focusing, and as well changes the ratio between the beam's peak fluence and F^{o}_{Cu}. As consequence, without any information of the focusing, the same spot on the Cu plate could be related to two very different beam profiles with different peak fluence. Moreover, as described in Section 5.3, our targets

[6]This is the reason why I switched from a f=50cm focal lens, as initially part of the setup, to a f=75cm

are not made of copper, instead they contain many different phases whose ablation threshold can be very much different form that of copper.

Second: The ablated area that appears on the Cu plate does not exactly correspond to the area where $F \geqslant F^o_{Cu}$. Indeed, heat diffusion from the ablated area can spread the size of the melt, especially since heat loss from the target accounts to as much as 75% of the pulse energy [52] and that copper is a very good heat conductor. This effect gets more and more pronounced as the pulse energy increases, such that the same beam can produce different spots if one does not always use the same energy. Furthermore, the ablated spot increases in size with the number of pulses. While it does saturate at some point, it is not clear what this saturation value corresponds to, but it should be expected that it depends on both beam energy and focusing, especially for the case of laser impinging at 45^o.

Third: The discontinuity between the fresh and the ablated/melted area on the target is not neat, it is rather blurry. On top of that, if the shape of the ablated area is not extremely regular, as it happens with the Nd:Yag laser, the estimate will entail geometrical approximations or averages among different measures. If then one uses a mm marked calibre to measure something which is just few $\mathrm{mm}^2 s$, this just by itself leads to an error of about 30% or worse. My recommendation, should the spot area be measured, may it be done with an optical microscope or scanner with a suitable software.

5.5.2 Analytical tools

Ray optics approximation:

To estimate the spot size one can use simple equations from linear optics. In this work what is referred to as "spot size" is the image of the aperture $\mathrm{X_b} \times \mathrm{Y_b}$ projected by the lens on the target plane, as illustrated in figure 5.6. The incoming rays passing through the lens can be treated as parallel rays converging to the focal point. Therefore, the image of the aperture $\mathrm{X_b} \times \mathrm{Y_b}(\mathrm{D})$ as function of the lens-target distance D is given by:

$$\mathrm{X_b} \times \mathrm{Y_b}(\mathrm{D}) = \mathrm{X_b} \times \mathrm{Y_b} * \left(\frac{\mathrm{f} - \mathrm{D}}{\mathrm{f}}\right)^2 * \sqrt{2} \tag{5.1}$$

where the factor $\frac{\mathrm{f-D}}{\mathrm{f}}$ accounts for the linear focussing on both X_b and Y_b and the factor $\sqrt{2}$ accounts for the $\theta_i = 45^o$ angle of incidence between the beam and the target normal.

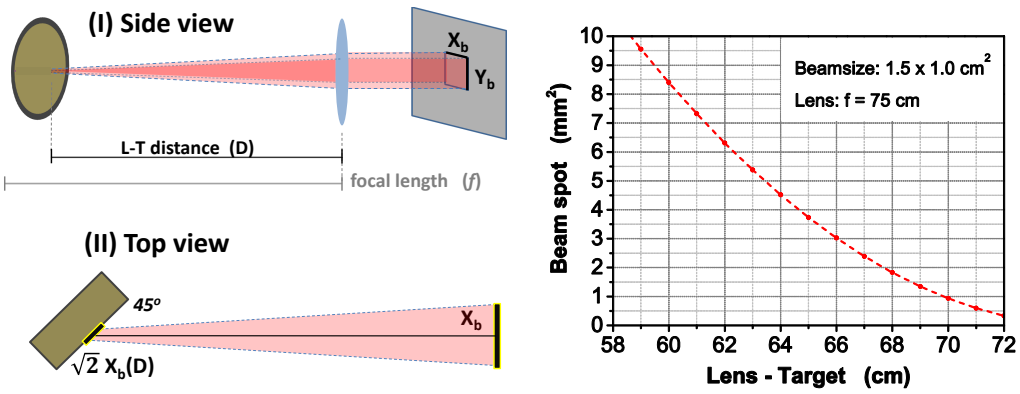

Figure 5.6: (Left): Laser spot as image of the aperture $X_b \times Y_b$ in geometric optics approximation. Note that this picture is simplified and does not contain the rastering mirror, which is placed between the aperture and the focal lens.
(Right): Laser spot size on the target as function of the lens-target distance, with $\mathrm{X_b} = 10\mathrm{mm}, \mathrm{Y_b} = 15\mathrm{mm}$ and $\theta_i = 45^o$.

Chapter 6

Pulsed Laser Deposition of thin films of CZTS and CTS

Summary: The atomic composition of thin films of CZTS and CTS produced by PLD from multi-crystalline sintered targets is strongly related to the laser fluence. Ablation of this kind of targets is understood as a phase-sensitive process. A qualitative understanding of the atomic composition versus fluence is given on the basis of the enthalpy of evaporation of the different phases in the target. The mechanism of Cu-S droplets formation and ejection is also discussed. After obtaining CZTS precursors with the desired stoichiometry, a 5.2% efficiency solar cell with a state-of-the-art device fabrication processing developed at the University of New South Wales (UNSW), Sidney, is demonstrated . The content of this chapter is currently submitted for publication to the journal "Progress in Photovoltaics - Research and Application" as a Research Article. The article is a full part of the Chapter.

6.1 Introduction - what is laser ablation?

This chapter intends to offer a broader context to the results presented in the paper enclosed at the end. We start our discussion with some extra specifications on what PLD is, with the goal of better clarifying what is meant with*"PLD allows a stoichiometric transfer"*. In fact, while "Pulsed Laser Deposition" appears to be a clear definition, *i.e.* what is deposited (somewhere) after shooting a laser pulse onto a target, "laser ablation" embodies such a vast range of different light-matter interactions that it is impossible to write a unified theory.
Ablation comes from the Latin word *ablatio*, literally "taken away", removal.

Light-induced material removal can happen in many different ways; lasers are used to cut marble rocks or to remove biological tissue. We must apply some restrictions to our definition. Anisimov suggests [45] that a somewhat coherent and general theory of PLD can be drawn if we consider a process such that:

1. ablation is directly related to the absorption of laser energy in the material;

2. in principle, ablation can proceed in vacuum or an inert medium;

3. laser ablation results in the production of a vapor $\pm$ gas (vapor $\pm$ plasma) plume of ablation products

The first two restrictions exclude, respectively, removal by cracking and laser-induced chemical etching. The third one is the most important: the products are in a volatile phase (gas and/or plasma) the dynamics of which is described by the plume model [48], thus excluding a simple process of thermal evaporation, which does not produce any plume.
Let us restrict the discussion here to what happens in vacuum for UV nanosecond laser pulses, and see what this plume should be like. The point of this discussion is to decide if, in this work, we have done some PLD, in the sense intended by Anisimov[1].
The discussion that follows is perhaps better understood with the help of Figure 6.1.

Since the laser pulses are in the nanosecond range, and electron-phonon interactions (heating) take place in a matter of picoseconds, the heating process is primarily driven by the incoming laser pulse, as shown in Figure 6.1 (left). Can the local temperature exceed the boiling point? Yes, and probably at that point it is already meaningless to think of a "boiling point", since this quantity is defined in the context of equilibrium thermodynamics. At some point in time, well before the laser pulse is terminated, the material starts to vaporize, and this vapor, in turn, starts to absorb part of the incoming laser light, becoming partly ionised and increasing its temperature well above that of the target. Ionic species with kinetic energy in excess of 100 eV are normally observed [80]. To make it short, when the laser pulse is terminated (tens of ns) we are left with a very hot and confined gas/plasma which extends over the ablated area for 10-100 μm, a much smaller length scale than the size of the irradiated area of about 1 mm^2. Expansion of this "2D" vapor sheet is adiabatic and highly forward directed with respect to

[1]Yes, we did.

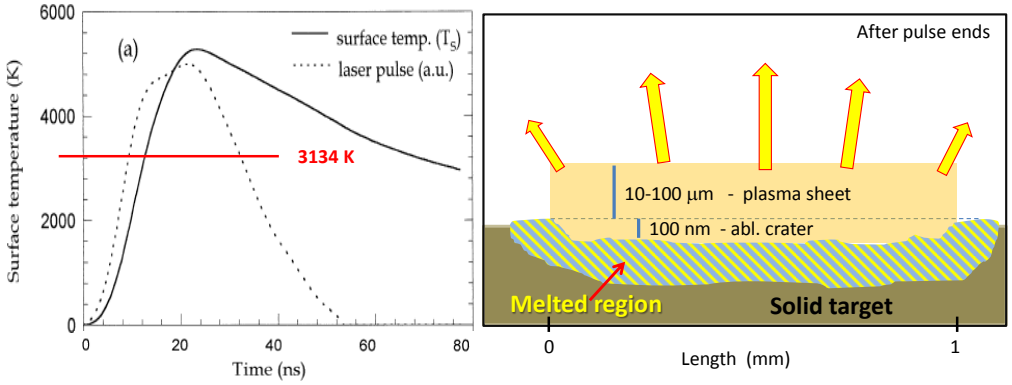

Figure 6.1: Left: Modeled surface temperature for an iron target irradiated with a 26 ns UV laser pulse at 4.5 J/cm^2, with iron boiling point of 3173 K indicated by the red line. Figure is taken from [64]. Right: Schematics of the target-plasma situation at the end of the laser pulse. The plasma is still confined and arrows indicate the direction of expansion. Not in scale.

the target plane, due to the initial planar geometry (each unit volume in the plasma sheet expands pursuing the highest density gradient, see arrows in Figure 6.1, right) and the fact that expansion is blocked on one side by the target itself. The bigger the size of the ablated area, the more confined and forward directed is the plume expansion.

Indeed, two key experimental signatures of laser ablation are:

1. the thickness gradient of the deposited material reflects the plume geometry.

2. the kinetic energy of the atomic species in the plume is significantly higher than the thermal energy associated to evaporation.

In our setup we cannot measure the velocity of the ionic species, but we can visualize the thickness gradient of the deposited material thanks to Newton's inference fringes, as shown in Figure 6.2. The comparison is between two images taken: (left) after a deposition at very low fluence (the Zn-Sn-S film of which in Section 4.4) and (right) after a deposition at 0.6 J/cm^2, as used for making solar cells. Do we see ablation or evaporation? or both? or one and one?
We recall that the risk of moving towards the "below threshold"-regime was that one may fall into the "incongruent evaporation regime" [50]. Should we not suspect that, at least, our Zn-Sn-S film was done under an evaporation regime?

From Figure 6.2, it seems that both cases agree with an ablation case, rather than evaporation. The spreading of the Newton rings, in fact, change significantly according to the laser fluence. Since the energy/pulse was roughly the same in the two cases, the two depositions differed mostly in the laser spot area that was used for the ablation process.

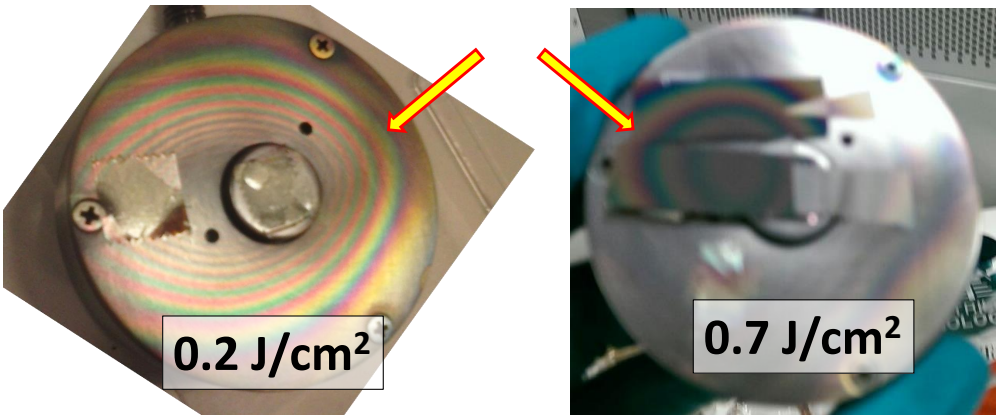

Figure 6.2: Left: image of the target holder after the deposition of the Zn-Sn-S film, done with a big spot size >8 mm^2 which leads to a very narrowly forwarded plume. Right: target holder after a deposition at 0.6 J/cm^2, as used for making solar cells, thus with a smaller spot size of 4 mm^2 and a relatively wider plume.

If it were simple evaporation processes in both cases, we should not see any big difference in the distribution of the deposited material. Is it laser ablation in both cases? Yes, indeed. In fact, if we imagine that the image on the left (very low fluence) was only the result of an evaporation process, we should then explain why an even narrower spatial distribution of the deposited material is seen, as compared to the image on the right. Further, the very peculiar composition and morphology of the Zn-Sn-S film would also support the conclusion that the process was not an equilibrium-type of deposition.
If we accept this discussion, we must conclude that the fabrication of the Zn-Sn-S film, and of all the other films in this thesis, was indeed Pulsed Laser Deposition in the sense of Anisimov. Furthermore, we must also conclude that the ablation process induced onto a multi-phase target is, more generally, a phase-selective ablation process. The question whether the transfer in PLD is stoichiometric or not, does not properly apply to the case of multi-phase targets of the kind used in this work. We are left with some open questions, which are probably more interesting by themselves than in regards to this particular system:

- If we had a single phase target, would the transfer be stoichiometric?

- Is the surface temperature in the multi-phase irradiated area uniform?
- When some Cu is transferred, are Cu-S phases getting heated mostly as consequence of light absorption, or do the hot plasma play a mayor role in etching them away?

6.2 The effects of laser fluence and wavelength

The laser fluence has a very relevant impact on atomic composition and morphology of the deposited films. Similar, but not identical trends are observed for the two PLD systems (248 nm and 355 nm) used in this work, indicating that the laser wavelength is also an important parameter. We characterize the stoichiometry of the precursors in terms of the compositional ratios Cu/Zn (or Cu/Sn) and Cu/(Zn+Sn), which are the most important, since the sulfur content changes during the annealing. For the sake of completeness, here we also include the results for the CTS target. For the discussion of the results, the reader is referred to Section 3.1 "Precursors preparation", of the paper enclosed at the end of the chapter.

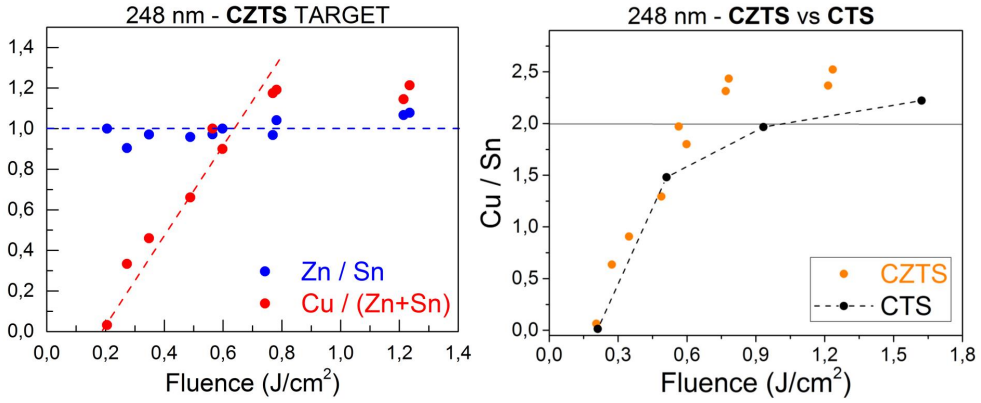

Figure 6.3: Left: Compositional ratios Zn/Sn (blue) and Cu/(Zn+Sn) (red) as function of the laser fluence for CZTS films deposited with the excimer laser PLD equipment(λ=248 nm, τ=20 ns). The non-stoichiometric transfer of copper is underlined by the red dashed line, which is just a guide to the eye.
Right: Compositional ratio Cu/Sn as function of the laser fluence for films deposited from the two different targets, CZTS (orange) and CTS (black) dots.

We start our comparison by looking at the results obtained with the excimer laser PLD equipment (248 nm and 26 ns) in Figure 6.3. Regarding the CZTS target, the transfer is decidedly non-stoichiometric in what concerns the Cu content, while the Zn/Sn ratio is always close to the stoichiometric

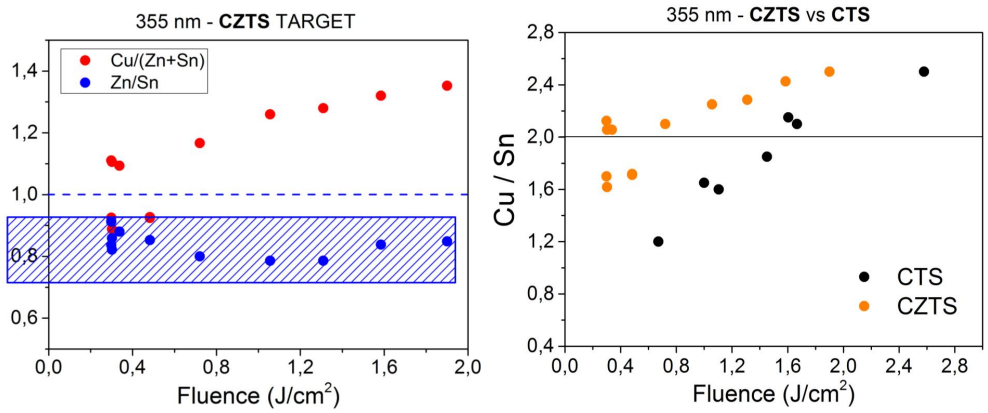

Figure 6.4: Left: Compositional ratios Zn/Sn (blue) and Cu/(Zn+Sn) (red) as function of the laser fluence for CZTS films deposited with the Nd:YAG PLD equipment (λ=355 nm, τ=7 ns). The Zn/Sn ratio, which is always well below the stoichiometric value, which shows significant difference compared to what was observed for the other PLD equipment. Right: Compositional ratio Cu/Sn as function of the laser fluence for films deposited from the two different targets, CZTS (orange) and CTS (black) dots. The data for the CZTS targets were taken by Stela Canulescu.

value. As discussed in the paper at the end of this chapter, SnS and ZnS have the same enthalpy of evaporation, while Cu-S phases requires much more energy before they reach the gas phase. These few observations are enough to account, in a first, crude approximation, for the results observed. Moreover, the argument holds in the same fashion also for the CTS, which is indeed what is seen experimentally. However, if we look at the results from the Nd:YAG PLD equipment (355 nm and 7 ns) in Figure 6.4, we readily see that, despite the fact that ZnS and SnS have a very similar enthalpy of evaporation, their transfer is now off-stoichiometric, as indicated by the dashed blue area. One possible reason for this difference is the much lower absorption coefficient of ZnS at 355 nm compared to that of SnS. We recall from Section 5.1 that a photon at the wavelength of 355 nm has an energy slightly (0.1 eV) below the badgap of ZnS, while its energy is more than 1 eV above the badgap of SnS, which is also a direct bandgap semiconductor. Thus, in this latter case, the non-stoichiometric transfer arises from a combination of different factors, which span from energy absorption to kinetics of vaporization. Moreover, it does not seem possible to choose a fluence value such that a stoichiometric transfer is allowed.

6.3 Structure of the precursors

In this work, precursors for solar cells are thin films of CZTS deposited by PLD on 3×1.5 cm^2 Mo-coated SLG. The substrate temperature is kept at room temperature, so the structure is completely amorphous, as revealed by the completely flat XRD pattern, Figure 2.5. The experimental part was done according to the descriptions of Chapter5. Briefly: background pressure $<10^{-6}$ mbar, Target-Substrate distance of 4 cm, excimer laser (248 nm, 15 Hz p.r.r, 20 ns pulse width, 25 mJ pulse energy, 20 min deposition time).
Regarding precursors, there are two very important parameters to control: the thickness and the composition. Films thicker than 800 nm exfoliate during the annealing and many detrimental secondary phases form if the stoichiometry is not Cu-poor and Zn-rich. The thickness profile and the morphology of a Cu-poor CZTS film are shown in Figure 6.5.

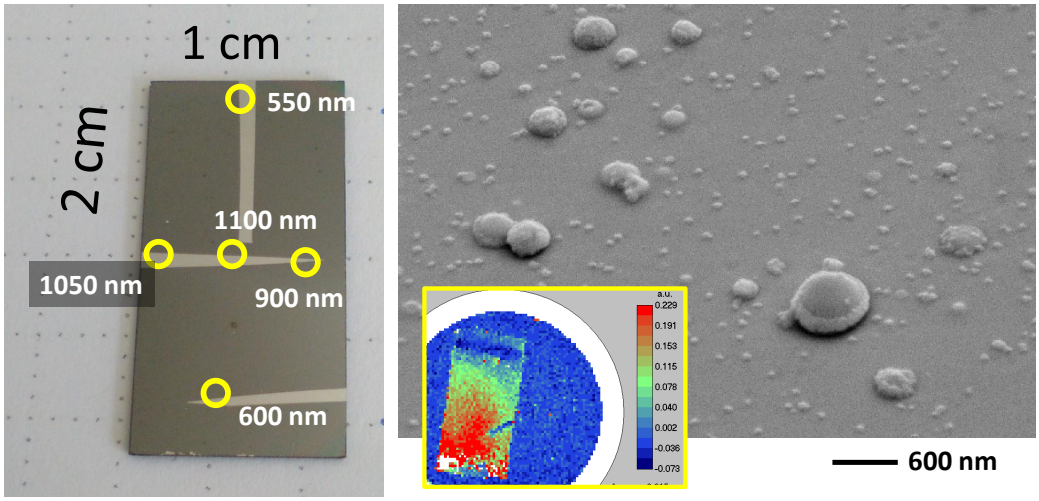

Figure 6.5: Left: Example of the typical thickness gradient for CZTS films produced with our setup on Mo-coated SLG substrate. During the deposition part of the substrate was covered with tape to allow measuring the thickness in different spots with a Dektak stylus profilometer. Samples used for measuring the composition with EDX were deposited for a longer time to ensure a thickness of more than 1 μm in the center.
Right, SEM image of the same film, which consists of an amorphous layer studded by molten droplets of Cu-S composition. In the inset, PL intensity mapping of a similarly fabricated sample after annealing. The color scale refers to the intensity of the signal at 920 nm.

As can be seen, our precursors are typically characterized by a thickness gradient of about 50% moving from center to edge, and we find that some device properties correlate with this thickness gradient, for instance the intensity of the PL signal. Thus, the thickness indicated refers to the centre

of the sample, where the film is thickest. It is important that the CZTS film does not exceed $\sim$ 800 nm thickness, at which severe exfoliation results during the annealing, as experienced many times by us, Figure 4.6, and as variously reported by other groups [34]. The film should not exfoliate anywhere on the sample surface. In fact, during CBD of CdS, the amount of exfoliated material usually increases. Moreover, it is not desirable to have external contaminants in the solution, in order to avoid precipitates or to affect the kinetic of the reactions.

6.4 Other groups doing PLD of CZTS

There are very few papers in literature reporting the use of PLD for the fabrication of CZTS thin-film solar cells [75, 76, 77, 78, 79]. They have few points in common:

- S-poor and Cu-rich stoichiometry is often reported, but no relation to laser fluence is observed. In [75] is noted that the amount of droplets diminishes if one reduces the laser fluence.
- All the works were done using a quaternary CZTS sintered target. PLD is done at room temperature and is followed by annealing in sulfurized atmosphere.
- The main reason reported for using PLD is the ability of PLD to preserve the stoichimetry during the transfer.

The first works were done in Japan in 2006-08 [75, 76] and were among the first studies on CZTS in general. The authors point out that decreasing the fluence reduces the number of droplets and that precursors are Sn-rich. The maximum power conversion efficiency demonstrated for their devices is 1.7%. To my judgement, these are the best papers on PLD of CZTS published so far.
There is a fair report by Sun et al. [77] where it is observed a Cu-rich and S-poor composition for the films produced in the temperature range 300 to 450°C, but no solar cell is reported. There are several papers from an indian-korean group [78], where the authors claim to have fabricated a 4% efficiency device, but their claim is obviously inconsistent with the data presented, such that no further comments are needed.
Last but not least, I shall discuss rather extensively the paper by Jin et al. [79], where the authors claim to have reached a device efficiency of 4.94% with a 400 nm thin absorber layer. This is very similar to our result, and

the paper was published on "Solar Energy Materials and Solar Cells" exactly when we were about to submit our work *"Ultra-thin Cu_2ZnSnS_4 solar cell prepared by pulsed laser deposition"* to the journal "Progress in Photovoltaics, R&A". Before I move on, I anticipate that I do not fully trust the content of this paper. There are missing some crucial informations, which makes it difficult to argue pro-or-contra the claimed 4.94% efficiency. Plus, the paper contains obscure sentences and several contradictions. The solar cell characterization gives inconsistent results.

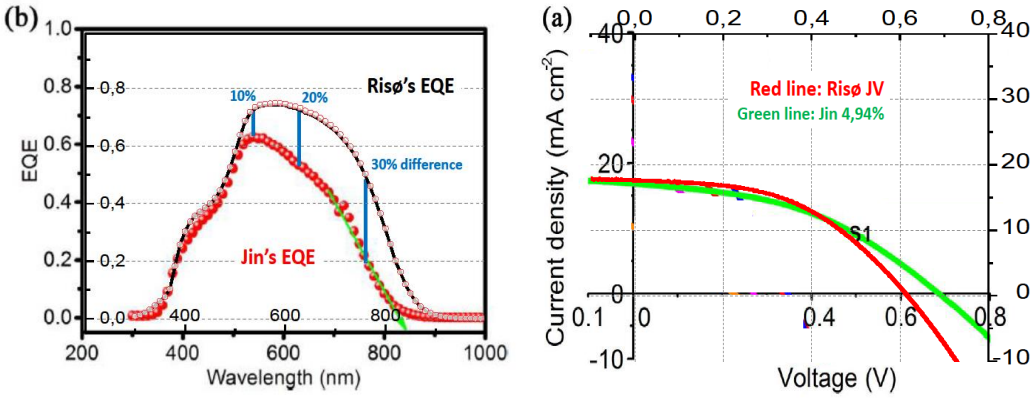

Figure 6.6: Left: Comparison of the EQE curves for our 5.2% efficiency device and Jin's 4.94% device. Data taken from [79]

Briefly, the authors propose a new fabrication technique for multi-component oxide targets. They claim that the resulting targets are more compact and homogeneous in chemical composition than the traditional ones made with sintering, and this greatly enhances the quality of the deposited films: "*due to the congruent transfer behaviour for PLD technique, even a slightly composition fluctuation of the target would greatly influence the deposited film*". However, admittedly their target is still multiphase, as can be seen from the XRD pattern presented and as written by the authors themselves in the text. Their strategy is the following: room temperature PLD of the quaternary oxide target (CZTO) followed by high temperature sulfurization or selenization in a dedicated furnace. They deposit on 3×3 cm^2 substrates and investigate different S/Se ratios. All the absorbers containing some selenium show very poor device efficiency, while the sample containing only sulfur gets the highest efficiency of 4.94% and a V_{oc} of 684 mV, which is the second best ever reported value for a solar cell made with a CZTS/CdS heterojunction, after IREC's 701 mV record value [37]. The authors, however, do not even comment on this fact. The short circuit current measured with the JV curve

is 16.82 mA/cm^2, very similar to our measured value of 17,4 mA/cm^2. No other diode parameters are extracted from the JV curve. In Figure 6.6, I have made a straight comparison of their reported EQE and JV curves with those from our device. A striking difference in the EQE curves is readily seen, with our device considerably over-performing that of Jin et al. in the spectral region of maximal collection (550-650 nm). According to this plot, a difference of less than 1% in the short circuit density (17.4% vs 16,8%) would be impossible. Perhaps, they may have done something wrong with the measurements of the EQE curve, for instance not using the light bias, as we already discussed in Section 4.3, but the authors do not write in the paper which instrument or illumination conditions ere used. What I can say is that, for our 5,2% efficiency device, the difference between the light biased EQE and the zero bias EQE is always below 5%. The solar cell has an area of 0.1 cm^2 and no other information is given to allow assessing the validity of the claim of 4.94% efficiency. Besides the efficiency claim, the solar cell seems to anyway exist and to produce a measurable PV activity. Further, the idea of using an oxide target to reduce the sulfur contamination on the vacuum equipment is worth keeping into consideration, if sulfurization can be effectively carried out afterwards.

Ultra-thin Cu_2ZnSnS_4 solar cell prepared by pulsed laser deposition

Andrea Cazzaniga[†1], Andrea Crovetto[†*2,3], Chang Yan[3], Kaiwen Sun[3], Xiaojing Hao[3], Joan Ramis Estelrich[1], Stela Canulescu[1], Eugen Stamate[4], Nini Pryds[4], Ole Hansen[2,5], and Jørgen Schou[1]

[1]DTU Fotonik, Technical University of Denmark, DK-4000 Roskilde, Denmark
[2]DTU Nanotech, Technical University of Denmark, DK-2800 Kgs. Lyngby, Denmark
[3]School of Photovoltaic and Renewable Energy Engineering, University of New South Wales, NSW 2052, Sydney Australia
[4]DTU Energy, Technical University of Denmark, DK-4000 Roskilde, Denmark
[5]CINF, Center for Individual Nanoparticle Functionality, Technical University of Denmark, DK-2800 Kgs. Lyngby, Denmark

[†] The authors A. Cazzaniga and A. Crovetto contributed equally to this work
* Correspondence: ancro@nanotech.dtu.dk

Abstract

We report on the fabrication of a 5.2% efficiency Cu_2ZnSnS_4 (CZTS) solar cell made by pulsed laser deposition (PLD) featuring an ultra-thin absorber layer (less than 450 nm). Solutions to the issues of reproducibility and micro-particulate ejection often encountered with PLD are proposed. At the optimal laser fluence, amorphous CZTS precursors with optimal stoichiometry for solar cells are deposited from a single target. Such precursors do not result in detectable segregation of secondary phases after the subsequent annealing step. In the analysis of the solar cell device, we focus on the effects of the finite thickness of the absorber layer. Depletion region width, carrier diffusion length, and optical losses due to incomplete light absorption and back contact reflection are quantified. We conclude that material and junction quality is comparable to that of thicker state-of-the-art CZTS devices.

1 Introduction

Considerable research effort is presently devoted to alternative earth-abundant and non-toxic materials for photovoltaic applications. In this context, the p-type chalcogenide semiconductor Cu_2ZnSnS_4 (CZTS) has become very popular due optimal direct bandgap at 1.5 eV, high absorption coefficient $> 10^4$ cm^{-1} and its rapid technological development in the last decade [1, 2]. Still, the current record efficiency of 12.6% for CZTSSe [3] and of 9.1% for pure-sulfide CZTS [4] is far below the 21.7% efficiency demonstrated by the very similar CIGS technology [5], from which they borrow most of the device architecture. Regarding the pure sulfide CZTS, different vacuum deposition techniques have been successfully employed, such as co-sputtering [4, 6–8] and co-evaporation [9–12]. The most successful strategies to date consist of a two stage process, where precursors are prepared at a substrate temperature below 300°C, followed by a high temper-

ature annealing (>500°C) done separately at much higher pressures. Among vacuum techniques, pulsed laser deposition (PLD) was firstly studied in 2007-08 by Moriya et al. [13, 14], who demonstrated a power conversion efficiency up to 1.74% with a two stage approach consisting of room temperature deposition of the precursors followed by high temperature annealing in a mixture of N_2 and H_2S. With a similar approach, but using a quaternary oxide target, a power conversion efficiency of 4.94% was claimed very recently by Jin et al. [15]

Pulsed laser deposition is a non-equilibrium technique that enables the fabrication of high quality thin films with complex stoichiometry, particularly oxides, nitrides, and amorphous materials [16–18]. Briefly, a pulsed UV laser beam is focused onto a solid target and laser ablation occurs, which result in highly non-thermal removal of the target material. The ablated material, which is an expanding plasma cloud, is finally collected onto a substrate placed a few cm away. The fact that the energy source is outside of the vacuum chamber and decoupled from the deposition process enables one to investigate many experimental parameters (background gas pressure, substrate temperature, ablation energy density) over a wider physical range than with other vacuum techniques. Since the laser heating and subsequent plasma formation are confined in a very small region of the target, there is no risk of contaminating the growing film with materials coming from components of the chamber other than the target itself. The kinetic energy of the atoms and ions in the deposition flux is related to the laser fluence and is usually of few eV. Particularly relevant to this work, PLD has proven to be a very successful technique in the growth of high quality films of amorphous structure [18, 19]. This ability comes from a few combined features: the possibility to keep the substrate at room temperature, with relative ease, the sticking coefficient close to unity for all incoming species, and both compactness and flatness of deposited films due to the highly energetic instantaneous material flux [16, 19]. However, reproducibility is often reported to be an issue, mostly because it is difficult to keep the laser ablation parameters within the desired range throughout the whole deposition process, especially in the case of strong coating on the laser view-port [20]. Droplet production and target deterioration are also issues in PLD [16]. Such problems have already been recognized as hurdles to production of high-efficiency solar cells by PLD [21].

However, in this work we demonstrate that it is possible to circumvent most of the above problems and obtain a CZTS solar cell efficiency above 5%. Interestingly, this result is achieved with an "ultra-thin" absorber layer, with thickness below 450 nm.

2 Experimental Details

A 10×10 cm^2 soda lime glass (SLG) substrate was sequentially cleaned in acetone and isopropanol in an ultrasonic bath (5 min each), rinsed in deionized water, and dried with nitrogen. A Mo bilayer was deposited by DC magnetron sputtering at 10 W/cm^2 power density. The first layer was 200 nm thick and deposited at a working pressure of 1.3×10^{-2} mbar for good adhesion to the substrate. The second layer was 300 nm thick and deposited at a working pressure of 3.9×10^{-3} mbar to achieve a lower sheet resistance. The sheet resistance of the Mo bilayer was 0.7 Ω/sq ±50% depending on position on the SLG substrate. The Mo-coated glass was cut into 1.5×3 cm^2 substrates, which were cleaned in the same way as above prior to pulsed laser deposition of CZTS precursors. Precursors were deposited with our PLD equipment, depicted schematically in Figure 1, under high vacuum with $p < 5 \times 10^{-6}$ mbar. The KrF excimer laser beam (248 nm wavelength, 20 ns pulse-width, 15 Hz pulse repetition rate) was focused onto a sintered target with overall CZTS stoichiometry (2.5 cm diameter, Testbourne

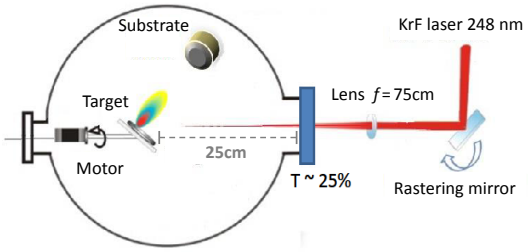

Figure 1: Sketch of the PLD setup. The laser pulses are focused on the target at 45 degrees from normal incidence with a focal lens. The fluence on the target was 0.6 J/cm^2 with a spot size of 4 mm^2.

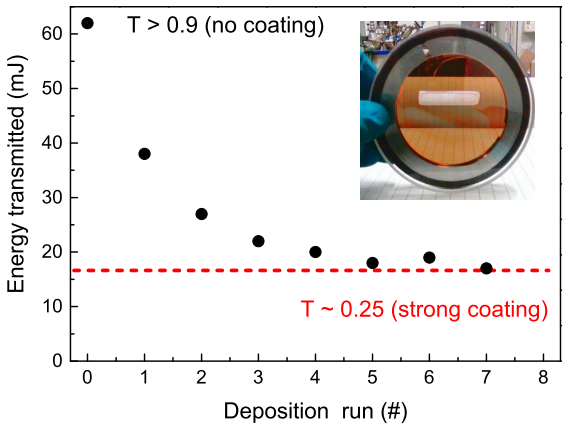

Figure 2: Laser energy transmitted through the viewport as a function of cumulative number of CZTS deposition runs. In the inset: photograph of the viewport after more than five deposition runs, when transmission of the laser through the viewport has reached an equilibrium value of about 25%. One deposition run corresponds to a 20 min deposition at 10 Hz pulse repetition rate.

Ltd, 2CuS:ZnS:SnS) at a laser fluence of 0.6 J/cm^2 and a spot size of 4 mm^2.

The laser energy on the target was measured inside the chamber to avoid errors due to strong coating of the viewport with ablated material. The depositions were done after the laser beam-viewport system had reached equilibrium, as shown in Figure 2.

Rastering of the laser and rotation of the target were used to maximize film uniformity and target utilization. The target-substrate distance was set to 4 cm and the substrate was kept at room temperature. Morphology of the precursors, and of the finished solar cell devices, was examined with a scanning electron microscope (SEM) equipped with a field emission gun (Supra 60VP, Zeiss). The chemical composition of the precursors was measured in the same instrument by energy dispersive X-ray spectroscopy (EDX) using a silicon drift detector (X-Max^N 50, Oxford Instruments) and a beam voltage of 15 kV. The CZTS precursors were vacuum packed and taken to the University of New South Wales for the sulfurization treatment and the buffer/window layer deposition. Sulfurization was conducted at 560°C in the presence of S and SnS powder in a rapid thermal processor (AS-One 100). The CdS buffer layer (60 nm) was deposited by a standard chemical bath deposition process [22], followed by RF magnetron sputtering of 50 nm intrinsic ZnO (i-ZnO) and 200 nm indium tin oxide (ITO) having a sheet resistance around 30 Ω/sq. A 1.5 mm^2 dot-shaped silver paste contact was applied on the ITO layer, followed by evaporation of 100 nm MgF_2 as an anti-reflection coating. Solar cell devices of 0.2 cm^2 were defined by mechanical scribing.

Illuminated current-voltage (J-V) measurements were performed after 5 min light soaking under standard AM 1.5 solar spectrum (100 mW/cm^2) using a solar simulator from PV Measurement calibrated with a standard Si reference and a Keithley 2400 source meter. Due to the coarse nature of the top contact, in this work we present the active area efficiency of the solar cell instead of the total area efficiency. Dark J-V and capacitance-voltage (C-V) curves were measured with an Agilent B1500A semiconductor device analyzer. C-V scans were performed between -4 V (reverse bias) and +2 V at a frequency of 100 kHz and an AC voltage of 50 mV.

External quantum efficiency (EQE) curves were measured at 0V and -1V dc bias in the range 300 to 1000 nm with a QEX10 spectral response system (PV measurements, Inc.) calibrated by the National Institute of Standards and Technology (NIST)-certified reference Si and Ge

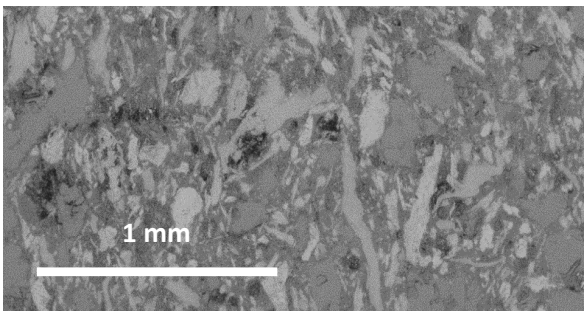

Figure 3: SEM image of the 2CuS:ZnS:SnS sintered target. The different phases are clearly visible and extend over a typical length scale of a few hundred μm. The melting point and the vapor pressure of the main phases are summarized in Table 1. The ablated area corresponds to a beam spot size of 4 mm^2.

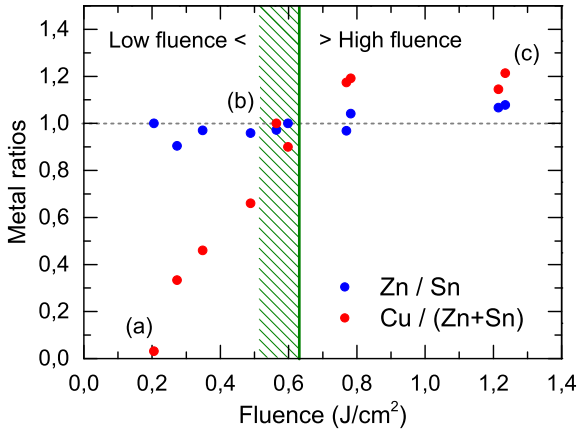

Figure 4: The metal ratios as a function of laser fluence as measured by EDX in the films deposited at room temperature. Letters denote the films shown in Figure 5. The fluence range used for preparing the solar cells precursors is indicated by the green shaded area. The fluence value (approximately 0.6 J/cm^2) that results in stoichiometric transfer is marked with a green line. Below and above this reference fluence, we speak of "low fluence" and "high fluence" in the main text.

photodiodes. The band gap of CZTS was extracted from the inflection point of the EQE curve, i.e., as the photon energy at which $-\mathrm{d(EQE)/d}\lambda$ has a maximum [23].

Steady-state photoluminescence (PL) spectra were measured on completed solar cells with an Accent RPM2000 system at an excitation wavelength of 532 nm and power density 100 W/cm^2. Raman spectra and time-resolved photoluminescence (TR-PL) decay were measured on a bare absorber layer fabricated similarly to those used for the solar cell.

Raman spectra with multiple excitation wavelengths (455, 532, and 780 nm) were measured on a similarly fabricated CZTS film using a DXR Raman microscope (Thermo Scientific) in backscattering configuration, with a laser power of 1.6 mW and a spot size of approximately 2×2 μm^2.

TR-PL was measured using the time-correlated single photon counting (TCSPC) technique (Microtime200, Picoquant). The excitation wavelength was 470 nm and the power density was 1 W/cm^2, with a pulse frequency of 10 MHz and a 780-820 nm detection range.

3 Results and discussion

3.1 Precursors preparation

In this study we aimed for maximally amorphous precursors by keeping the substrate at room temperature during deposition. Thus, stoichiometry and morphology of the films are primarily related to the laser beam-target interaction, which is very complex here due to the multi-phase structure of the target, as shown in Figure 3. Since a single crystal target is not commercially available, the target used in this work is made from sintered powders (2CuS:ZnS:SnS). The different phases extend over many hundreds of μm and have very different physical properties in terms of energy absorption, decomposition mechanisms and volatility in vacuum, as summarized in Table 1.

As a matter of fact, the Cu/(Zn+Sn) and Zn/Sn ratios in the precursors are of paramount importance to achieve good quality devices [27]. Therefore, we start our discussion with the stoichiometry of

films deposited in the laser fluence range from 0.2 to 1.2 J/cm^2, as shown in Figure 4. Noteworthy, the copper content in the as-deposited films is found to be strongly related to the laser fluence, while the Zn/Sn ratio is always close to the target stoichiometry. First, a threshold fluence for copper transfer is clearly visible at 0.2 J/cm^2. In the "low fluence" range from 0.2 to 0.8 J/cm^2, the Cu content steadily increases from 0% to its stoichiometric value, same as the target. In the "high fluence" range above 0.6 J/cm^2 the films become Cu-rich and the Cu content saturates above its stoichiometric value. The sulfur content is not shown here, but a behaviour opposite to copper is seen, i.e., it steadily decreases from low to high laser fluences. Changes in films composition are also followed by changes in films morphology. SEM images of three films deposited with different laser fluences are shown in Figure 5. The as-deposited films are amorphous and, in particular, (b) and (c) are studded with micron-sized droplets which are primarily a mixture of copper and sulfur [28]. From Figures 4 and 5 it is clear that, by increasing the laser fluence, both the copper content in the films and the amount of Cu-S droplets are increasing.

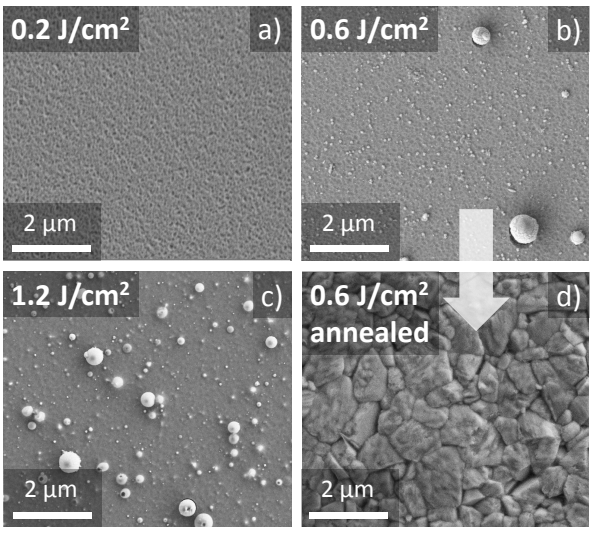

Figure 5: (a to c): top view of as-deposited films using three different laser fluences. (a) 0.2 J/cm^2 (low fluence); (b) 0.6 J/cm^2 (intermediate fluence); and (c) 1.2 J/cm^2 (high fluence). No peaks are detected in the XRD pattern (not shown here), indicating that the films and the droplets are amorphous. Image (d) represents film (b) after annealing in sulfurized atmosphere as used for making solar cells.

While laser ablation is not an evaporation process at thermodynamic equilibrium, still, a qualitative understanding of the fluence dependence of composition and morphology of the deposited films can be proposed on the account of thermodynamical parameters of the different phases in the target, which are listed in Table 1. As can be seen, ZnS and SnS phases readily sublime in vacuum, either congruently (SnS) or incongruently (ZnS), due to low enthalpy of evaporation. On the other hand, Cu-containing phases only release S_2 gas when heated above the melting point, see Equations 1, 2. Only when Cu_2S is formed it can then release gaseous Cu after dissociation. Hence the minimum temperature for Cu evaporation is above the melting point of Cu_2S, at 1129°C, and the process requires more energy than SnS and ZnS sublimation. Furthermore, the specific heat of ZnS and SnS phases is lower than those of Cu-S phases, meaning that the laser energy can be more effective in raising the local temperature of the volatile phases. Cu_2S formation from CuS and $Cu_{1.75}S$ is a relatively energy-intensive process, which occurs through two sequential solid state reactions [25]:

$$CuS \rightarrow Cu_{1.75}S_{(s)} + S_{2(g)} \quad (1)$$

$$Cu_{1.75}S_{(s)} \rightarrow Cu_2S_{(s)} + S_{2(g)} \quad (2)$$

The enthalpies of formation of the reactions in Equations 1 and 2 are 178 ±4 kJ/mol and 268 ±7 kJ/mol, respectively [25].

We can speculate that at very low fluence, below 0.2 J/cm^2, all the energy is readily absorbed by the volatile phases ZnS and SnS, which very quickly dissociate and create the plasma, while the energy density on the target never reaches the critical value to dissociate $Cu_{2-x}S$ phases and copper is not transferred to the films, as shown in Figure 4, sample (a). The relatively low heat of

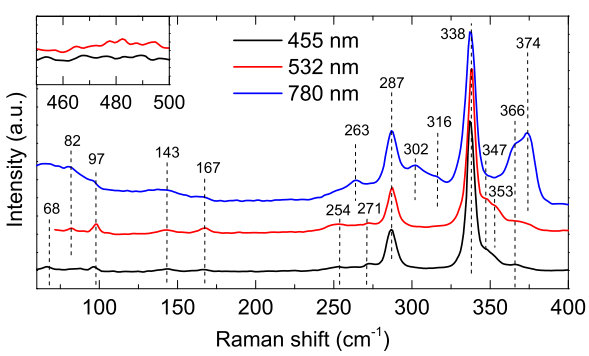

Figure 6: Raman spectra of the CZTS absorber layer at three different excitation wavelengths after high temperature sulfurization. Raman spectroscopy was also performed on the bottom surface of CZTS after lift-off from the Mo substrate, and no peaks related to secondary phases were found. The dashed bars indicate the identified peaks related to kesterite CZTS, according to [29]. The inset graph shows the spectral range where $Cu_{2-x}S$ has the strongest Raman peak.

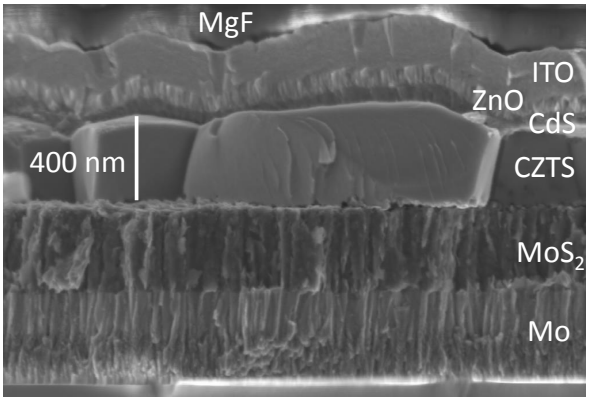

Figure 7: SEM image of the cross section of our champion device.

fusion of Cu_2S can partly explain why some of the material is not fully ablated, but instead transferred as a molten droplet when the hydrostatic pressure of the plasma on the target is enough for inducing material removal from the target. At very high fluence (>0.8 J/cm^2), we believe that the Cu-rich composition of the as-deposited films is a direct consequence of non-directional evaporation of volatile species ZnS and SnS from the target, while the ablated particles are emitted preferentially toward the substrate.

For the preparation of the solar cell absorbers we utilized precursors made at the laser fluence of 0.6 J/cm^2, which corresponds to sample (b) in Figure 5. The overall composition at this fluence, estimated by EDX, is Cu-poor $Cu/(Zn + Sn) \sim 0.85$, as prescribed for high efficiency CZTS devices [27]. The Zn/Sn ratio is ~ 1 and the S/(Cu+Zn+Sn) ratio is between 0.9 and 1. We note that precursors (b) contain Cu-S droplets. We have verified that these droplets can be removed via KCN etching, but pinholes and voids are left in the precursors, which is not desirable for making solar cells. However, removal of droplets does not seem to be necessary. In fact, after high temperature sulfurization, no localized Cu excess is detected by EDX mapping (not shown), no traces of secondary phases are visually evident by SEM (Figure 5(d)), and no $Cu_{2-x}S$ is detected by Raman spectroscopy (inset of Figure 6). This indicates that the Cu atoms diffuse effectively in the film during annealing.

3.2 Solar cell characterization

3.2.1 Morphology and thickness

In Figure 7 a SEM cross section of our champion device with 5.2% active area efficiency is shown. The morphology is compact and most grains extend from bottom to top. No obvious segregation of smaller grains and secondary phases exists at the interfaces, and no voids are visible, in contrast to what is often observed even in state-of-the-art devices [9, 30]. We emphasize that these features are common to all our annealed films, regardless of the specific point where the image is taken. We speculate that the absence of voids and secondary phases in the annealed films may be a consequence of the compact and maximally disordered structure of the precursors obtained by PLD. The CZTS absorber layer rests on a relatively thick (390 nm) MoS_2 layer. The image was taken about 2-3 mm from the solar cell area and, with a conservative estimate on the expected thickness gradient, the CZTS layer in the solar cell does not ex-

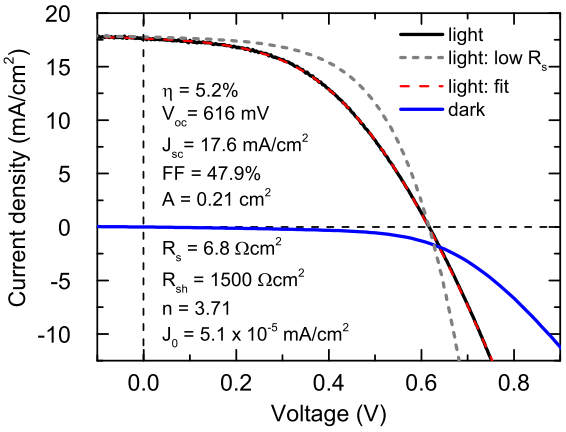

Figure 8: The dark and illuminated (1 sun) J-V curve of our champion device fitted with a single diode model (red dashed curve). All parameters, with the exception of the dark saturation current density J_0, were extracted by fitting the illuminated J-V curve. The high series resistance is due to non-ideal top contact geometry, as discussed in Section 3.3.3. Assuming a series resistance of 1 $\Omega\,\mathrm{cm}^2$ (grey dashed curve), the fill factor and efficiency increase to 58% and 6.3%, respectively.

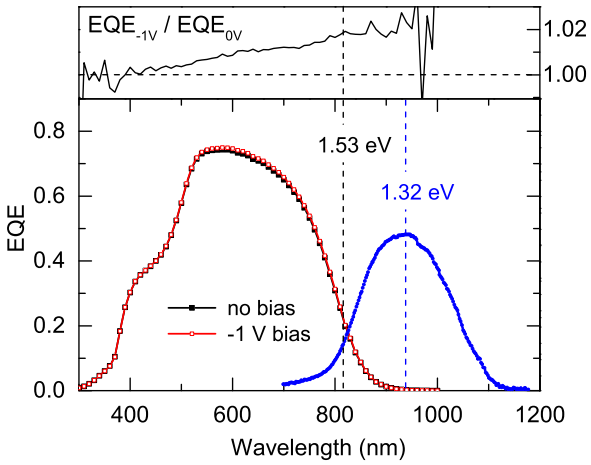

Figure 9: External Quantum Efficiency curves under 0 V bias (black symbols) and -1 V bias (red symbols). The inflection point of the $\mathrm{EQE}_{0\mathrm{V}}(\lambda)$ curve at 810 nm (1.53 eV) is indicated with a black dashed line. The inset shows the ratio $\mathrm{EQE}_{-1\mathrm{V}}(\lambda)/\mathrm{EQE}_{0\mathrm{V}}(\lambda)$. The PL spectrum at room temperature of the finished device (blue symbols) has a maximum at 1.32 eV (blue dashed line).

ceed a thickness of 450 nm, which is among the lowest values reported for high efficiency CZTS devices [15, 30].

Chalcogenide absorbers below 700 nm thickness are sometimes referred to as "ultra-thin" in the literature [31, 32]. In general, if the material properties of the absorber were independent of thickness, one would expect only the short circuit current to be reduced in an ultra-thin absorber, due to 1) incomplete light absorption, and 2) lower collection efficiency, as more minority carriers are generated near the back contact where they can recombine. However, keeping a high material quality in ultra-thin absorbers has been proven to be very challenging for CdTe [31], CIGS [33] and CZTS [30]. Even though back contact recombination can be successfully reduced by introduction of a back surface passivation layer [33], device efficiencies at thicknesses below 500 nm are still consistently lower than expected from short circuit current losses alone [31]. In fact, in all the above studies there was a noticeable decrease in both the open circuit voltage and the fill factor. A common observation was that the morphology of ultra-thin absorbers was inferior to that of thicker films grown under the same conditions, mainly in terms of reduced grain size and increased density of shunt paths. While it is difficult to evaluate the effect of the former on device efficiency, the latter is documented by a decrease of the device shunt resistance with decreasing thickness [30, 31, 33]. The only systematic investigation of CZTS thickness effects on device efficiency was done for co-sputtered CZTS [30]. There, the effect was particularly strong: a 500 nm absorber achieved only 50% of the efficiency of a 2 μm absorber, compared to 80% for both CdTe and CIGS [31, 33]. This was attributed to the increasing role played by secondary phases (SnS, ZnS), both at the front and back interface of CZTS. In the following section these issues will be quantified in our own device.

3.2.2 Electrical and optical properties

The dark and illuminated (1 sun) J-V curves, steady state PL, and EQE (at zero and reverse bias) are shown in Figures 8 and 9. The CZTS band gap of 1.53 eV, indicated in Figure 9, corresponds to to the inflection point of the EQE curve. The PL spectrum has a peak at a lower energy (1.32 eV), similarly to previous investigations on CZTS devices [9, 34]. This is believed to be due to a high density of band-edge tail states that reduces the achievable open circuit voltage [23].

The short circuit current J_{sc} = 17.6 mA/cm^2 derived from the illuminated J-V curve is in good agreement with the value of 17.4 mA/cm^2 obtained by integration of the EQE measured under white light bias. Despite the very thin absorber, this is a fairly high value for CZTS solar cells, which hints to a high collection efficiency, as will be discussed later. The shunt resistance R_{sh} and the dark saturation current J_0 are also comparable to state-of-the-art CZTS devices with larger thickness and efficiency $> 7\%$ [4, 6, 7, 9]. The high shunt resistance is consistent with the absence of voids and shunting paths as revealed by SEM imaging (Figure 7). On the other hand, the open circuit voltage V_{oc} = 616 mV is somewhat lower and the fill factor $FF = 47.9\%$ is much lower than in benchmark devices. The latter is mostly due to high series resistance R_s and a high diode ideality factor n.

As mentioned above, short circuit current losses are always expected in ultra-thin absorbers, so it can be instructive to quantify them. The calculated losses due to incomplete light absorption are reported in Figure 10 and explained in the caption. The potential gain in short circuit current by complete light absorption due to the extra generated carriers is not negligible (+1.9 mA/cm^2). This could be achieved either by a thicker absorber, or by an ideal back reflector, and would result in a 10% relative gain in efficiency, up to 5.7%. The J_{sc} would then be close to 20 mA/cm^2, which is comparable to the state-of-the-art CZTS solar cells [4, 6, 7, 9].

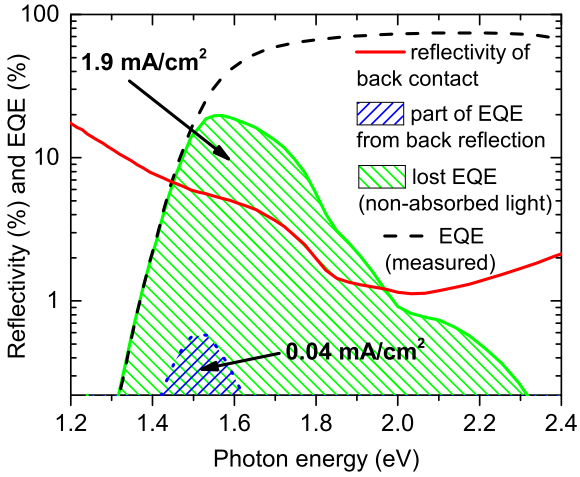

Figure 10: Calculated losses on the short circuit current due to the limited thickness of the device. In dashed green the current loss due to non absorbed light (assuming 90% collection efficiency). In dashed blue the contribution to current gain from reflection at the CZTS/MoS_2 interface. Note the logarithmic scale. The solid red curve is the calculated reflectivity of the back contact, which includes contributions from a single CZTS-MoS_2 reflection and a single MoS_2-Mo reflection minus absorbtion in the MoS_2 layer. The optical functions of CZTS, MoS_2 and Mo were taken from the literature [35, 36]. The thickness of MoS_2 in the calculation is 390 nm as in our solar cell. The reflectivities of the two interfaces were calculated using the Fresnel reflection coefficient.

However, with our back contact structure (390 nm MoS_2/Mo), the calculated contribution of back contact reflection to the short circuit current is as low as 0.04 mA/cm^2, which is negligible. This difference can be explained as follows. The reflection at the CZTS/MoS_2 interface is negligible due to the small mismatch between the optical functions of the two materials. While the MoS_2/Mo reflectivity is higher (about 20% in the high wavelength range), still the remaining 80% is completely absorbed in the Mo and there is a large additional contribution from absorption in the thick MoS_2 layer. Even if the MoS_2 was only 50 nm thick, the contribution of back

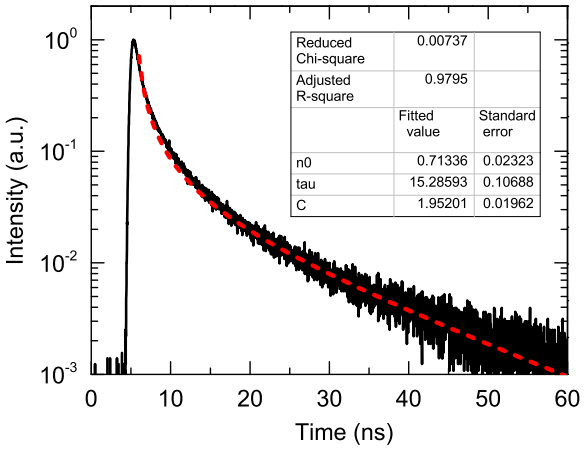

Figure 11: Time-resolved photoluminescence of a bare CZTS film after sulfurization. The red dashed line is the fit following Equation 4 with the coefficients n_0, τ, and C as indicated in the figure.

contact reflection would still be relatively low (0.3 mA/cm^2). In the limiting case of a direct CZTS/Mo interface, the contribution would increase slightly to 0.5 mA/cm^2.

The fact that our measured short circuit current, corrected for optical losses due to finite thickness, is comparable to state-of-the-art CZTS devices, points to the fact that collection efficiency is reasonably high and not significantly degraded by the small thickness of the absorber. To confirm this hypothesis, we investigated the ratio between the EQE at zero voltage bias (EQE_{0V}) and at -1 V reverse bias (EQE_{-1V}) of our device, as shown in the upper panel of Figure 9. Remarkably, the two curves never differ by more than 2% for photon energies above the CZTS band gap and the difference steadily reduces at shorter wavelengths. This resembles closely the measurement in [9], where the maximum difference in EQE at 0 V and -1 V was slightly more than 3% for a 600 nm-thick, 8.6%-efficient device. In [30], a deviation of more than 10% was observed even at a reverse bias of only -0.5 V, indicating dramatic problems with collection efficiency attributed by the authors to secondary phases at the interfaces. These results suggest that our device is relatively unaffected by collection losses, and that the diffusion length L_d of minority carriers is larger than the quasi-neutral region W_N of our absorber. We attribute the small increase in EQE at reverse bias to back surface recombination losses that are inevitable for a thin absorber in the absence of a back surface field.

A diffusion length greater than the quasi-neutral region, $L_D > W_N$, is also supported by the analysis of time-resolved photoluminescence (TR-PL), as illustrated in Figure 11. The TR-PL signal does not follow a simple exponential decay and is best described by a rate equation which contains both a linear and a quadratic term in the excess carrier density n:

$$\frac{dn}{dt} = -An - Cn^2 \qquad (3)$$

Following [37], and substituting $A = 1/\tau$ for the linear term, which represents the minority-carrier lifetime in the low injection regime, the solution to Equation 3 is:

$$n(t) = \frac{n_0 \exp(-t/\tau)}{1 + n_0 C\tau[1 - \exp(-t/\tau)]} \qquad (4)$$

By fitting the whole range of the PL decay according to this model, we obtain a value of about 15 ns for the carrier lifetime. We note that, if the same fitting method as [9] is applied, we obtain about 10 ns lifetime. While carrier lifetimes reported in the literature cannot always be compared directly due to the different models used by different authors to fit the TR-PL data, we emphasize that this value is at the high end for CZTS absorbers [9].

To provide a lower bound value for the minority carrier diffusion length, we estimate the width of the depletion region by means of C-V scan measurements. In Figure 12 we show the density of charged states at different depths into the CZTS absorber, which constitutes an upper limit to its real doping density. The plot has been derived from C-V scans by applying a standard model for a p-n$^+$ junction, where all the measured capacitance is due to ionized acceptors in the depletion region, which is assumed to extend exclusively in the p-type absorber. Due to the significant series resistance present in the device, we corrected the

measured capacitance and conductance at each DC voltage bias based on an equivalent circuit with an AC resistance in series with the junction [38]. The value of the AC resistance was estimated as 8.1 Ω cm^2 from the characteristics of the capacitance decline at high frequency in a separate capacitance-frequency (C-f) measurement. The resulting charged state density stabilizes to about $3 \times 10^{16}\,\mathrm{cm}^{-3}$ within the depletion region, which is interpreted as an upper limit for the true doping density of CZTS. Outside the depletion region, the charged state density seems to increase rapidly. We believe this to be a data analysis artifact due to the simplified model for the device response to the C-V measurement. Indeed, in thin-film materials trap states can be an additional sources of capacitance besides the ionized shallow acceptors. [39]. Following [38], the width of the depletion region at zero bias W_D is estimated to be 190 nm, similarly to that in Ref. [9]. However, this value is obtained under the strong assumptions that both the CdS and the i-ZnO layers are much more heavily doped than the CZTS absorber, which is questionable [40, 41]. In the case of a completely depleted 60 nm-thick CdS layer, the depletion region width in CZTS can be extracted by assuming the measured capacitance C_m to be due to two equivalent capacitors in series: one encompasses the full CdS buffer layer (C_b), and the other is due to the depletion region of the CZTS absorber (C_a), so that:

$$\frac{1}{C_\mathrm{m}} = \frac{1}{C_\mathrm{a}} + \frac{1}{C_\mathrm{b}} \qquad (5)$$

Here $C_\mathrm{a} = \varepsilon_0\varepsilon_\mathrm{a}\Sigma/W_\mathrm{D}$ and $C_\mathrm{b} = \varepsilon_0\varepsilon_\mathrm{b}\Sigma/d$, where ε_0 is the vacuum permittivity, ε_a (ε_b) is the relative permittivity of the absorber (buffer) layer, Σ is the solar cell area, and d is the thickness of the buffer layer. Under these assumptions, the extracted CZTS depletion region width reduces to 150 nm, and further to 110 nm if both the CdS and the i-ZnO layers are assumed to be completely depleted. Hence, we estimate an interval from 110 to 190 nm for the depletion width in CZTS. From this we conclude that the minority carrier diffusion length must be at least 300 nm. Indeed, if the diffusion length is simply calculated using the measured lifetime of 15 ns and a CZTS electron mobility of 3 cm^2/Vs [42], the result is 350 nm.

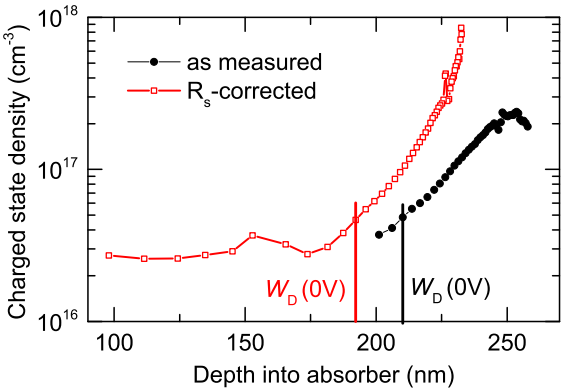

Figure 12: Depth profile of the density of charged states in the CZTS absorber extracted from a capacitance-voltage measurement. Black filled symbols: uncorrected data assuming zero series resistance. Open red symbols: data corrected for an AC series resistance of 8.1 Ω cm^2. W_D is the width of the depletion region at zero bias, assuming that the CdS and i-ZnO layers have much heavier doping than CZTS.

3.2.3 Performance limitations

The main deficit of our device with respect to state-of-the-art CZTS solar cells is the low fill factor of 47.9%, which is due to a high ideality factor and high series resistance. To investigate the possible origin of the latter, we studied the dependence of series resistance on device area. This was done on an adjacent solar cell on the same chip (with similar series resistance) by measuring its dark J-V characteristic after reducing its total area A by mechanical scribing. Four scribing-measurement iterations were performed. As shown in Figure 13, the series resistance of the solar cell increases linearly with area. Hence, we conclude that the main contribution to the high series resistance must be the lateral spreading resistance of the ITO layer. By proper design of a top contact grid, this contribution can be minimized with a minimal loss in short circuit current due to shadowing. Therefore,

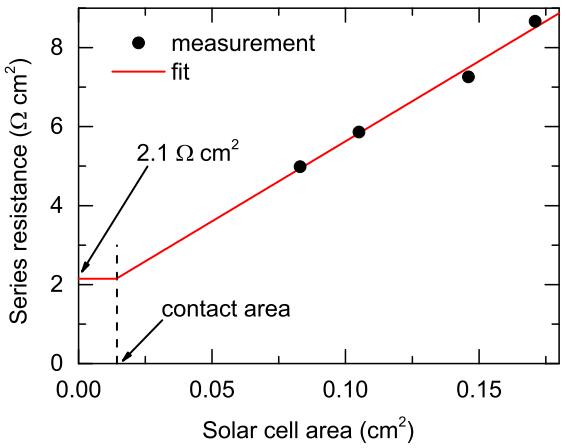

Figure 13: Dependance of dark series resistance on device area, with a linear fit to the measured points. The area of the silver paste dot contact is 0.015 cm^2. The area-independent dark series resistance is extrapolated as 2.1 Ω cm^2. This corresponds to the case where the lateral spreading resistance of the ITO layer is no longer the limiting factor for the series resistance.

we plotted in Figure 8 also the simulated J-V curve under illumination with the same parameters of the fitted experimental J-V curve but a lower realistic series resistance of 1 Ω cm^2. As a result the fill factor improves up to a value of 58%, close to the values reported for state-of-the-art CZTS solar cells, which would lead to a device efficiency of 6.3% (Figure 8).

The origin of the high ideality factor can only be speculated at the moment. However, it was observed in a study on ultra-thin CdTe solar cells [43] that the ideality factor increased with decreasing absorber thickness, up to a value of 3.9 for a thickness of 500 nm. The authors attributed the fact to voltage-dependent collection in the thin solar cell. This explanation may apply to our device as well, since our estimated collection depth is not much larger than the thickness of the absorber. This implies that significant collection losses may occur under forward bias, where the depletion region shrinks.

The V_{oc} of our device is inferior to [9] by about 50 mV. Since our carrier lifetimes are relatively high, this discrepancy could be due to enhanced back surface recombination in the thin absorber, or alternatively to a voltage-dependent collection efficiency under forward bias as proposed above.

4 Conclusion

We reported a pure-sulfide CZTS solar cell device with 5.2% active area efficiency using an ultra-thin absorber (< 450 nm) prepared by pulsed laser deposition. Careful control of the laser fluence allows deposition of high-quality amorphous CZTS precursors with the optimal stoichiometry for solar cells. Such precursors do not result in detectable segregation of secondary phases in the subsequent annealing step. We believe this is the main reason why the present device performs well compared to previously reported CZTS devices of similar thickness. In particular, the short circuit current is comparable to (thicker) state-of-the-art CZTS devices, when the losses related to incomplete light absorption are taken into account. Despite the small absorber thickness, there are no signs that material and junction quality are significantly lower than that of thicker absorbers: grain size, carrier lifetimes, collection efficiency, shunt resistance, and dark saturation current are all similar to benchmark CZTS solar cells. The main deficit compared to benchmark CZTS solar cells is in the fill factor, which, however, does not appear to be a thickness-related effect. Instead, it is mostly due to non-optimal contact geometry, which should not represent a severe development roadblock. In absolute terms, the low open circuit voltage remains the main problem preventing > 10% efficiencies to be achieved in CZTS solar cells.

5 Acknowledgements

This work was supported by a grant from the Danish Council for Strategic Research. CINF is funded by the Danish National Research Foundation (DNRF54). The authors are grateful to Fangzhou Zhou (UNSW) for assistance with device fabrication and pack-

aging, to Fangyang Liu (UNSW) for assistance with efficiency measurement, and to John Stride (UNSW) for lab access. A. Crovetto acknowledges the Nanocarbon and Nanoprobes groups (DTU Nanotech) for usage of the Raman setup.

References

[1] Ito K. *Copper Zinc Tin Sulfide-Based Thin-Film Solar Cells*. Wiley, 2015.

[2] Liu X, Feng Y, Cui H, Liu F, Hao X, Conibeer G, Mitzi DB, Green M. The current status and future prospects of kesterite solar cells: a brief review. *Progress in Photovoltaics: Research and Applications* 2016; doi:10.1002/pip.2741.

[3] Wang W, Winkler MT, Gunawan O, Gokmen T, Todorov TK, Zhu Y, Mitzi DB. Device Characteristics of CZTSSe Thin-Film Solar Cells with 12.6% Efficiency. *Advanced Energy Materials* 2013; **4**(7):1301 465, doi: 10.1002/aenm.201301465.

[4] Tajima S, Itoh T, Hazama H, Ohishi K, Asahi R. Improvement of the open-circuit voltage of Cu_2ZnSnS_4 solar cells using a two-layer structure. *Applied Physics Express* 2015; **8**(8):082 302, doi:10.7567/APEX.8.082302.

[5] Jackson P, Hariskos D, Wuerz R, Kiowski O, Bauer A, Friedlmeier TM, Powalla M. Properties of $Cu(In,Ga)Se_2$ solar cells with new record efficiencies up to 21.7%. *physica status solidi (RRL) - Rapid Research Letters* 2015; **9**(1):28–31, doi:10.1002/pssr.201409520.

[6] Sun K, Yan C, Liu F, Huang J, Zhou F, Stride JA, Green M, Hao X. Over 9% Efficient Kesterite Cu_2ZnSnS_4 Solar Cell Fabricated by Using $Zn_{1-x}Cd_xS$ Buffer Layer. *Advanced Energy Materials* 2016; doi: 10.1002/aenm.201600046.

[7] Scragg JJ, Kubart T, Wätjen JT, Ericson T, Linnarsson MK, Platzer-Björkman C. Effects of Back Contact Instability on Cu_2ZnSnS_4 Devices and Processes. *Chemistry of Materials* 2013; **25**(15):3162–3171, doi: 10.1021/cm4015223.

[8] Fairbrother A, Fontané X, Izquierdo-Roca V, Espíndola-Rodríguez M, López-Marino S, Placidi M, Calvo-Barrio L, Pérez-Rodríguez A, Saucedo E. On the formation mechanisms of Zn-rich Cu_2ZnSnS_4 films prepared by sulfurization of metallic stacks. *Solar Energy Materials and Solar Cells* 2013; **112**:97–105, doi: 10.1016/j.solmat.2013.01.015.

[9] Shin B, Gunawan O, Zhu Y, Bojarczuk NA, Chey SJ, Guha S. Thin film solar cell with 8.4% power conversion efficiency using an earth-abundant Cu_2ZnSnS_4 absorber. *Progress in Photovoltaics: Research and Applications* 2011; **21**(1):72–76, doi: 10.1002/pip.1174.

[10] Wang K, Gunawan O, Todorov T, Shin B, Chey SJ, Bojarczuk NA, Mitzi D, Guha S. Thermally evaporated Cu_2ZnSnS_4 solar cells. *Applied Physics Letters* 2010; **97**(14):143 508, doi:10.1063/1.3499284.

[11] Mise T, Tajima S, Fukano T, Higuchi K, Washio T, Jimbo K, Katagiri H. Improving the photovoltaic performance of co-evaporated Cu_2ZnSnS_4 thin-film solar cells by incorporation of sodium from NaF layers. *Progress in Photovoltaics: Research and Applications* 2016; :n/a–n/adoi:10.1002/pip.2745.

[12] Schubert BA, Marsen B, Cinque S, Unold T, Klenk R, Schorr S, Schock HW. Cu_2ZnSnS_4 thin film solar cells by fast coevaporation. *Progress in Photovoltaics: Research and Applications* 2011; **19**(1):93–96, doi:10.1002/pip.976.

[13] Moriya K, Tanaka K, Uchiki H. Fabrication of Cu_2ZnSnS_4 Thin-Film Solar Cell Prepared by Pulsed Laser Deposition. *Japanese Journal of Applied Physics* 2007; **46**(9A):5780–5781, doi: 10.1143/JJAP.46.5780.

[14] Moriya K, Tanaka K, Uchiki H. Cu_2ZnSnS_4 Thin Films Annealed in H_2S Atmosphere for Solar Cell Absorber Prepared by Pulsed Laser Deposition. *Japanese Journal of Applied Physics* 2008; **47**(1):602–604, doi: 10.1143/JJAP.47.602.

[15] Jin X, Yuan C, Zhang L, Jiang G, Liu W, Zhu C. Pulsed laser deposition of $Cu_2ZnSn(S_xSe_{1-x})_4$ thin film solar cells using quaternary oxide target prepared by combustion method. *Solar Energy Materials and Solar Cells* 2016; **155**:216–225, doi: 10.1016/j.solmat.2016.06.022.

[16] Willmott PR. Deposition of complex multielemental thin films. *Progress in Surface Science* 2004; **76**(6-8):163–217, doi: 10.1016/j.progsurf.2004.06.001.

[17] Norton D. Pulsed Laser Deposition of complex materials: Progress towards applications. *Pulsed Laser Deposition of Thin Films*, Eason R (ed.). John Wiley & Sons, Inc.: Hoboken, NJ, USA, 2008; 3–31, doi: 10.1002/0470052120.

[18] Frumar M, Frumarova B, Nemec P, Wagner T, Jedelsky J, Hrdlicka M. Thin chalcogenide films prepared by pulsed laser deposition – new

amorphous materials applicable in optoelectronics and chemical sensors. *Journal of Non-Crystalline Solids* 2006; **352**(6):544–561, doi:10.1016/j.jnoncrysol.2005.11.043.

[19] Krebs H. Characteristic properties of laser-deposited metallic systems. *International Journal of Non-equilibrium Processing* 1997; **10**(1).

[20] Ohnishi T, Lippmaa M, Yamamoto T, Meguro S, Koinuma H. Improved stoichiometry and misfit control in perovskite thin film formation at a critical fluence by pulsed laser deposition. *Applied Physics Letters* 2005; **87**(24):1–3, doi:10.1063/1.2146069.

[21] Dittrich H, Klose M, Brieger M, Schaffler R, Schock H. $CuInSe_2$ thin film solar cells by pulsed laser deposition. *Conference Record of the Twenty Third IEEE Photovoltaic Specialists Conference*, 1993; 617–620, doi:10.1109/PVSC.1993.347022.

[22] Yan C, Liu F, Sun K, Song N, Stride JA, Zhou F, Hao X, Green M. Boosting the efficiency of pure sulfide CZTS solar cells using the In/Cd-based hybrid buffers. *Solar Energy Materials and Solar Cells* 2016; **144**:700–706, doi:10.1016/j.solmat.2015.10.019.

[23] Gokmen T, Gunawan O, Todorov TK, Mitzi DB. Band tailing and efficiency limitation in kesterite solar cells. *Applied Physics Letters* 2013; **103**(10):103 506, doi:10.1063/1.4820250.

[24] Piacente V, Foglia S, Scardala P. Sublimation study of the tin sulphides SnS_2, Sn_2S_3 and SnS. *Journal of Alloys and Compounds* 1991; **177**(1):17–30, doi:10.1016/0925-8388(91)90053-X.

[25] Brunetti B, Piacente V, Scardala P. Study on sulfur vaporization from covellite (CuS) and anilite ($Cu_{1.75}S$). *Journal of Alloys and Compounds* 1994; **206**(1):113–119, doi:10.1016/0925-8388(94)90018-3.

[26] Haynes WM. *CRC Handbook of Chemistry and Physics, 96th Edition*. CRC Press, 2015.

[27] Katagiri H. Survey of development of CZTS-based thin film solar cells. *IEEE 3rd International Conference on Photonics*, 2012; 345–349, doi:10.1109/ICP.2012.6379533.

[28] Ettlinger RB, Crovetto A, Canulescu S, Cazzaniga A, Ravnkilde L, Youngman T, Hansen O, Pryds N, Schou J. Formation of copper tin sulfide films by pulsed laser deposition at 248 and 355 nm. *Applied Physics A* 2016; **122**(4):466, doi:10.1007/s00339-016-9939-4.

[29] Dimitrievska M, Fairbrother A, Fontané X, Jawhari T, Izquierdo-Roca V, Saucedo E, Pérez-Rodríguez A. Multiwavelength excitation Raman scattering study of polycrystalline kesterite Cu_2ZnSnS_4 thin films. *Applied Physics Letters* 2014; **104**(2):021 901, doi:10.1063/1.4861593.

[30] Ren Y, Scragg JJS, Frisk C, Larsen JK, Li SY, Platzer-Björkman C. Influence of the Cu_2ZnSnS_4 absorber thickness on thin film solar cells. *physica status solidi (a)* 2015; **212**(12):2889–2896, doi:10.1002/pssa.201532311.

[31] Paudel N, Wieland K, Compaan A. Ultrathin CdS/CdTe solar cells by sputtering. *Solar Energy Materials and Solar Cells* 2012; **105**:109–112, doi:10.1016/j.solmat.2012.05.035.

[32] Li-Kao ZJ, Naghavi N, Erfurth F, Guillemoles JF, Gérard I, Etcheberry A, Pelouard JL, Collin S, Voorwinden G, Lincot D. Towards ultrathin copper indium gallium diselenide solar cells: proof of concept study by chemical etching and gold back contact engineering. *Progress in Photovoltaics: Research and Applications* 2012; **20**(5):582–587, doi:10.1002/pip.2162.

[33] Lundberg O, Bodegård M, Malmström J, Stolt L. Influence of the $Cu(In,Ga)Se_2$ thickness and Ga grading on solar cell performance. *Progress in Photovoltaics: Research and Applications* 2003; **11**(2):77–88, doi:10.1002/pip.462.

[34] Larsen JK, Li SY, Scragg JJS, Ren Y, Hägglund C, Heinemann MD, Kretzschmar S, Unold T, Platzer-Björkman C. Interference effects in photoluminescence spectra of Cu2ZnSnS4 and Cu(In,Ga)Se2 thin films. *Journal of Applied Physics* 2015; **118**(3):035 307, doi:10.1063/1.4926857.

[35] Li SY, Hägglund C, Ren Y, Scragg JJ, Larsen JK, Frisk C, Rudisch K, Englund S, Platzer-Björkman C. Optical properties of reactively sputtered Cu_2ZnSnS_4 solar absorbers determined by spectroscopic ellipsometry and spectrophotometry. *Solar Energy Materials and Solar Cells* 2016; **149**:170–178, doi:10.1016/j.solmat.2016.01.014.

[36] Crovetto A, Chen R, Ettlinger RB, Cazzaniga AC, Schou J, Persson C, Hansen O. Dielectric function and double absorption onset of monoclinic Cu_2SnS_3: Origin of experimental features explained by first-principles calculations. *Solar Energy Materials and Solar Cells* 2016; **154**:121–129, doi:10.1016/j.solmat.2016.04.028.

[37] Ohnesorge B, Weigand R, Bacher G, Forchel A, Riedl W, Karg FH. Minority-carrier lifetime and efficiency of $Cu(In,Ga)Se_2$ solar cells. *Applied Physics Letters* 1998; **73**(9):1224–1226, doi:10.1063/1.122134.

109

[38] Schroder DK. *Semiconductor material and device characterization*. John Wiley & Sons: Hoboken, New Jersey, 2006; 63–84.

[39] Hegedus SS, Shafarman WN. Thin-film solar cells: device measurements and analysis. *Progress in Photovoltaics: Research and Applications* 2004; **12**(23):155–176, doi: 10.1002/pip.518.

[40] Misic B, Pieters BE, Theisen JP, Gerber A, Rau U. Shunt mitigation in ZnO:Al/i-ZnO/CdS/Cu(In,Ga)Se_2 solar modules by the i-ZnO/CdS buffer combination. *physica status solidi (a)* 2015; **212**(3):541–546, doi: 10.1002/pssa.201431496.

[41] Shafarman WN, Siebentritt S, Stolt L. Cu(InGa)Se_2 Solar Cells. *Handbook of Photovoltaic Science and Engineering*, Luque A, Hegedus S (eds.). chap. 13, John Wiley & Sons, Ltd: Chichester, UK, 2010; 579, doi: 10.1002/9780470974704.

[42] Shin B, Gershon T, Guha S. CZTS-Based Thin-Film Solar Cells Prepared via Coevaporation. *Copper Zinc Tin Sulfide-Based Thin-Film Solar Cells*, Ito K (ed.). chap. 15, Wiley, 2015; 344–345.

[43] Bai Z, Yang J, Wang D. Thin film CdTe solar cells with an absorber layer thickness in micro- and sub-micrometer scale. *Applied Physics Letters* 2011; **99**(14):143 502, doi: 10.1063/1.3644160.

Solid Phase	Specific heat C_p J/(K*mol)	Melting point °C	Heat of Fusion kJ/mol	Heat of vaporization kJ/mol	Vapor products
CuS	47.8	220*	s.s.r 1		$S_{2(g)}$
$Cu_{1.75}S$	76.3	507*	s.s.r 2		$S_{2(g)}$
Cu_2S	76.3	1129	9.62	N.A.	N.A.
SnS	49.3	881	31.6	220 (subl.)	$SnS_{(g)}$
ZnS	46.0	1827	30.0	206 (subl.)	$ZnS_{(g)}$, Zn, $S_{2(g)}$

Table 1: Physical properties of the most relevant solid state phases in the sintered target. Other binary and ternary chalcogenide phases are not excluded, but no metallic phases were found. Subscripts (s)/(g) indicate solid/gas. Melting temperatures marked with * relate to the solid state reaction (s.s.r.) mentioned in the text. Heat of vaporization is only given for compounds that can be fully evaporated, either congruently or via dissociation product. Data from [24–26].

Chapter 7

Double absorption onset of monoclinic Cu2SnS3: experimental features explained by DFT

Last, but not least.

Achieving reproducibility made the study entitled "Dielectric function and double absorption onset of monoclinic Cu_2SnS_3: Origin of experimental features explained by first-principles calculations" possible. The work, of which an excerpt is given here in Figure 7.2, was published in the journal "Solar Energy Materials and Solar Cells" and is the second most important outcome of my phD. While it does not take long time to discuss it, it rightfully deserves the status of a chapter.

Short story: my colleague Rebecca once made a (seemingly) phase-pure monoclinic CTS thin-film which featured interesting optical properties, as revealed by spectroscopic ellipsometry. Unfortunately, reproducibility was an issue and the consistency of the results was doubtful. After my study on the fluence dependence for CZTS films, we thought it was finally possible to also replicate that interesting CTS sample. We did, and in the work we furthermore clarified the nature of the absorption mechanism, which was a debated question in literature. Aim of this pico-chapter is also to convince the reader (and myself) that the lengthy discussion in the "Guidelines for PLD of chalcogenide targets", Chapter 5 had its own utility, and it was not just me being pedantic over irrelevant details.

7.1 Pico-introduction to CTS material

Cu_2SnS_3 (CTS) is another earth-abundant non-toxic *p*-type chalcogenide material investigated as absorber for thin film solar cells, see for example [83]. It is again a direct bandgap semiconductor with record efficiency of 4.6% [81] and Cu-poor compositions are again suitable for the fabrication of solar cell absorbers. Despite the lower number of elementary constituents than CZTS, its physical properties are by no means easier to understand. CTS is reported to exist in three different phases [82, 83]: monoclinic, cubic and tetragonal. All these phases have a zinc-blend structure, and differs only in the degree of disorder among the cations Cu and Sn, resulting in phases with different crystal symmetries and defect densities. The record 4.6% [81] is obtained with a CTS/CdS heterojunction and the CTS absorber is reported to be monoclinic, the most ordered phase.

7.2 Experimental work

The experimental challenges were (1) finding the conditions to fabricate a monoclinic CTS film and (2) measuring its optical functions with spectroscopic ellipsometry. Due to the high sensitivity of spectroscopic ellipsometry to surface roughness, the samples had to be compact and very flat. Precursors of thickness below 100 nm were deposited at room temperature on Mo-coated SLG, as those used for making solar cells. The PLD equipment used for this work is the one with the solid state Nd:YAG laser described in Section 5.1. The use of SLG/Mo substrates introduces complexity to the ellipsometry analysis, especially since we were going to investigate the absorption edge of CTS. However, for the study to be relevant, one must try

to keep the experimental conditions as close as possible to device fabrication. Aiming for the maximally ordered phase, our intuition suggests that the Cu/Sn ratio should be as close as possible to its stoichiometric value. Indeed, from the literature survey [84], the use of a large amount of SnS powder during the annealing is suggested. We deposited several Cu-poor CTS precursors and added in the graphite box both S and SnS powders for the annealing step. We tested different precursors (in terms of Cu/Sn%) and different annealing strategies (temperature and amount of SnS powder). The thin films were characterized in Lyngby by Andrea Crovetto with SEM imaging, Raman spectroscopy and grazing incidence XRD. Contrary to CZTS, the different phases of CTS are distinguishable under standard Raman investigations.

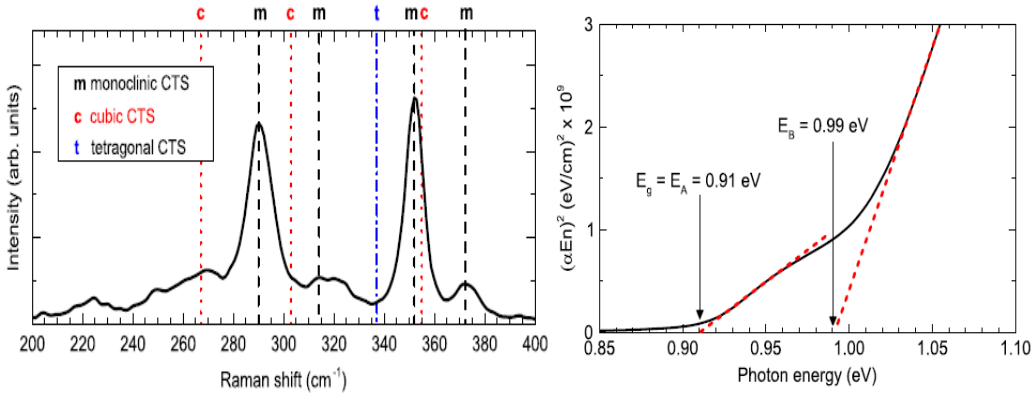

Figure 7.1: The key experimental finding of the paper: the double absorption onset commonly observed in CTS films (plot on the right) is an attribute of the pure monoclinic phase (Raman spectrum on the left). Not shown here, the experimental optical functions are in excellent agreement with those calculated using a DFT model for a defect-free, monoclinic CTS phase.

7.3 Conclusion

We showed that the double onset in the absorption coefficient originates from optical transitions at the Γ-point from three energetically close-lying valence bands to a single conduction band. Structural imperfection, like secondary phases, are not needed to explain the absorption spectrum. Finally, we show that the absorption coefficient of CTS is particularly large in the near-bandgap spectral region when compared to similar photovoltaic materials.

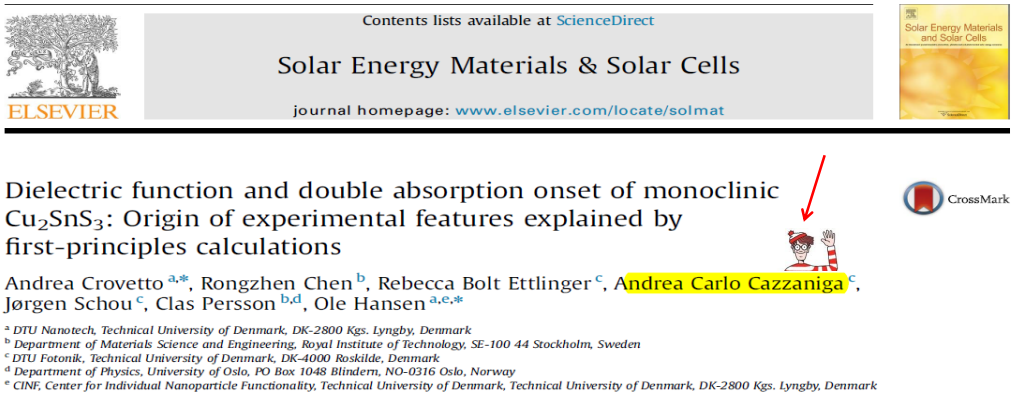

Contents lists available at ScienceDirect

Solar Energy Materials & Solar Cells

journal homepage: www.elsevier.com/locate/solmat

Dielectric function and double absorption onset of monoclinic Cu_2SnS_3: Origin of experimental features explained by first-principles calculations

Andrea Crovetto [a,*], Rongzhen Chen [b], Rebecca Bolt Ettlinger [c], Andrea Carlo Cazzaniga [c], Jørgen Schou [c], Clas Persson [b,d], Ole Hansen [a,e,*]

[a] DTU Nanotech, Technical University of Denmark, DK-2800 Kgs. Lyngby, Denmark
[b] Department of Materials Science and Engineering, Royal Institute of Technology, SE-100 44 Stockholm, Sweden
[c] DTU Fotonik, Technical University of Denmark, DK-4000 Roskilde, Denmark
[d] Department of Physics, University of Oslo, PO Box 1048 Blindern, NO-0316 Oslo, Norway
[e] CINF, Center for Individual Nanoparticle Functionality, Technical University of Denmark, Technical University of Denmark, DK-2800 Kgs. Lyngby, Denmark

Figure 7.2: Front page of the paper presented in this chapter. The full paper is not included, since its content is beyond the topic of this thesis. My contribution to this work was related to the fabrication of the CTS films, which I have done following the principles described in Chapter 5.

Conclusions

Whereof one cannot speak, thereof one must be silent
Ludwig Wittgenstein

Perhaps my last few words on this project, and on a topic that has drawn my attention for the past three years. It was easier to write the Preface.

The very scientific novelty in this project, before the specific choice on CZTS material, consisted in a real, long-standing effort to use PLD for the production of thin-film solar cells. This was a very unique experiment, and rightfully deserves a thoughtful discussion. Should I listen to Wittgenstein, this part of the conclusions would never be written. Rather, I intend to offer my own view on the topic, which has the few merits of being stark, partial and refutable.

If you browse "PLD + solar cells" (*and do a lot of search), the outcome is nothing but a handful of papers. I counted eight, and put them into the table below. Eight papers, 8. Considering that solar cells are fashionable since forever, that PLD is out there since the early 90's, and that in the last decade the number of publications about *-whatever-* has grown out of proportion, this is a ridiculously low number. Is there something wrong with PLD and solar cells? Yes.
At least if we talk about polycrystalline materials. They are not deposited on 5×5 mm^2 single crystal substrates, the growth is not epitaxial. The main strengths of PLD do not find application here. Still, these are not motivations for why PLD should fail. And indeed, there are no fundamental limitations why it should, as we could demonstrate in this work. By bringing our precursors to UNSW, and letting them do the annealing and finishing the device, we got a *state-of-the-art* CZTS device. Our record in-house device is still stuck at 2.6%.
Indeed, the most successful techniques used for depositing the absorber layers

are those enabling accurate control and reproducibility; they are not successful because of any unique physics[1]. This, I believe, is the reason why so very few people have succeed in using PLD for making solar cells: the low sample throughput of typical PLD setups, and the very different background knowledge. PLD is hardly used in connection with complex devices, where the overall process is more important than each single step. PLD is used for fundamental studies, one layer or one interface at time. I did say that this was part was refutable, isn't it?

ref.	Material	Year	Efficiency
[85]	CIGS	1993	8.5%
[86]	CdTe	2012	6.7%
[87]	CdTe	1991	>8%
[88]	CdTe	1993	6.4%
[75]	CZTS	2006	1.7%
[76]	CZTS	2008	0.64%
[79]	CZTS	2016	4.9%

Table 7.1: Collection of all the papers found in the literature reporting the fabrication of a thin film solar device where the absorber layer was fabricated with Pulsed Laser Deposition. The search was restricted to CIGS, CdTe and CZTS. It's worth noting that the first ever reported solar cells with CIGS and CdTe absorbers had an efficiency of >5% and >8%, respectively.

Being it such a humongous effort, is there any need for using PLD in this field? Yes.
Precisely because PLD bears some unique physics in the deposition process, this should be exploited with the goal of bringing about new insights to our fundamental understanding of the physics of thin-film PV devices. In this respect, the objection that PLD is a non-scalable technique is completely irrelevant. Even further, it makes a lot more sense to use PLD for making solar cells with a clear scientific goal, rather than investigating low cost deposition techniques for materials that have not proven yet viable for commercialization.
The features that PLD can bring to the TF-PV community were discussed in Section 0.5 with regards to CZTS material, and the contents can easily be generalized to any other PV materials.

About CZTS. The main problem is the low Voc, and I have not developed any original contribution on this issue. Two less discussed problems

[1] If that were the case, how could many different deposition techniques be successful?

are exfoliation and reproducibility of the results. In particular, the annealing step is very critical to both these issues.
(1) Against the graphite box. I would very much favour the use of H_2S gas during the annealing instead of using a graphite box filled with some sulfur powder. The graphite box is porous, such that one never knows how much sulfur is in there, nor if it was contaminated with something else or not. The sulfur gas dynamics in this system is not-known. If screwing or not the lid of the graphite box makes a big difference, as I was told at a conference, this method is not reliable. Using H_2S gas (or similar) would enable an exact knowledge of the sulfurizing gas during the whole process. From the literature there is usually no hope that one can understand how the sulfurization process was conducted in a particular study. H_2S is toxic and dangerous, it is definitively more expensive than using the graphite box. Still, we are doing research and the goal is not yet, unfortunately, to make it cheaper. The goal is to make it work! Plus, how much does it cost in terms of time, work, and chemicals, the optimization of this graphite-box approach? Maybe I am missing something on the utility of this method.
(1.bis) If a graphite box has to be used, I would make my new one ultra thin, so that the amount of sulfur that can accumulate inside is very low and easy to remove with a fast bake-out.
(2) Exfoliation is a problem that affects CZTS devices, but not CZTSe or CZTSSe. It happens during the sulfurization process, when the CZTS grains grow and a MoS_x layer forms at the bottom contact. Contrary to what seen for the $MoSe_x$ layer, the MoS_x layer does not seem beneficial to the CZTS device, as discussed in Section 0.3.3. Could depositing the CZTS onto a *already-selenized* Mo back contact reduce exfoliation and produce a better bottom contact?

About this project. We achieved a basic understanding of the physics behind PLD of CZTS, such that the deposition of CZTS precursors is now a stable and reproducible process. This was illustrated in Chapter 5, and the outlined working procedure is very easy to implement in any other PLD setup.
Further, the results on the non-stoichiometric transfer, Chapter 6, are probably of general validity for any case of PLD on multi-crystalline sintered targets. Since the expertise in PLD is largely on the use of a single crystal (or single phase) target, this case-study may turn out to be useful for future projects devoted to finding "new materials" for "old applications", where compound targets are usually the only option available.

Acknowledgements

I very much thank my supervisor Jørgen Schou for the trust he has always accorded to me and for the opportunity to work in this interesting research field. I hope I did not delude any expectations. The freedom of work and the participation to many international conferences made me a better physicist, and that's not something one can find everywhere. I thank all the people in our group, Stela, Sara and Rebecca for the time shared in the lab and outside. Many people have given their valuable contribution, professors Ole Hansen and Nini Pryds, reading our last manuscript was maybe a pleasure, reading the first ones was surely not. I should also mention all the people who I met at Risø, colleagues and friends, I don't make a list so nobody is forgotten. Thanks Simone for the time at the neutron house, and thanks Joan for actually depositing the 5.2% sample!
Last, but not least, this work, and my whole phD, have invaluably benefited from the contribution of Ancro and Alice, in different ways but in about the same amount of phone calls.

Bibliography

[1] **A. Cazzaniga**, R.B. Ettlinger, S. Canulescu, J. Schou and N. Pryds, *Nanosecond laser ablation and deposition of silver, copper, zinc and tin*, Appl. Phys. A (2014) 117:89–92;

[2] R. B. Ettlinger, **A. Cazzaniga**, S. Canulescu, N. Pryds and J. Schou, *Pulsed laser deposition from ZnS and Cu2SnS3 multicomponent targets*, Appl. Surf. Sci. 336, 385-390 (2015);

[3] A. Crovetto, **A. Cazzaniga**, R. B. Ettlinger, J. Schou and O. Hansen, *Optical properties and surface characterization of pulsed laser-deposited Cu2ZnSnS4 by spectroscopic ellipsometry*, Thin Solid Films 582 , 203-207 (2015);

[4] R. B. Ettlinger, A. Crovetto, S. Canulescu, **A. Cazzaniga**, L. Ravnkilde, T. Youngman, O. Hansen, N. Pryds and J. Schou, *Formation of copper tin sulfide films by pulsed laser deposition at 248 and 355 nm*, Appl. Phys. A 122, 1-10 (2016);

[5] **A. Cazzaniga**, A. Crovetto, R. B. Ettlinger, S. Canulescu, O. Hansen, N. Pryds and Jørgen Schou, *ZnS toplayer for enhancement of the crystallinity of CZTS absorber during the annealing.* 2015 IEEE 42ND PHOTOVOLTAIC SPECIALIST CONFERENCE (PVSC), Book Series: IEEE Photovoltaic Specialists Conference, pp.1-4. Published: 2015;

[6] A. Crovetto, R. Chen, R. B. Ettlinger, **A. Cazzaniga**, J. Schou, C. Persson, O. Hansen, *Dielectric function and double absorption onset of monoclinic Cu2SnS3 : Origin of experimental features explained by first-principles calculations*, Solar Energy Mat. and Solar Cells, 154, 121-129 (2016);

[7] **A. Cazzaniga**, A. Crovetto, C. Yan, K. Sun, X. Hao, J. Ramis Estelrich, S. Canulescu, E. Stamate, N. Pryds, O. Hansen, and Jørgen Schou *Ultra-thin Cu2ZnSnS4 solar cell prepared by pulsed laser deposition*, Submitted to "Progress in Photovoltaics: Research and applications" (July 2016);

Chapter 0 - Introduction

[8] B. Shin, O. Gunawan, Y. Zhu, N. A. Bojarczuk, S. Chey and S. Guha *Thin film solar cell with* 8.4% *power conversion efficiency using an earth-abundant Cu2ZnSnS4 absorber*, Prog. Photovolt: Res. Appl. (2013) 21:72–76;

[9] S. Tajima, T. Itoh, H. Hazama, K. Ohishi and R. Asahi, *Improvement of the open-circuit voltage of Cu2ZnSnS4 solar cells using a two-layer structure*, Appl. Phys. Express 8, 082302 (2015);

[10] Fraunhofer ISE: Photovoltaics Report, updated: 26 August 2015;

[11] P. Singh and N.M. Ravindra, *Temperature Dependence of Solar Cell Performance—an Analysis*, solmat, 101: 36–45, 2012;

[12] I. Repins, M. Romero, J. Li, S.H. Wei, D. Kuciauskas, C. Jiang, C. Beall, C. DeHart, J. Mann, W. Hsu, G. Teeter, A. Goodrich, and R. Noufi, *Kesterite successes, ongoing work, and challenges: a perspective from vacuum deposition*, IEEE Journal of Photovoltaics, 3, 439–445, 2013;

[13] J. Li and B. Clemens, *The Role of Grain Boundaries in CZTS-Based Thin-Film Solar Cells*, pag. 313, in: "Copper Zinc Tin Sulfide Based Thin-Film Solar Cells", ed. by K. Ito, Wiley, 2015;

[14] U.S. Geological Survey, *Rare Earth Elements—Critical Resources for High Technology*, USGS Fact Sheet 087-02 (2002);

[15] H. Katagiri, "Sulfurization of Physical Vapor Deposited Precursor Layers", pag.192 in: "Copper Zinc Tin Sulfide Based Thin-Film Solar Cells", ed. by K. Ito, Wiley, 2015;

[16] I. Olekseyuk, I. Dudchak, and L. Piskach, *Phase equilibria in the CU2S-ZnS-SnS2 system.* Journal of Alloys and Compounds, 368(1–2), 135–143, 2004;

[17] A. Walsh, S. Chen, S.-H. Wei, and X Gong, *Kesterite Thin-Film Solar Cells: Advances in Materials Modelling of Cu2ZnSnS4*, Adv. Energy Mater. 2012, 2, 400–409;

[18] J. Scragg, J. Larsen, M. Kumar, C. Persson, J. Sendler, S. Siebentritt, and C. Platzer Bjorkman, *Cu–Zn disorder and band gap fluctuations in Cu2ZnSn(S,Se)4: Theoretical and experimental investigations*, Phys. Status Solidi B 253, No. 2, 247–254 (2016);

[19] G. Rey, A. Redinger, J. Sendler, T. P. Weiss, M. Thevenin, M. Guennou, B. El Adib, and S. Siebentritt, *The band gap of Cu2ZnSnSe4: Effect of order-disorder*, APL 105, 112106 (2014);

[20] S. Chen, A. Walsh, X.-G. Gong, and S.-H. Wei, *Classification of lattice defects in kesterite Cu2ZnSnS4 and Cu2ZnSnSe4 Earth-abundant solar cell absorbers*, Adv. Mater. 25, 1522 (2013);

[21] J. Scragg, T. Ericson, T. Kubart, M. Edoff and C. Platzer-Bjorkman, *Chemical Insights into the Instability of Cu2ZnSnS4 Films during Annealing*, Chem. Mater. 2011, 23, 4625–4633;

[22] A. Redinger, D.M. Berg, P.J. Dale and S. Siebentritt, *The Consequences of Kesterite Equilibria for Efficient Solar Cells*, J. Am. Chem. Soc. (2011), 133 3320–3323;

[23] T. Gershon, T. Gokmen, O. Gunawan, R. Haight, S. Guha and B. Shin, *Understanding the relationship between Cu2ZnSn(S,Se)4 material properties and device performance*,MRS Communications (2014) doi:10.1557/mrc.2014.34;

[24] W. Wang, M.T. Winkler, O. Gunawan, T. Gokmen, T.K. Todorov, Y. Zhu, and D.B. Mitzi, *Device characteristics of CZTSSe thin-film solar cells with 12.6% efficiency*, Adv. Energy Mater. 4, (2014);

[25] R. Geisthardt, M. Topic, and J.R. Sites *Status and Potential of CdTe Solar-Cell Efficiency*, IEEE JOURNAL OF PHOTOVOLTAICS, VOL. 5, NO. 4, JULY 2015;

[26] S. Chen, L.W. Wang, A. Walsh, X. Gong, and S.-H. Wei, *Abundance of CuZn + SnZn and 2CuZn + SnZn defect clusters in kesterite solar cells*, Appl. Phys. Lett. 101, 223901 (2012).

[27] C. Persson, *Electronic and optical properties of Cu2ZnSnS4 and Cu2ZnSnSe4*, J. Appl. Phys. 107, 053710 (2010);

[28] M. Contreras, K. Ramanathan, J. AbuShama, F. Hasoon, D. L. Young, B. Egaas and R. Noufi *Diode Characteristics in State-of-the-Art ZnO/CdS/Cu(In1xGax)Se2 Solar Cells*, Prog. Photovolt: Res. Appl. 2005; 13:209–216;

[29] J. Scragg, T. Kubart, J. Watjen, Tove Ericson, M. Linnarsson, and C. Platzer-Bjorkman, *Effects of Back Contact Instability on Cu2ZnSnS4 Devices and Processes*, Chem. Mater. 2013, 25, 3162−3171;

[30] K. Sun, C. Yan, F. Liu, J. Huang, F. Zhou, J. Stride, M. Green, and X. Hao, *Over 9% Efficient Kesterite Cu2ZnSnS4 Solar Cell Fabricated by Using Zn1–xCdxS Buffer Layer*, Adv. Energy Mater. 2016, 1600046;

[31] C. Platzer-Bjorkman, C. Frisk, J. K. Larsen, T. Ericson, S.-Y. Li, J. J. S. Scragg, J. Keller, F. Larsson, and T. Torndahl, *Reduced interface recombination in Cu2ZnSnS4 solar cells with atomic layer deposition Zn1−xSnxOy buffer layers* , Applied Physics Letters 107, 243904 (2015);

[32] W. Shockley and H.J. Queisser, *Detailed Balance Limit of Efficiency of pn Junction Solar Cells*, J. Appl. Phys. 32, 510 (1961);

[33] S. Siebentritt and A. Redinger, *Loss Mechanisms in Kesterite Solar Cells*, in: "Copper Zinc Tin Sulfide Based Thin-Film Solar Cells", ed. by K. Ito, Wiley, 2015;

[34] K. Tai, O. Gunawan, M. Kuwahara, S. Chen, S.G. Mhaisalkar, C. Huan and David B. Mitzi, *Fill Factor Losses in Cu2ZnSn(SxSe1−x)4 Solar Cells: Insights from Physical and Electrical Characterization of Devices and Exfoliated Films* , Adv. Energy Mater. (2015), 1501609;

[35] D. Aaron, R. Barkhouse, Richard Haight, Noriyuki Sakai, Homare Hiroi, Hiroki Sugimoto, and David B. Mitzi, *Cd-free buffer layer materials on Cu2ZnSn(SxSe1-x)4: Band alignments with ZnO, ZnS, and In2S3*, Appl. Phys. Lett. 100, 193904 (2012);

[36] S. Tajima, K. Kataoka, N. Takahashi, Y. Kimoto, T. Fukano, M. Hasegawa, and H. Hazama, *Direct measurement of band offset at the interface between CdS and Cu2ZnSnS4 using hard X-ray photoelectron spectroscopy*, Appl. Phys. Lett. 103, 243906 (2013);

Chapter 1 - Introduction

[37] A. Fairbrother, X. Fontane, V. Roca, S. Marino, M. Placidi, E. Saucedo, *On the formation mechanisms of Zn-rich Cu2ZnSnS4 films prepared by sulfurization of metallic stacks*, Solmat, 112(2013)97–105;

[38] S. Chen, X. Gong, A. Walsh and S.H. Wei, *Defect physics of the kesterite thin-film solar cell absorber Cu2ZnSnS4*, Appl. Phys. Lett. 96, 021902 (2010);

[39] A. Polizzotti, I. Repins,R. Noufi, S.H. Wei and David B. Mitzi, *The state and future prospects of kesterite photovoltaics*, Energy Environ. Sci., 2013, 6, 3171;

[40] A. Weber, R. Mainz, and H. W. Schock, *On the Sn loss from thin films of the material system Cu–Zn–Sn–S in high vacuum*,J. Appl. Phys. 107, 013516 (2010);

[41] O. Gunawan, T. Gokmen, and D.B. Mitzi, *Suns-VOC characteristics of high performance kesterite solar cells*, J. of App. Phys. 116, 084504 (2014);

[42] P.R. Willmott, *Deposition of complex multielemental thin films*, Progress in Surface Science 76 (2004) 163–217;

[43] J. Schou, *Physical aspects of the pulsed laser deposition technique: The stoichiometric transfer of material from target to film*, Applied Surface Science 255 (2009) 5191–5198;

[44] H. Fujioka, *Pulsed Laser Deposition (PLD)*, in "Handbook of Crystal Growth", 2nd ed.(2014), Vol. *Thin films and Epitaxy.* Edited by:Tom Kuech, ISBN: 978-0-444-63304-0;

[45] S.I. Anisimov and B.S. Luk'yanchuk,*Selected problems of laser ablation theory*, Physics, Uspekhi 45 (3) 293 324 (2002);

[46] S. Anisimov, D Bauerle, B Lukyanchuk: Phys. Rev. B. 48,12076 (1993);

[47] S. Amoruso, B. Toftmann and J. Schou, Phys Rew E 69, 056403, (2004);

[48] J. Schou, S. Amoruso, and J.G. Lunney, *Plume dynamics*, in: Laser Ablation and its Applications, ed. by Claude Phillips, Springer 2007;

[49] P.R. Willmott, Reviews of Modern Physics, Vol. 72, No. 1, January 2000, p. 315;

[50] D. Dijkkamp, T. Venkatesan, X.D. Wu, S.A. Shaheen, N. Jisrawi, Y.H. Min-Lee, W.L. McLean, M. Croft, Appl. Phys. Lett. 51 (1987) 619;

[51] H. Sankur, W.J. Gunning, J. deNatale, J.F. Flintoff, J. Appl. Phys. 65 (1989) 2475;

[52] P.R. Willmott, P. Manoravi, K. Holliday, Appl. Phys. A 70 (2000) 425:

[53] A. Ohtomo, H.Y. Hwang, *A high-mobility electron gas at the LaAlO3/SrTiO3 heterointerface*, Nature (2004) 427 423;

[54] H.U. Krebs, "Characteristic properties of laser deposited systems", Int. Jour. of Non-Eq. Proc.; 1997, Vol. 10, pp. 3-24 1368-9290, 1997;

[55] D. O'Mahony and J.G. Lunney *Group III Nitride Growth* in: "Pulsed Laser Deposition of Thin Films: Applications-Led Growth of Functional Materials", Ed. by R. Eason (2007), John Wiley;

[56] R. Timm, P. R. Willmott, and J. R. Huber, *Ablation and blowoff characteristics at 248 nm of Al, Sn and Ti targets used for thin film pulsed laser deposition*, J. Appl. Phys. 80, 1794 (1996);

[57] F. Rong, *Liquid target pulsed laser deposition*, Applied Physics Letters 67, 1022 (1995);

[58] D. H. Lowndes, in *Laser Ablation Desorption*, Exp. Methods Phys. Sci. Vol 30, edited by J. C. Miller and R. F. Haglund (Academic Press, New York, 1998), pp. 475–571;

[59] L. Chen, in *Pulsed Laser Deposition of Thin Film*, edited by D. B. Crisey and G. K. Hubler, 1st ed. (Wiley, 1994), pp. 167–198;

[60] N. Arnold and D. Bäuerle, *Uniform target ablation in pulsed-laser deposition*, Appl. Phys. A 68, 363–367 (1999);

[61] T. Ohnishi, M. Lippmaa, T. Yamamoto, S. Meguro, and H. Koinuma, *Improved stoichiometry and misfit control in perovskite thin film formation at a critical fluence by pulsed laser deposition*, Appl. Phys. Lett. 87, 241919 (2005);

[62] T. Ohnishi, K. Shibuya, T. Yamamoto, and M. Lippmaa, *Defects and transport in complex oxide thin films*,J. Appl. Phys. 103, 103703 (2008);

[63] T. Ohnishi, H. Koinuma, M. Lippmaa, *Pulsed laser deposition of oxide thin films*, Appl. Surf. Sci., 252 (2006) 2466–2471;

Chapter 2 and 3 - PLD of Cu, Zn, and Sn

[64] J. Lunney, *Pulsed laser deposition of metal and metal multilayer films*, Applied Surface Science 86 (1995) 79-85;

[65] R. Dietsch, Th. Holz, H. Mai,F. Meyer, R. Scholz, B. Wehner, *High precision large area PLD of X-ray optical multilayers*, Applied Surface Science 127–129 1998 451–456;

[66] J. Shena, Zheng Gaib, J. Kirschnerc, *Growth and magnetism of metallic thin films and multilayers by pulsed-laser deposition*, Surface Science Reports 52 (2004) 163–218;

[67] F. Doring, A.L. Robisch, C. Eberl, M. Osterhoff, A. Ruhlandt, T. Liese, F. Schlenkrich, S. Hoffmann, M. Bartels, T. Salditt, and H.U. Krebs, *Sub-5 nm hard x-ray point focusing by a combined Kirkpatrick-Baez mirror and multilayer zone plate*, Optics Express, 19322, Vol. 21, No. 16 (2013);

Chapter 4 - PLD of CZTS, first attempts

[68] A. Nagaoka and K. Yoshino, *Growth of CZTS Single Crystals*, in: "Copper Zinc Tin Sulfide Based Thin-Film Solar Cells", ed. by K. Ito, Wiley, 2015;

[69] D.M. Bishop, B.E. McCandless, R. Haight, D. Mitzi, and R. Birkmire, *Fabrication and Electronic Properties of CZTSe Single Crystals*, DOI: 10.1109/JPHOTOV.2014.2363552;

[70] K. Wang et al.,*Thermally evaporated Cu2ZnSnS4 solar cells*, Appl. Phys. Lett. 97, 143508 (2010);

[71] T. Gershon et al., *Photoluminescence characterization of a high-efficiency Cu2ZnSnS4 device*, Journal of Applied Physics 114, 154905 (2013);

[72] A. Redinger et al., *Cu-Rich Precursors Improve Kesterite Solar Cells*, Adv. Energy Mater. 2014, 4, 1300543;

[73] Yi Ren, J. Scragg, C. Frisk, J.K. Larsen, S. Li, and C.P. Bjorkman "*Influence of the Cu2ZnSnS4 absorber thickness on thin film solar cells*". Phys. Status Solidi A, 1-8 (2015);

Chapter 5 and 6 - Pulsed Laser Deposition of thin films of CZTS and CTS

[74] A. Forbes, "*Flat-top beams*", in: Laser Beam Propagation: Generation and Propagation of Customized Light, ed. by Andrew Forbes, CRC press, chap.7.

[75] Moriya K., Tanaka K., Uchiki H., *Fabrication of Cu2ZnSnS4 Thin-Film Solar Cell Prepared by Pulsed Laser Deposition.*, Japanese Journal of Applied Physics 2007; 46(9A):5780-5781

[76] Moriya K., Tanaka K., Uchiki H., *Cu2ZnSnS4 Thin Films Annealed in H2S Atmosphere for Solar Cell Absorber Prepared by Pulsed Laser Deposition.*, Japanese Journal of Applied Physics 2008; 47(1):602-604;

[77] L. Sun, J. He,H. Kong, F. Yue,P. Yang, J. Chu, *Structure, composition and optical properties of Cu2ZnSnS4 thin films deposited by Pulsed Laser Deposition method*, SOLMAT, 95(2011)2907–2913;

[78] A.V. Moholkar, S.S. Shinde, G.L. Agawane, S.H. Jo, K.Y. Rajpure, P.S. Patil, C.H. Bhosale, J.H. Kim, *Studies of compositional dependent CZTS thin film solar cells by pulsed laser deposition technique: An attempt to improve the efficiency*, Journal of Alloys and Compounds 544 (2012) 145–151;

[79] X. Jin, L. Zhang, G. Jiang, W. Liu, C. Zhu, *Pulsed laser deposition of Cu2ZnSn(SxSe1x)4 thin film solar cells using quaternary oxide target prepared by combustion method*, SOLMAT, 155(2016)216–225;

[80] B. Toftmann and J. Schou, *"Time-resolved and integrated angular distributions of plume ions from silver at low and medium laser fluence"*, Appl Phys A (2013) 112:197–202;

Chapter 7 - Double absorption onset of monoclinic Cu2SnS3

[81] M. Nakashima1, J. Fujimoto, T. Yamaguchi, and M. Izaki, *Cu2SnS3 thin-film solar cells fabricated by sulfurization from NaF/Cu/Sn stacked precursor*, Appl. Phys. Expr. 8, 042303, 2015;

[82] Y.T. Zhai, S. Chen, J. Yang, H.J Xiang, X.G. Gong, A Walsh, J. Kang, and S.H. Wei, *Structural diversity and electronic properties of Cu2SnX3 (X = S, Se): A first-principles investigation*, Phys. Rev. B 84, 075213 (2011);

[83] N. Aihara, H. Araki, A. Takeuchi, K. Jimbo, and H. Katagiri, *Fabrication of Cu2SnS3 thin films by sulfurization of evaporated Cu-Sn precursors for solar cells*, Phys. Status Solidi C, 10, No. 7–8, 1086–1092 (2013);

[84] L. Baranowski, K. McLaughlin, P. Zawadzki, S. Lany, A. Norman, H. Hempe, R. Eichberger, T. Unold, E. Toberer, and A. Zakutayev, *Effects of disorder on carrier transport in Cu2SnS3*, Phys Rev. Applied 4, 044017, 2015;

[85] H. Dittrich, M. Klose, M. Brieger, R. Schaffler and H.W. Schock, Cu2InSe3, *thin film solar cells by pulsed laser deposition*, 0-7803-1220-1/93, (1993) IEEE conference proceedings.

[86] B. Li, J. Liu, G. Xu, R. Lu, L. Feng, and J. Wu, *Development of pulsed laser deposition for CdS/CdTe thin film solar cells*, Appl. phys. lett. 101, 153903 (2012);

[87] A. Compaan, A. Bhat, C. Tabory, S. Liu, Y. Li, M.E. Savage, M. Shao, L. Tsien, and R.G. Bohn *polycrystalline CdTe solar cells by pulsed laser deposition*, CH2953-8/91/0000-0957 (1991) IEEE conference proceedings.

[88] P. Harrison, J. Meeth, B. Li, J. Liu, R. Lu, L. Feng, J. Wu, *The Effects of Pressure on the Fabrication of CdS/CdTe Thin Film Solar Cells Made via Pulsed Laser Deposition*, 2013 IEEE 39th (PVSC), DOI: 10.1109/PVSC.2013.6745003;